THE UNIVERSITY OF OKLAHOMA

GRADUATE COLLEGE

EXCITATION OF ATOMIC HYDROGEN

A DISSERTATION

SUBMITTED TO THE GRADUATE FACULTY

in partial fulfillment of the requirements for the

degree of

DOCTOR OF PHILOSOPHY

BY

JAMES D. WALKER, JR.

Norman, Oklahoma

1970

EXCITATION OF ATOMIC HYDROGEN

APPROVED BY

Robert M. St. John

William N. Haugh

Kent J. Carroll

Richard A. Long

Ronald R. Bucaro

DISSERTATION COMMITTEE

ACKNOWLEDGMENTS

I would sincerely like to acknowledge Dr. R. M. St. John who directed the research reported in this dissertation. The excellent facilities for the measurement of electron excitation cross sections provided by him were invaluable in this work.

I wish to specially thank Dr. J. D. Jobe for the great amount of time he contributed in discussing and demonstrating the experimental techniques of electron excitation cross section measurements. The help of my associates Dr. P. N. Stanton, Dr. F. A. Sharpton, and Mr. K. G. Walker is also appreciated.

I wish to recognize the stimulating and enlightening discussions and/or correspondence regarding this work with Dr. G. H. Dunn, Dr. W. L. Fite, Dr. R. A. Day, Dr. D. W. O. Heddle, Dr. I. D. Latimer, Dr. C. C. Lin, and Dr. S. J. Smith.

Mr. R. G. Stermer is due special recognition for performing the glassblowing required in this work. Significant contributions to the design of the apparatus in this work arose from frequent discussions with him.

Finally, I wish to thank my wife Liz for her invaluable understanding and encouragement during the course of this work.

J. D. Walker, Jr.

TABLE OF CONTENTS

TABLE OF CONTENTS (Continued)

LIST OF TABLES

LIST OF FIGURES

LIST OF FIGURES (Continued)

CHAPTER I

INTRODUCTION

The hydrogen atom with one electron and proton is the simplest of all atomic systems. It has therefore been the most important atom used in the development of atomic quantum theory. The first atomic quantum theory by Niels Bohr was successful in allowing the calculation of the discrete energy levels of atomic hydrogen which had been observed by spectroscopists. Several later refinements of the quantum theory, such as the Lamb shift, were first applied to the hydrogen atom and compared with the observed spectrum.

Due to the simplicity of the hydrogen atom, properties such as its electron excitation cross sections can readily be calculated. Such calculations are generally accepted as valid above incident electron energies of 30-50 times the threshold energy for the excitation of a state. Experimental measurements of these cross sections are desirable in order to provide accurate values at low energies and to check for systematic errors in the calculated cross sections at high energies.

While the hydrogen atom is the simplest atom to treat by theoreticians, experimental measurements on it are difficult due to the tendency for hydrogen atoms to form diatomic molecules. Hydrogen in equilibrium at room temperature is nearly completely molecular. Although hydrogen molecules can readily be dissociated in the laboratory, the "lifetime" of the resulting atoms at low pressure is limited by surface recombination. Spectroscopists can escape this problem by producing excited hydrogen atoms by hydrogen molecule-electron collisions in a glow discharge. An atomic hydrogen population need not be created. However, in order to obtain a relatively pure atomic hydrogen spectrum, the material of the walls of the discharge tube must be selected and treated in order to obtain a low probability of recombination. The glow discharge can then dissociate essentially 100% of the hydrogen molecules.

In the measurements of the electron excitation cross sections of atomic hydrogen it is necessary to separate the source of hydrogen atoms and the exciting electron beam in order to prevent their interaction. Hydrogen atoms must therefore be transferred from their source to the electron beam before they recombine. The difficulty in accomplishing this has led most workers in the field of electron excitation cross section measurement to defer work on the hydrogen atom.

The excitation cross sections of atomic hydrogen can be readily applied to astrophysics since hydrogen is the most abundant element in the Universe and it generally occurs in its atomic state. For example, from observations of the H_α line from the Sun, information on the Sun's atomic hydrogen density and electron density and temperature can be obtained by using the atomic hydrogen excitation cross sections.

Previous Work

The first measurements of atomic hydrogen excitation cross sections were made by Ornstein and Lindeman[1]. They flowed hydrogen atoms from a Wood's discharge tube source to an electron beam through a glass tube. The metal parts of the electron gun were shielded by a glass plate in order to hinder the recombination of hydrogen atoms. In this way they obtained 7-10 μ of atom rich hydrogen in the electron beam. By photographing the spectrum from the electron beam, they obtained the relative H_α, H_β, and H_γ optical excitation functions.

The general method used by Ornstein and Lindeman in transferring hydrogen atoms from the dissociation source to the electron beam can be called the "containment" method. This method relies on a low probability for hydrogen atoms impinging on the container wall to recombine. Since all surfaces satisfying this requirement are also electrical

nonconductors, charging of these surfaces and distortion of the electron beam energy is to be expected. The alternative to the containment method is the atomic beam method. Although the densities obtainable in an atomic beam are relatively small due to the physical limit on pumping speed, the material surrounding the electron gun can be entirely metallic, allowing proper operation of the electron beam.

Lamb and Retherford[2] developed an atomic hydrogen beam from a tungsten oven source. They crossed this beam with an electron beam and measured the energy splitting between the $2S_{1/2}$ and $2P_{1/2}$ states, which is now called the Lamb shift, by means of radio frequency quenching of the $2S_{1/2}$ state. Using a tungsten oven source of hydrogen atoms Fite and Brackmann[3] developed a crossed electron-atomic hydrogen beam system capable of measuring electron-hydrogen atom collision processes. The accuracies of their measurements were significantly increased by modulating their atomic beam with a chopping wheel. In this way the signals from electron-atomic beam collisions and electron-molecular background collisions could be separated.

Fite and Brackmann[3] measured the Lyman α intensity from their crossed electron-atomic beams in order to obtain the 2P optical excitation cross section of atomic hydrogen. Since the density of hydrogen atoms in their electron beam

could not be determined, their measurement could not be absolute. It was therefore normalized at high energy to the Born approximation. All of the measurements of the excitation cross sections of atomic hydrogen following those of Fite and Brackmann[3] employed the crossed electron-atomic beam technique. All of these measurements, previous to this work, employed tungsten oven sources of hydrogen atoms. Measurements of the 2P excitation cross section were made by: Fite, Stebbings, and Brackmann[4]; Chamberlain, Smith, and Heddle[5]; Long, Cox, and Smith[6]; and Williams, Curley, and McGowan[7].

Lichten and Schultz[8] measured the excitation cross section of the metastable 2S state of atomic hydrogen using the electron ejection technique for the detection of metastable atoms. They calculated the hydrogen atom density in the electron beam from their furnace temperature and pressure and from the geometrical factors of their apparatus. They used the published efficiency of their metastable atom detector to determine the absolute number of metastable atoms produced. In this way they obtained an absolute 2S excitation cross section which was within 30% of the theoretical cross section near onset. The work of Lichten and Schultz[8] represents the only absolute excitation cross section measurement on atomic hydrogen prior to this work. A

relative measurement of the 2S excitation cross section was made by Stebbings, Fite, Hummer, and Brackmann[9] by quenching the 2S states in an electric field downbeam from the electron beam. The Lyman α radiation from the quenched 2S states was detected and the ratio of the 2S to 2P excitation cross sections was measured.

Kleinpoppen and Kraiss[10] measured the optical excitation cross section and the polarization of the n = 3 state of atomic hydrogen by observation of the H_α line.

This Work

The abundance of the published measurements of the cross sections of the 2S and 2P states of atomic hydrogen does not encourage one to construct an apparatus to remeasure these cross sections. A further deterrent is the great amount of design, fabrication, and assembly required in the construction of such an apparatus as described by Long et al.[6]

In order to measure excitation cross sections for higher n states than those previously reported, a greater density of hydrogen atoms in the electron beam is required to offset the decreasing cross sections with increasing n. Therefore, in this work a new design of a crossed electron-atomic hydrogen beam apparatus was developed which yielded

an atomic hydrogen density in the electron beam which was greater than those obtained in the previous works by a factor of approximately 10^5. A Wood's discharge tube source of hydrogen atoms was developed in this work and used with the crossed beam apparatus. Measurements of the Balmer optical excitation cross sections were made for n = 3-13. The high degree of dissociation obtained in the electron beam allowed the absolute measurements of these cross sections by a technique developed in this work.

CHAPTER II

PROCEDURE OF THE EXPERIMENT

Definitions of Electron Excitation Cross Sections

The cross section for the production of an excited electronic state of an atom or molecule due to a collision with an incident electron will be referred to here as the excitation cross section. Such cross sections can be measured by passing a monoenergetic electron beam through a low pressure gas of atoms and molecules. By observing the radiative decay of the resulting excited atomic or molecular states their optical excitation cross sections can be obtained. The term state is used here to refer to a group of quantum states which cannot be optically resolved. Observation of the i to j atomic or molecular transition yields the optical excitation cross section of state i, Q_{ij}, as

$$Q_{ij} = \frac{R_{ij}}{NJ/e} , \qquad (1)$$

where R_{ij} is the rate of photon emission per unit volume at a given point in the electron beam due to the i to j transition,

J is the electron beam current density at the same point in the electron beam,

N is the density of atoms or molecules at the same point in the electron beam, and

e is the charge of an electron.

Eq. (1) can be altered by integrating over the plane perpendicular to the direction of motion of the electrons, plane A, as

$$Q_{ij} \int_A N(J/e)dA = \int_A R_{ij}dA. \qquad (2)$$

Performing the indicated integration we obtain

$$Q_{ij} = \frac{P_{ij}}{N^* I/e}, \qquad (3)$$

where P_{ij} is the rate of photon emission per unit length of the electron beam at a given point due to the i to j transition,

I is the electron beam current at the same point in the electron beam crossing plane A, and

N^* is the average value of N weighted by J/I over the plane A. (Note that if N is constant we have the simple relation $N^* = N$.)

The optical excitation cross section as given by Eq. (3) is a function of directly measurable quantities.

It should be noted that the optical excitation cross section, Q_{ij}, represents only the cross section for excitations to the i state which subsequently radiatively decay by the i to j transition. The branching ratio of the i to j transition, B_{ij}, is defined as

$$B_{ij} = \sum_k A_{ik}/A_{ij}, \qquad (4)$$

where A_{ij} is the Einstein transition probability from state i to state j.

The sum in Eq. (4) is over all lower states connected to state i by radiative decay. The apparent excitation cross section of state i, Q_i', can be obtained from the optical excitation cross section as

$$Q_i' = B_{ij}\, Q_{ij}. \qquad (5)$$

The apparent excitation cross section of state i includes excitations to state i by several modes. These include direct excitation from the ground state to state i, direct excitation from the ground state to upper states and subsequent cascade into state i, excitation to states which are very close to the energy level of state i and subsequent transfer of excitation to state i due to collisions with ground state atoms (or conversely the transfer of excitation from state i), and ionization of the atom by electron impact and subsequent recombination to state i. The apparent excitation cross section can be written as a sum of these components as

$$Q_i' = Q_i^D + Q_i^C + Q_i^T + Q_i^R, \qquad (6)$$

where Q_i^D is the component due to direct excitation of state i and is called the level excitation cross section,

Q_i^C is the component due to cascade from upper directly excited states,

Q_i^T is the component due to transfer of excitation, and

Q_i^R is the component due to recombination.

In order to experimentally separate these components, use can be made of their functional dependencies on electron beam current and gas density. Q_i^D and Q_i^C are independent of beam current and gas density, Q_i^T is directly proportional to gas density and independent of electron beam current, and Q_i^R is directly proportional to the electron beam current and independent of gas density. By reducing the electron beam current and gas density sufficiently it is possible to eliminate essentially the recombination and transfer components leaving only the direct excitation and cascade components. This work was carried out under these conditions. Indeed, the low gas densities obtained in the atomic beam in this work prohibited the observation of the transfer of excitation.

It should be noted that optical, apparent, and level excitation cross sections have been defined for incident electrons of a particular energy. Indeed, the cross sections are strongly dependent on incident electron energy. This functional dependence is called the electron excitation function.

Measurements of excitation cross sections are made under conditions where not more than 1% of the beam electrons suffer inelastic collisions. We therefore require that $\Delta x\, N^* \sum_i Q_i^D \leq .01$, where Δx is the length of the electron beam

and the sum is over all level excitation cross sections Q_i^D including the ionization cross section to the continuum. If this condition is not met, electrons are obtained in the beam of less energy than the monoenergetic value. The resulting mixture of energies would lead to incorrect excitation cross sections.

Measurements with the Crossed Beam System

The crossed electron and atomic hydrogen beam system used for the measurement of the excitation cross sections of atomic hydrogen is shown in Figs. 1 and 2. The details of construction and operation are given in Chapter III. The source of hydrogen atoms was a glow discharge of the R. W. Wood[11] type. Hydrogen molecules were admitted to the discharge by a needle valve, dissociated, and emitted from a nozzle which formed an atomic beam which was crossed with an electron beam.

Eq. (3) shows that in order to obtain the optical excitation cross section of state i we must know P_{ij}, I, and N^*. The first two of these can be absolutely measured in a straightforward manner discussed later in this chapter. In the case of an atomic beam, however, considerable inaccuracy arises in the absolute measurement of N^*. N^* can readily and accurately be held constant, enabling the measure-

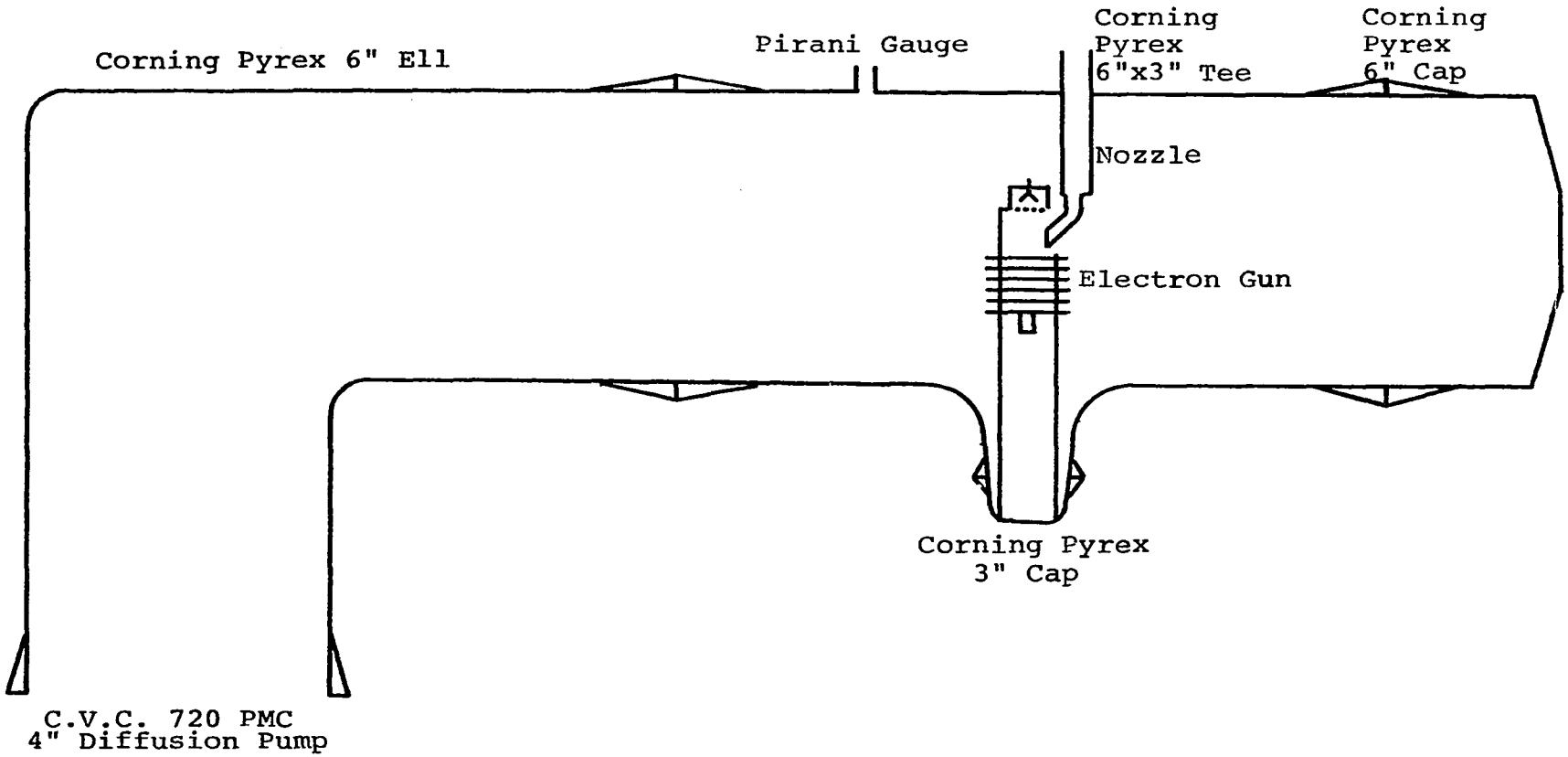

Figure 1. Crossed Beam System.

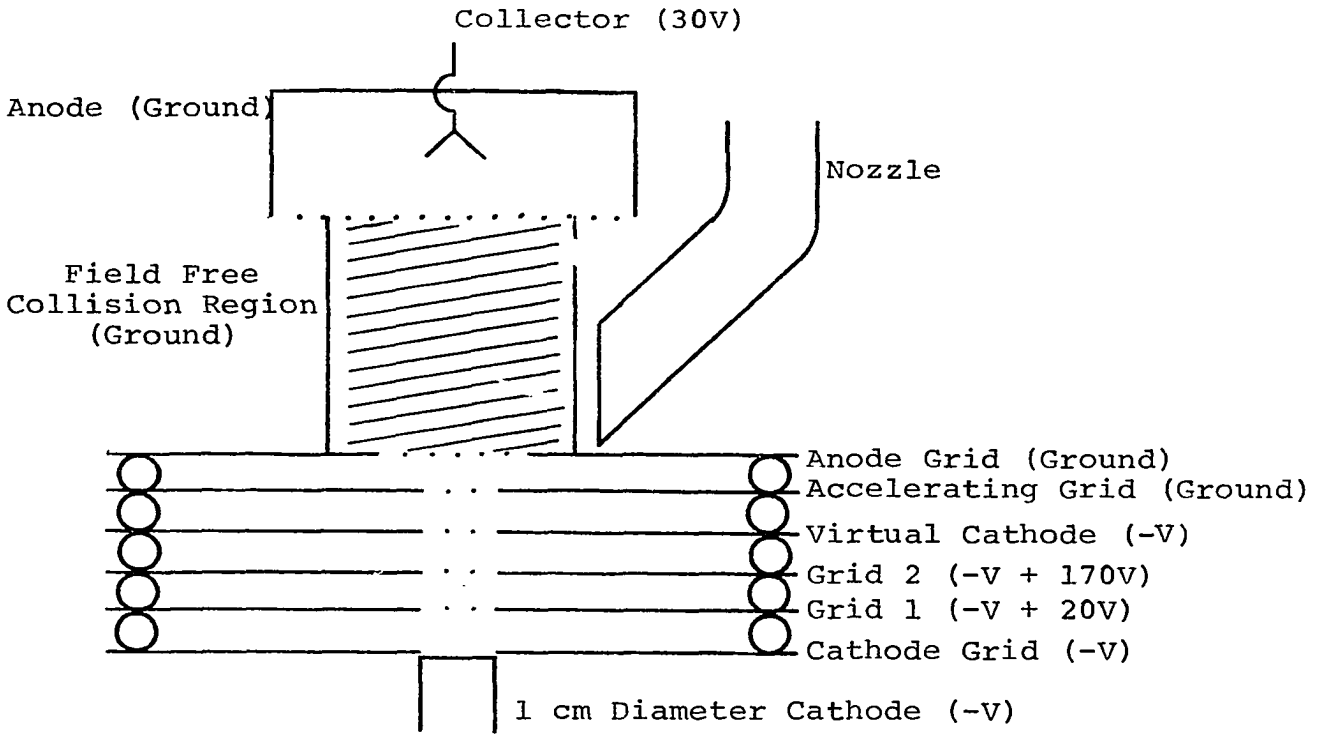

Figure 2. Electron Gun.

ments of excitation functions and the ratios of the excitation cross sections of the same atom or molecule where N^* cancels. A review of previous atomic beam excitation experiments[3,6] revealed that these two types of measurements were generally all that had been accomplished for atomic hydrogen or any other atomic or molecular species, although Lichten and Schultz[8] calculated the atomic hydrogen density in their atomic beam in order to obtain the absolute 2S excitation cross section.

Relation of Atomic and Molecular Hydrogen Densities in the Electron Beam

In the present work the absolute measurement of N^* was circumvented in the following manner. Let us consider atoms or molecules of two different species designated "A" and "B". The ratio of their optical excitation cross sections as defined by Eq. (3) is given by

$$\frac{Q_{Aij}}{Q_{Blm}} = \frac{P_{Aij}\, N^*_B\, I_B}{P_{Blm}\, N^*_A\, I_A} . \qquad (7)$$

Eq. (7) shows that the measurement of the ratio N^*_B/N^*_A is necessary to obtain the absolute value of Q_{Aij}. In this work it was possible to measure the ratio of atomic to molecular hydrogen densities in the electron beam with an estimated 20% accuracy in the manner described below.

The condition of constant mass flux through any plane cross section of the flow system with the Wood's tube on or off was readily obtained by holding the setting of the needle valve supplying the Wood's tube constant. Let us consider a unit area at some point τ in the electron beam shown in Fig. 3. Here v is the velocity of an atom or molecule in the atomic beam and θ and ϕ give the direction of motion. Let the normal to this unit area be parallel to the drift direction of the atomic beam. It will become

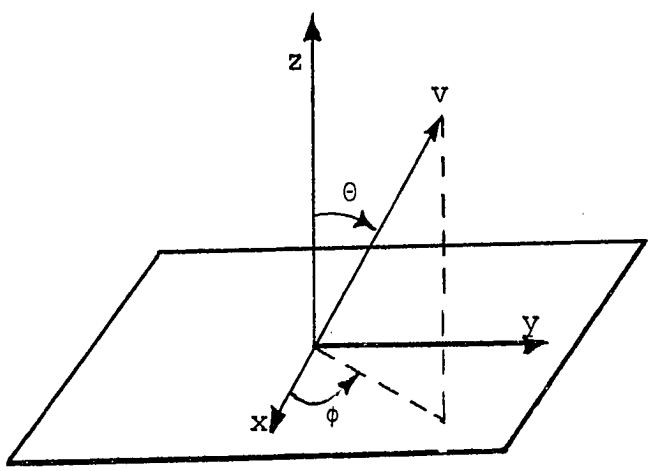

Figure 3. Coordinates for Mass Flux in the Electron Beam.

evident that the precise alignment of this normal will have no effect on the following analysis. The mass flux per unit area, $F_{H_2B}(\tau)$, at point τ in the electron beam due to hydrogen molecules emitted directly from the nozzle when the Wood's tube is off is given by

$$F_{H_2B}(\tau) = \int_0^{\infty} \int_0^{2\pi} \int_0^{\pi/2} m_{H_2} N_{H_2B}(\tau) G_{H_2B}(v, \theta, \phi, \tau) v^3 x \qquad (8a)$$

$$x \sin\theta \cos\theta \, d\theta \, d\phi \, dv,$$

where $G_{H_2B}(v, \theta, \phi, \tau)$ is the velocity and direction distribution function at point τ of hydrogen molecules emitted directly from the nozzle with the Wood's tube off,

$N_{H_2B}(\tau)$ is the density of hydrogen molecules at point τ due to direct emission from the nozzle with the Wood's tube off, and

m_{H_2} is the mass of a hydrogen molecule.

The mass flux per unit area, $F'_{H_2B}(\tau)$, at point τ due to hydrogen molecules emitted directly from the nozzle when the Wood's tube is on is given by

$$F'_{H_2B}(\tau) = \int_0^{\infty} \int_0^{2\pi} \int_0^{\pi/2} m_{H_2} N'_{H_2B}(\tau)\, G'_{H_2B}(v, \theta, \phi, \tau)\, v^3 x \qquad (8b)$$

$$x \sin\theta \cos\theta \, d\theta \, d\phi \, dv,$$

where $G'_{H_2B}(v, \theta, \phi, \tau)$ is the velocity and direction distribution function at point τ of hydrogen molecules emitted directly from the nozzle with the Wood's tube on, and

$N'_{H_2B}(\tau)$ is the density of hydrogen molecules at point τ due to direct emission from the nozzle with the Wood's tube on.

The mass flux per unit area, $F_{HB}(\tau)$, at point τ due to hydrogen atoms emitted directly from the nozzle with the Wood's tube on is given by

$$F_{HB}(\tau) = \int_0^{\infty} \int_0^{2\pi} \int_0^{\pi/2} m_H N_{HB}(\tau)\, G_{HB}(v, \theta, \phi, \tau)\, v^3 x \qquad (8c)$$

$$x \sin\theta \cos\theta \, d\theta \, d\phi \, dv,$$

where $G_{HB}(v, \theta, \phi, \tau)$ is the velocity and direction distribution function at point τ of hydrogen atoms emitted directly from the nozzle with the Wood's tube on,

$N_{HB}(\tau)$ is the density of hydrogen atoms at point τ due to direct emission from the nozzle with the Wood's tube on, and

m_H is the mass of a hydrogen atom.

The velocity distribution of a gas passing through an orifice has been found to be Maxwellian for large Knudsen numbers (the ratio of the mean free path to the orifice radius).

Wise and Wood[12] have measured the interdiffusion coefficient, D_{H,H_2}, of H through H_2 for a pressure of H_2 of 30×10^{-3} mm Hg to be 4.70×10^4 cm^2/sec at 293°K. The relation between the diffusion coefficient and the mean free path, λ, is given by Cobine[13] as

$$D = \frac{\lambda \bar{v}}{3}, \qquad (9)$$

where $\bar{v}$ is the average atomic or molecular velocity (in the case of a binary mixture $\bar{v}$, λ, and D refer to the species which is diffusing).

Using 2.5×10^5 cm/sec for $\bar{v}_H$ at 300°K[14] we obtain a value of .565 cm for λ. Since the mean free path is inversely proportional to the pressure, at ten microns of H_2 the mean free path of H is 1.69 cm. For the one centimeter diameter orifice of the nozzle used in this experiment a Knudsen number

of 3.38 is obtained. From Cobine[15] we find that the mean free path of H_2 through itself is 18.3×10^{-6} cm at N.T.P. At ten microns pressure the mean free path becomes 1.39 cm and results in a Knudsen number of 2.78 for the one centimeter orifice. The close agreement in the Knudsen numbers for H through H_2 and H_2 through itself can be understood from the work of Vanderslice *et al.*[16] in which the cross sections for high temperature H-H, H-H_2, and H_2-H_2 collisions were calculated. They noted that the interaction energy between two free H atoms is approximately twice that between two H atoms of which either one or both is a part of a larger molecule. We therefore conclude that the Knudsen number for atomic hydrogen through itself for the one centimeter orifice is approximately equal to those for H through H_2 and H_2 through itself at the same pressure.

The upper limit on the pressure at the orifice with the Wood's tube off in the experiment was ten microns of hydrogen molecules. If the mass flow rate is held constant and the hydrogen molecules are completely converted to atoms, the pressure at the orifice will increase by a factor of $\sqrt{2}$. This condition would result in a Knudsen number for H through itself of approximately 2.0. At these Knudsen numbers Scott *et al.*[17] have measured the velocity distribution of argon and xenon passing through an orifice to be approximately

Maxwellian. They found that for Knudsen numbers below three, departures from the Maxwellian velocity distribution began. Their work suggested that collisions in the vicinity of the orifice resulted in preferential depletion of low-velocity particles with particle replacement occurring at higher velocities. The trends of the average velocity with Knudsen number were shown to be the same for argon and xenon, resulting in only second order deviations in the ratio of their average velocities at the same Knudsen number from the Maxwellian case. The results of Scott et al. were similar to those obtained by Marcus and McFee[18] with potassium.

Since the Wood's tube becomes warm when it runs, we must determine whether the hydrogen atoms and molecules reach thermal equilibrium with the walls of the nozzle, shown in Fig. 1, before they effuse into the electron beam. The accomodation coefficient, α, of a surface for an impinging gas particle is defined by Hartnett[19] as

$$\alpha = \frac{e_g - e_r}{e_g - e_w}, \qquad (10)$$

where e_g is the energy of a gas particle incident on the wall,

e_w is the energy of the wall, and

e_r is the energy of the gas particle reflected from the wall.

The deviation from thermal equilibrium of gas particles leaving the nozzle in this experiment is given as

$$\Delta E = \Delta E_o (1 - \alpha)^n, \qquad (11)$$

where ΔE_o is the average energy difference between the gas particles and the wall upon entry to the nozzle,

ΔE is the average energy difference between the gas particles and the wall upon exit from the nozzle, and

n is the average number of wall collisions per gas particle in passing through the nozzle.

In this experiment ΔE_o was estimated to be 3/2 k 50°K. Keesom and Schmidt[20] have measured the accommodation coefficient for glass to be 0.67 for helium with the surface covered by a layer of helium and 0.70 for neon with the surface covered by a layer of neon. The average number of wall collisions per gas particle passing through the nozzle in this experiment was calculated to be greater than 300. Using the

values of 0.70 for α^i and 300 for n we find that ΔE equals $(\Delta E_o\ 10^{-157})$. Thus thermal equilibrium with the walls of the nozzle was obtained.

Applying the velocity distribution measurements by Scott et al.[17] on argon and xenon and by Marcus and McFee[18] on potassium to atomic and molecular hydrogen at the same Knudsen numbers, we conclude that close approximations to the Maxwellian velocity distribution for hydrogen atoms and molecules emitted from the nozzle were obtained in this work. Since only the ratios of the average velocities are used here, the velocity distributions will be treated as Maxwellian. We also conclude that the temperature of these distributions was that of the nozzle which was at room temperature. The Maxwellian velocity distribution function for a gas is given by Dushman[21] as

$$f(v) = \frac{4}{\sqrt{\pi}} \left(\frac{m}{2kT} \right)^{3/2} v^2 e^{-mv^2/(2kT)} . \tag{12}$$

It is possible to separate the velocity distribution functions from the direction of motion distribution functions in Eqs. (8a), (8b), and (8c) as

---

[i] Here the assumption is made that atomic and molecular hydrogen has the same accommodation coefficient on glass as neon. This is justified by observing from the table given by Hartnett[19] that α is strongly a function of the surface and not the gas species.

$$G_{H_2B}(v, \theta, \phi, \tau) = \frac{f_{H_2B}(v)}{4\pi v^2} g_{H_2B}(\theta, \phi, \tau) \tag{13a}$$

$$G'_{H_2B}(v, \theta, \phi, \tau) = \frac{f_{H_2B}(v)}{4\pi v^2} g'_{H_2B}(\theta, \phi, \tau) \tag{13b}$$

$$G_{HB}(v, \theta, \phi, \tau) = \frac{f_{HB}(v)}{4\pi v^2} g_{HB}(\theta, \phi, \tau) \tag{13c}$$

where $g_{H_2B}(\theta, \phi, \tau)$, $g'_{H_2B}(\theta, \phi, \tau)$, and $g_{HB}(\theta, \phi, \tau)$ are the distribution functions for the direction of motion at point τ of hydrogen molecules with the Wood's tube off, hydrogen molecules with the Wood's tube on, and hydrogen atoms with the Wood's tube on, respectively, emitted directly from the nozzle.

Since the Knudsen number of the orifice in this experiment was at least 2, gas-wall collisions were much more important than gas-gas collisions in determining the distribution functions for the direction of motion of gas particles emitted directly from the nozzle. It should be noted that the small effect of gas-gas collisions on these distribution functions should have been quite similar for atomic and molecular hydrogen due to their mean free paths

being approximately equal. Therefore, in order to compare $g_{H_2B}(\theta, \phi, \tau)$, $g'_{H_2B}(\theta, \phi, \tau)$, and $g_{HB}(\theta, \phi, \tau)$, detailed information on the nature of the gas-wall collisions is needed. The assumption was made by Knudsen[22] that any surface, no matter how macroscopically smooth, is molecularly rough. This results in the reflection of gas particles in a direction which is totally independent of the direction of incidence. The wide use and success of this concept in calculating the conductance of tubes in the regime of molecular flow is shown by Dushman[23]. However, recent interest in the passage of vehicles through the low density regime constituting the upper atmosphere has stimulated detailed experimental and theoretical studies on the reflection of gas particles from solid surfaces. As a result, numerous molecular beam experiments[24-30] have demonstrated specular, or mirror like, reflection from surfaces. In the review by Stickney[31] further experimental work as well as theoretical work is presented. Eeder[32] reviews the quantum mechanical work on gas scattering (specular and diffuse) from the surface of crystals.

As a result of the specular reflection properties measured for various surfaces referred to above, the spacing of the irregularities of these surfaces projected onto the plane perpendicular to the direction of incidence must be

smaller than the de Broglie wavelength of the incident gas particles[24] (which is $[1.59/\sqrt{M}]$ Å for room temperature particles where M is the gram molecular weight of the gas).

The use of electron microscopes allows resolution by the replication technique of ~5 Å. Datz et al.[25] failed in making carbon replicas of a platinum surface due to the extreme surface smoothness. Naves and Sella[33] discovered granular structure in fractured glass on the order of 50 Å ~ 300 Å by the method of carbon, platinum, and irridium replication, but found no structure in polished glass. In a reflection type measurement performed at the University of Oklahoma Electron Microscope Laboratory on Corning 7740 Pyrex tubing we found no structure using a resolution of 300 Å.

In spite of the unanticipated extreme smoothness of many surfaces, random or diffuse reflection properties have been found to occur by several investigators. Stalder et al.[34] in a Knudsen flow wind tunnel experiment found that the measured drag on an iron cylinder at room temperature was given by the diffuse reflection model within experimental error. Davis, Levenson, and Milleron[35,36] measured the conductances of CO_2 and xenon through various tube geometries[i]

---

[i] The materials of these tubes were not specified, although they were probably some machinable metal. They were referred to as "commercial materials" in the articles.

at room temperature and found these to agree within the 10% probable experimental error with conductances calculated by the Monte Carlo method based on diffuse reflection of gas particles. Smith and Fite[26] found by the molecular beam method that diffuse scattering occurred for A and H_2 from a Ni surface at room temperature while highly specular reflection occurred at 600°C. Datz et al.[25] found by the molecular beam method that diffuse scattering occurred for He and D_2 from a Pt surface at room temperature while highly specular scattering occurred at 1100°C. The explanation for diffuse scattering given by Datz was the adsorption of the incident gas particles, long residence times in the adsorbed state, and diffuse evaporation. The rate of evaporation of adsorbed gas particles increases and the average residence time decreases with increasing surface temperature. Since the diffuseness of evaporated gas particles increases with increasing residence time, the diffuseness should decrease with increasing surface temperature.

Zwanzig[37] has given a simple model for surface adsorption such that impinging gas particles suffering inelastic collisions are adsorbed or reflected depending on whether their resultant kinetic energy is less than or greater than the surface potential energy well. Zwanzig's model for gas particle-lattice interaction is based on a one-dimensional

lattice with nearest neighbor interaction. The gas particle-lattice potential function is taken to be the same as that for two lattice atoms. The lattice atoms are taken to be initially at rest. Zwanzig found by classical methods that impinging gas particles are adsorbed or reflected depending on whether their incident kinetic energies are less than or greater than a critical energy K_c. K_c is of the order of m^3D where D is the depth of the potential well and m is the mass ratio (gas particle mass/surface atom mass).

The heat of adsorption of He on Pt is between 0.1 and 0.2 kcal/mol and that of D_2 is between 1.5 and 2.0 kcal/mol. Based on Zwanzig's adsorption theory, specular reflection should occur at gas temperatures above 0.1°K. However, Datz found that specular reflection did not occur at room temperature for either gas. A contaminant with a heat of adsorption of 26 kcal/mol could form on the surface at room temperature, however, and increase the adsorption probability of He and D_2 sufficiently to produce diffuse reflection. Indeed, Datz observed this phenomenon by lowering the temperature of Pt to room temperature from an elevated temperature. He observed the transition from specular to diffuse reflection as a function of time. This rate was the same whether the D_2 beam was run continuously or intermittently, ruling out the possibility of an adsorbed layer of D_2 explaining the transition. It should be noted that Datz

obtained the layer of contaminant on his Pt surface at room temperature in spite of the use of standard high vacuum techniques. Liquid nitrogen trapped mercury diffusion pumps produced a chamber pressure of 1×10^{-7} mm Hg. A mass spectroscopic analysis indicated that air and water vapor were the predominant species in the ambient gas.

The work of O'Keefe et al.[28] seems to indicate that the water vapor in Datz's experiment was responsible for the surface contamination. O'Keefe found specular reflection for H_2 from a freshly cleaved LiF crystal at room temperature by the molecular beam method. Since Bayh and Pflug[38] found that there are four monolayers of H_2O on freshly cleaved LiF, its reflection properties should be insensitive to H_2O contamination.

For the present work, the measurements of Hurlbut[39,40] of the reflection properties of N_2, A, and air from glass are of primary interest. His apparatus was capable of measuring reflection both in and out of the plane of incidence. For a glass surface at room temperature he obtained diffuse reflection with slight deviations only at grazing angles of incidence. Stickney[31] has claimed Hurlbut's surface was contaminated as the work of Datz et al.[25] would also indicate. Hurlbut obtained 2×10^{-6} mm Hg ambient pressure using a diffusion pump (with an unspecified fluid) and a liquid

nitrogen trap. It should be noted that the physical factors determining the surface condition in Hurlbut's experiment were essentially the same as those in this work.

Since no work has been done specifically on atomic and molecular hydrogen scattering from glass, we must infer the type of scattering which occurred from the 7740 Pyrex nozzle at room temperature in this work. Due to the consistent diffuse scattering results at room temperature by Hurlbut on glass and by the various other workers on other surfaces mentioned above, we conclude that diffuse scattering occurred from the nozzle in this work. The implication of this conclusion is that the distribution functions for the directions of motion are equal as shown by

$$g_{H_2B}(\theta, \phi, \tau) = g'_{H_2B}(\theta, \phi, \tau) = g_{HB}(\theta, \phi, \tau) . \tag{14}$$

By substituting the forms of $G_{H_2B}(v, \theta, \phi, \tau)$, $G'_{H_2B}(v, \theta, \phi, \tau)$, and $G_{HB}(v, \theta, \phi, \tau)$ given by Eqs. (13a), (13b), and (13c), respectively, into Eqs. (8a), (8b), and (8c), respectively, and integrating with respect to v, we obtain

$$F_{H_2B}(\tau) = \left(\frac{1}{4\pi}\right) m_{H_2} \bar{v}_{H_2B}(\tau) N_{H_2B}(\tau) \int_0^{2\pi} \int_0^{\pi/2} g_{H_2B}(\theta, \phi, \tau) x$$

(15a)

$$x \sin\theta \cos\theta \, d\theta \, d\phi$$

$$F'_{H_2B}(\tau) = \left(\frac{1}{4\pi}\right) m_{H_2} \bar{v}'_{H_2B}(\tau) N'_{H_2B}(\tau) \int_0^{2\pi} \int_0^{\pi/2} g'_{H_2B}(\theta, \phi, \tau) x$$

(15b)

$$x \sin\theta \cos\theta \, d\theta \, d\phi$$

$$F_{HB}(\tau) = \left(\frac{1}{4\pi}\right) m_{H} \bar{v}_{HB}(\tau) N_{HB}(\tau) \int_0^{2\pi} \int_0^{\pi/2} g_{HB}(\theta, \phi, \tau) x$$

(15c)

$$x \sin\theta \cos\theta \, d\theta \, d\phi,$$

where $\bar{v}_{H_2B}(\tau)$ is the average velocity at point τ of hydrogen molecules emitted directly from the nozzle with the Wood's tube off,

$\bar{v}'_{H_2B}(\tau)$ is the average velocity at point τ of hydrogen molecules emitted directly from the nozzle with the Wood's tube on, and

$\bar{v}_{HB}(\tau)$ is the average velocity at point τ of hydrogen atoms emitted directly from the nozzle with the Wood's tube on.

In this work $\bar{v}_{H_2B}(\tau)$, $\bar{v}'_{H_2B}(\tau)$, and $\bar{v}_{HB}(\tau)$ are constant functions of τ. Since in each case the gas was in thermal equilibrium with the nozzle at room temperature T_R we obtain the relations

$$\frac{1}{2} m_{H_2} \overline{v^2}_{H_2B}(\tau) = \frac{1}{2} m_{H_2} \overline{v^2}'_{H_2B}(\tau) = \frac{1}{2} m_H \overline{v^2}_{HB}(\tau) = \frac{3}{2} kT_R. \tag{16}$$

For the Maxwellian velocity distribution we find that the root mean square velocity, v_r, is simply related to the arithmetic mean velocity[41], v_a, as

$$v_r = \frac{1}{2}\sqrt{\frac{3\pi}{2}}\, v_a. \tag{17}$$

Using the atomic to molecular hydrogen mass ratio and the Maxwellian velocity distribution for each gas, we obtain the relations

$$\bar{v}_{H_2B}(\tau) = \bar{v}'_{H_2B}(\tau) \tag{18}$$

$$\bar{v}_{H_2B}(\tau) = \frac{1}{\sqrt{2}}\, \bar{v}_{HB}(\tau) \tag{19}$$

Equation (14) showing the direction of motion distribution functions in the electron beam to be equal implies that if the mass flux through any plane cross section of the flow system is constant with the Wood's tube on or off, then the mass flux through a unit area at point τ in the electron beam due to gas particles emitted directly from the nozzle is constant, as given by

$$F_{H_2B}(\tau) = F'_{H_2B}(\tau) + F_{HB}(\tau) . \tag{20}$$

Rewriting Eq. (20) we obtain

$$F_{HB}(\tau) = F_{H_2B}(\tau) - F'_{H_2B}(\tau) . \tag{21}$$

We can now substitute the expressions for $F_{H_2B}(\tau)$, $F'_{H_2B}(\tau)$, and $F_{HB}(\tau)$ in Eqs. (15a), (15b), and (15c) into Eq. (21) to obtain Eq. (22). Note that since the distribution functions for the direction of motion are equal, the integrals cancel.

$$\begin{aligned} m_H \bar{v}_H(\tau) N_{HB}(\tau) = {} & m_{H_2} \bar{v}_{H_2}(\tau) N_{H_2B}(\tau) \\ & - m_{H_2} \bar{v}'_{H_2}(\tau) N'_{H_2B}(\tau) . \end{aligned} \tag{22}$$

Combining Eqs. (18), (19), and (22), and using the atomic to molecular hydrogen mass ratio, we obtain

$$N_{HB}(\tau) = \sqrt{2}\left[N_{H_2B}(\tau) - N'_{H_2B}(\tau)\right] . \qquad (23)$$

Although the atomic and molecular hydrogen densities in the electron beam considered up to this point have been those emitted directly from the nozzle, background densities also exist due to scattering from the surfaces of the beam chamber. The background density in this work comprised approximately one half of the total density in the electron beam. If the background density consisted entirely of hydrogen molecules and therefore remained constant when the Wood's tube was on and off, the density of hydrogen atoms in the electron beam could be obtained from the difference in total molecular hydrogen densities with the Wood's tube on and off since the background densities would subtract out any yield $N_{HB}(\tau)$ by Eq. (23).

Smith[42] has shown that at low pressures, recombination of atomic hydrogen due to gas-gas collisions is insignificant compared with gas-surface collisions. Wise and Wood[43] have reviewed the work on the surface recombination coefficients of atomic hydrogen for various surfaces. In

this work the principal surfaces in the beam chamber, shown in Fig. 1, were Pyrex for the chamber walls and nozzle, 303 stainless steel for the electron gun plates, and nickel for the grid wires. The recombination coefficients range from 0.2 for nickel to 3×10^{-4} for water moistened Pyrex. The recombination coefficient for stainless steel was not given by Wise and Wood but it should be similar to that of nickel. Although the condition of a surface plays an important role in determining its recombination coefficient, the condition of the surfaces in the beam chamber in this work could not be determined. A monolayer of diffusion pump oil and/or water may have readily formed on the surfaces. Since this could raise as well as lower the recombination coefficients, the ones given above will be used. We must therefore consider the case in which hydrogen atoms are reflected back into the electron beam.

According to the previous discussion, the room temperature surfaces of the beam chamber should exhibit diffuse reflection for hydrogen atoms and molecules. All of the surfaces of the beam chamber were at room temperature except those of the electron gun. Due to its thermionic cathode the temperature of the electron gun was high. The accelerating plate nearest the atomic beam is estimated to have reached several hundred degrees centigrade. However,

the roughness of this plate should have greatly reduced any specular reflection. Further, any specular reflection should have been similar for hydrogen atoms and molecules. We therefore make the assumption that the reflection properties of the surfaces of the beam chamber were the same for hydrogen atoms and molecules. With a mean free path of 17 cm (at one micron pressure) in the 15 cm diameter beam chamber, gas-gas collisions should have played a secondary role in determining the paths of the gas particles. Further, the gas-gas collisions should have affected hydrogen atoms and molecules in a like manner according to the calculations of Vanderslice et al.[16] We therefore conclude that hydrogen atoms and molecules statistically followed the same paths in the beam chamber.

Let us now consider a particular surface in the beam chamber. With the Wood's tube off we find an incident mass flux F_{H_2} per unit area of hydrogen molecules. This mass flux is due to an incident density of hydrogen molecules N_{H_2}, a velocity distribution function $f_{H_2}(v)$, and a distribution function for the direction of motion $g_{H_2}(\theta, \phi)$. Upon reflection from the surface, a fraction $K(\tau)$ of the density N_{H_2} passes through point τ in the electron beam. When the Wood's tube is turned on, the condition of hydrogen atoms and molecules statistically following the same

paths and the conservation of mass gives the result that the incident mass flux per unit area on the surface equals that with the Wood's tube off. Thus, the sum of the incident mass flux per unit area of hydrogen molecules F'_{H_2} and the incident mass flux per unit area of hydrogen atoms F_H with the Wood's tube on equals F_{H_2}. Hydrogen atoms and molecules statistically following the same paths implies that the distribution functions for their directions of motion incident on the surface are equal. Further, we can use Maxwellian velocity distributions at room temperature for the hydrogen atoms and molecules in the chamber. We now have the same conditions obtained for the mass flux per unit area in the electron beam due to gas particles emitted directly from the nozzle. We can therefore apply the relation of densities in Eq. (23) to the densities incident on the surface in the beam chamber and obtain

$$N_H = \sqrt{2}\,(N_{H_2} - N'_{H_2}), \tag{24}$$

where N_H is the density of hydrogen atoms incident on the surface with the Wood's tube on and

N'_{H_2} is the density of hydrogen molecules incident on the surface with the Wood's tube on.

Upon striking the surface, a fraction γ of the atoms will recombine. Using the same reflection properties for hydrogen atoms and molecules we find that the number of hydrogen atoms reflected into point τ in the electron beam is $(1 - \gamma) K(\tau) N_H$. The total density of hydrogen molecules reflected into point τ with the Wood's tube on is $K(\tau) \left[N'_{H_2} + \frac{\gamma N_H}{\sqrt{2}} \right]$. It follows that the relation for the scattered atoms and molecules from the surface into point τ is

$$N_{HR}(\tau) = \sqrt{2} \left(N_{H_2R}(\tau) - N'_{H_2R}(\tau) \right), \qquad (25)$$

where $N_{HR}(\tau)$ is the density of hydrogen atoms at point τ reflected from the surface with the Wood's tube on,

$N_{H_2R}(\tau)$ is the density of hydrogen molecules at point τ reflected from the surface with the Wood's tube off, and

$N'_{H_2R}(\tau)$ is the density of hydrogen molecules at point τ reflected from the surface with the Wood's tube on.

Since the forms of Eqs. (23) and (25) are identical, it follows that we can write a relation for the total densities at point τ in the same form, given as

$$N_{HT}(\tau) = \sqrt{2}\left(N_{H_2T}(\tau) - N'_{H_2T}(\tau)\right), \qquad (26)$$

where $N_{HT}(\tau)$ is the total density of hydrogen atoms at point τ with the Wood's tube on,

$N_{H_2T}(\tau)$ is the total density of hydrogen molecules at point τ with the Wood's tube off, and

$N'_{H_2T}(\tau)$ is the total density of hydrogen molecules at point τ with the Wood's tube on.

Absolute H Cross Section Measurement with the Crossed Beam System

The primary factors in determining the distribution of current in the one centimeter diameter electron beam was the electron gun design, the beam current, the accelerating voltage, and space charge neutralization. For a given accelerating voltage, the beam currents used with atomic and molecular hydrogen were essentially the same. Since the ionization cross sections of atomic and molecular hydrogen are both large and the total density in the electron beam was essentially the same with the Wood's tube on and off, space charge neutralization should have readily been accomplished in either case. Of interest in this work is the overlap of the electron beam current density and the

atomic and molecular hydrogen densities. A one-dimensional representation, in the direction mutually perpendicular to the axes of the electron beam and the nozzle, of this overlap is shown in Fig. 4 based on estimates of the distibutions. The uniform nature of the electron beam is expected due to the design of the electron gun. The broad and flat characteristics of the atomic and molecular hydrogen distribution is due to the beaming effect from the nozzle which is discussed in Chapter III.

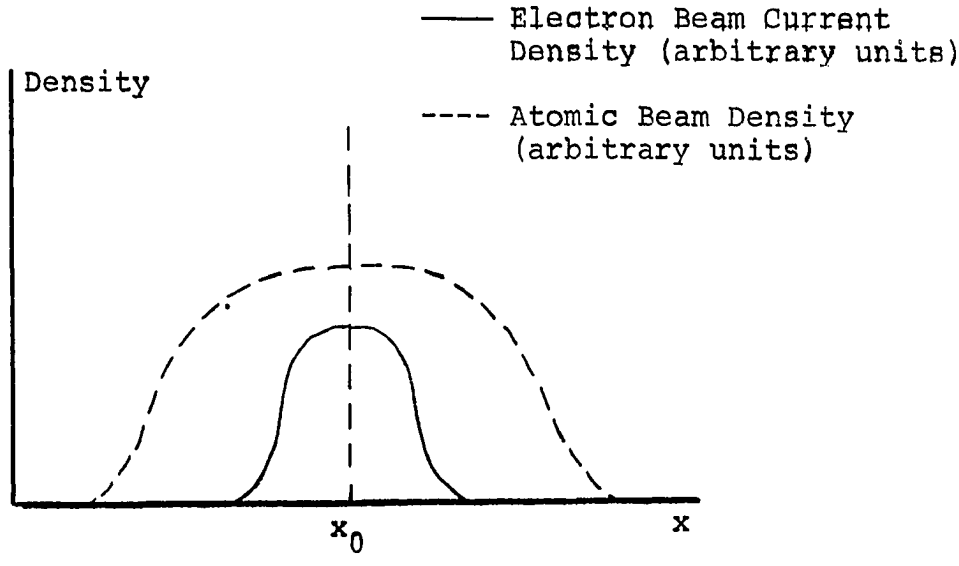

Figure 4. Spatial Distributions of the Electron and Atomic Beams.

Multiplying Eq. (26) by the electron beam current density at point τ and integrating over the cross-sectional area of the electron beam, we obtain

$$N^*_{HT} = \sqrt{2}\,(N^*_{H_2T} - N^{*'}_{H_2T}) . \tag{27}$$

From Fig. 4 it can be seen that small changes in the electron beam current distribution from the atomic to molecular case produce very small changes in the relation given in Eq. (27). The assumption of equal current distributions for equal accelerating voltages, therefore, introduces negligible error in the measurement of relative atomic and molecular hydrogen cross sections. The variation of current distribution with accelerating voltage was not great enough to cause a significant error in the measurement of excitation functions.

Eq. (3) shows that an expression for the weighted average density $N^*_{H_2T}$ can be written as

$$N^*_{H_2T} = \frac{P_{H_2ij}}{Q_{H_2ij}\, I/e} . \tag{28}$$

A similar expression can be written for $N^{*'}_{H_2T}$. By the measurement of P_{H_2ij}/I for a given molecular band we can

obtain $N^{*'}_{H_2T}/N^{*}_{H_2T}$. Using the relation in Eq. (27) we can then obtain $N^{*}_{HT}/N^{*}_{H_2T}$.

Let us denote the photon emission rate per unit length of the electron beam in the i to j transition P_{H_2ij}, P'_{H_2ij}, and P_{Hij} for hydrogen molecules with the Wood's tube off, hydrogen molecules with the Wood's tube on, and hydrogen atoms with the Wood's tube on. Let I_{on} and I_{off} denote the electron beam current with the Wood's tube on and off. Using Eq. (3) we obtain Eq. (29) which gives P_{Hij}/I_{on} in terms of directly measurable quantities, given as

$$\frac{P_{Hij}}{I_{on}} = \frac{(P_{Hij} + P'_{H_2ij})}{I_{on}} - \frac{N^{*'}_{H_2T}}{N^{*}_{H_2T}} \frac{P_{H_2ij}}{I_{off}} . \tag{29}$$

The optical excitation cross sections of atomic hydrogen can now be given in terms of the molecular hydrogen optical excitation cross sections by the relation given in Eq. (7) as shown in Eq. (30). All of the quantities in Eq. (30) are directly measurable or derivable from directly measurable quantities.

$$Q_{Hij} = Q_{H_2ij} \left(\frac{P_{Hij}}{I_{on}}\right) \left(\frac{I_{off}}{P_{H_2ij}}\right) \left(\frac{N^{*}_{H_2T}}{N^{*}_{HT}}\right) . \tag{30}$$

For the measurement of the radiation from the crossed electron-atomic hydrogen beams a 1/2-meter Jarrell-Ash Ebert mounted monochromator was used. The radiation was focused on the entrance slit of the monochromator with a quartz lens in such a way that a magnification factor of approximately one was obtained. With the entrance slit oriented perpendicular to the axis of the electron beam, the maximum slit width of 1 mm used in the measurements resulted in the observation of an approximately 1 mm length of the electron beam. The entrance and exit slits were kept equal in these measurements yielding the triangular relative transmission function $T(\lambda - \lambda_o)$ shown in Fig. 5. In measuring P_{ij} scale factors were encountered due to the following: the density of hydrogen atoms and molecules in the electron beam, the solid angle of observation of the electron beam, the length of the electron beam observed, the transmission of the window in the vacuum chamber, the transmission of the focusing lens, the transmission of the monochromator, the quantum efficiency and the amplification of the photomultiplier tube, and the net amplification of the succeeding noise rejection and amplifying circuits. Scale factors were also encountered in measuring I due to the amplifying circuits used. Finally, the resulting quantities proportional to P_{ij} and I were sent to an analog divider where they were further amplified and

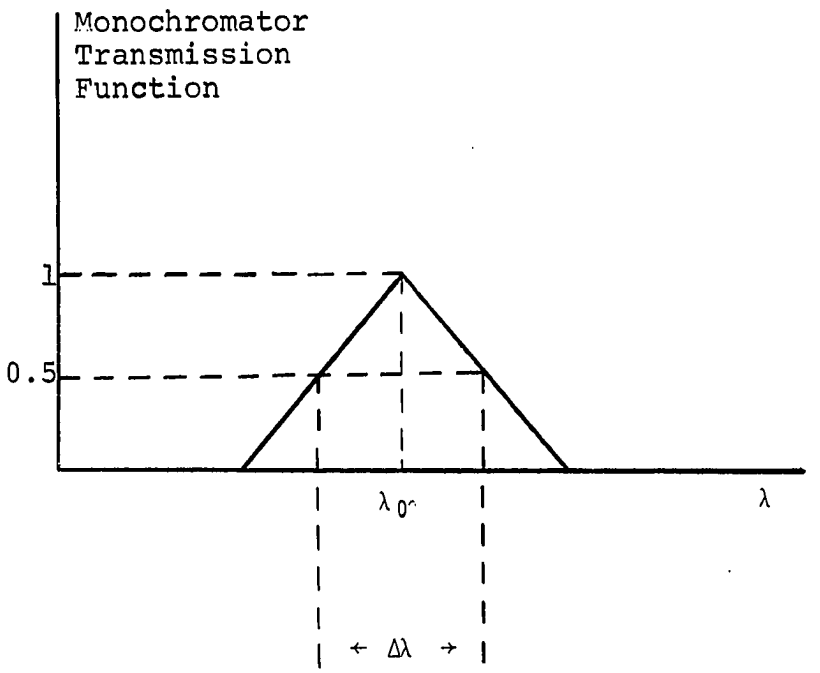

Figure 5. Transmission Function of the Monochromator.

then divided. We thus obtained a quantity proportional to P_{ij}/I. A detailed discussion of the equipment used in this process is given in Chapter III.

Since the measurement of the scale factor of P_{ij}/I by a calibrated tungsten ribbon lamp and a standard current

meter results in approximately 15% error, considerable error would result in Q_{Hij}, as given in Eq. (30), from the measurements of $(P_{Hij} + P'_{H_2ij})/I_{on}$ and P_{H_2ij}/I_{off} in this manner. It was therefore desirable to make the scale factors for these quantities equal so they would cancel in Eq. (30). Since the transmission factor of the monochromator and the response of the photomultiplier tube was highly wavelength dependent, it was desirable to measure atomic and molecular excitation cross sections at identical wavelengths. Such a case would allow one setting of the monochromator for both cross sections. In this way even if the lines were not "peaked" at the maximum of the relative transmission function of the monochromator, their transmissions would be identical. Such identical wavelengths exist for hydrogen due to molecular dissociation-excitation. These cross sections, being among the largest H_2 excitation cross sections, provided ratios P_{H_2ij}/I_{off} which could be measured with the same scale factors as the ratios $(P_{Hij} + P'_{H_2ij})/I_{on}$. Over the ten minute interval required to obtain excitation functions with the Wood's tube on and off, these scale factors were constant within 3%. The deviation from linearity in the measurement of P_{ij}/I was less than 3%. In a similar manner the scale factors in the measurement of $N^*_{H_2T}$ and $N^{*'}_{H_2T}$, cancel in Eqs. (29) and (30).

As stated previously, it was the measurement of $N^*_{HT}/N^*_{H_2T}$ which allowed the absolute measurement of Q_{Hij}. Eq. (27) indicates that N^*_{HT} is proportional to the difference $\left(N^*_{H_2T} - N^{*'}_{H_2T}\right)$. If this difference were less than the combined errors in the measurements of $N^*_{H_2T}$ and $N^{*'}_{H_2T}$, a highly inaccurate value of N^*_{HT} would result. This was the case obtained in the previous work by Fite and Brackmann[4] and Long et al.[6] using a tungsten oven source of hydrogen atoms, resulting in the measurement of only relative excitation functions. However, in this work $N^{*'}_{H_2T}/N^*_{H_2T}$ was approximately 0.5 allowing the determination of N^*_{HT} in the manner indicated above with relatively small error.

The hydrogen molecule exhibits a many-line spectrum. Since the radiation transmitted through a monochromator is inversely proportional to the resolution obtained, for a weak radiation source such as an electron beam through molecular hydrogen gas at low pressure, individual lines could not be resolved while transmitting detectable signals. Therefore, an optical excitation cross section measured for H_2 represents an effective cross section $Q^*_{H_2ij}$ given by Eq. (31) where the i to j transition represents the energy difference equivalent to λ_o which is at the center of the monochromator transmission function.

$$Q^{*}_{H_2 ij} = \sum_{l,m} Q_{H_2 lm}\, T(\lambda - \lambda_o), \qquad (31)$$

where λ is the wavelength of the l to m transition and $T(\lambda - \lambda_o)$ is the relative transmission function of the monochromator.

Absolute H_2 Cross Section Measurement with the Static System

The measurement of the absolute molecular hydrogen excitation cross sections was carried out with the apparatus described by Sharpton[44]. Since the gas did not flow in this apparatus, molecular densities could be determined by means of a McLeod gauge. The electron beam current was measured directly with a Sensitive Precision microammeter. The procedure for calibrating the P_{ij} measurement is described below.

Let us first consider emission from a tungsten strip standard lamp. Lamps supplied by the General Electric Company, such as the 20A/T24/2 used in this work, are calibrated in terms of brightness temperature T_B. The relation between the brightness temperature and the true temperature T of the ribbon is given by[45]

$$N_\lambda(T_B) = \varepsilon_\lambda(T)\, \tau_\lambda\, N_\lambda(T), \qquad (32)$$

where $N_\lambda(T)$ is the Plank Spectral Radiance Function,

$\varepsilon_\lambda(T)$ is the emissivity of a tungsten ribbon at wavelength λ and temperature T, and

τ_λ is the transmission of the standard lamp window at wavelength λ.

Plank's radiation function can be converted from power to photon rate by dividing by $\frac{hc}{\lambda}$. The quantity used in this work $P_{\Delta\lambda}(\lambda,T)$ was the photon rate from the standard lamp transmitted through the relative transmission function $T(\lambda - \lambda_o)$ of the monochromator given as

$$T(\lambda - \lambda_o) = 1 + \frac{\lambda - \lambda_o}{\Delta\lambda} \quad \text{for } \lambda_o - \Delta\lambda \leq \lambda \leq \lambda_o \tag{33a}$$

$$T(\lambda - \lambda_o) = 1 - \frac{\lambda - \lambda_o}{\Delta\lambda} \quad \text{for } \lambda_o \leq \lambda \leq \lambda_o + \Delta\lambda, \tag{33b}$$

where λ_o is the center of the relative transmission function and $\Delta\lambda$, called the bandpass, is the width of the triangular transmission function at half height. $P_{\Delta\lambda}(\lambda_o,T)$ is given by

$$P_{\Delta\lambda}(\lambda_o,T) = \int_{\lambda_o - \Delta\lambda}^{\lambda_o + \Delta\lambda} T(\lambda - \lambda_o)\, \varepsilon_\lambda(T) \frac{\lambda}{hc} N_\lambda(T)\, d\lambda. \tag{34}$$

$P_{16\ \mathring{A}}(\lambda,T)$ has been evaluated by Jobe[46] on an IBM 1410 computer for temperatures ranging from 1400°K to 3000°K and for wavelengths ranging from 2220 Å to 30,000 Å. The emissivities measured by DeVos[47] were used in this calculation. Since $\varepsilon_\lambda(T)$ is a slowly varying function of λ, $\varepsilon_{\lambda_o}(T)$ was used in the integration. Further, the constant and linear terms of the Taylor expansion of $\lambda N_\lambda(T)$ about λ_o were used. These approximations introduced negligible error for all bandpasses used in this work. $P_{\Delta\lambda}(\lambda,T) = \frac{\Delta\lambda}{16\ \mathring{A}} P_{16\ \mathring{A}}(\lambda,T)$. It should be noted that although a triangular transmission function was used, the same results hold for an arbitrary, but symmetric, transmission function with its center at λ_o. Setting the transmission function at λ_o equal to unity, the bandpass $\Delta\lambda$ is then equal to the area under the transmission curve.

The technique for calibrating the measurement of P_{ij} is to compare the reading for P_{ij} with the reading from the standard lamp P_{SL} using the same optics, detection, and amplification systems. Fig. 6 shows the optics arrangement used in this measurement. In order to make the optical systems in the measurements of P_{ij} and P_{SL} as nearly equal as possible, the focusing lens L was mounted on the same aluminum plate as the 1/2-meter Jarrell-Ash monochromator. This assembly was directed at the electron beam and the standard lamp retaining equal lens to source distances. The formula for the absolute optical excitation cross section defined in Eq. (3) is given in Eq. (35) in terms of

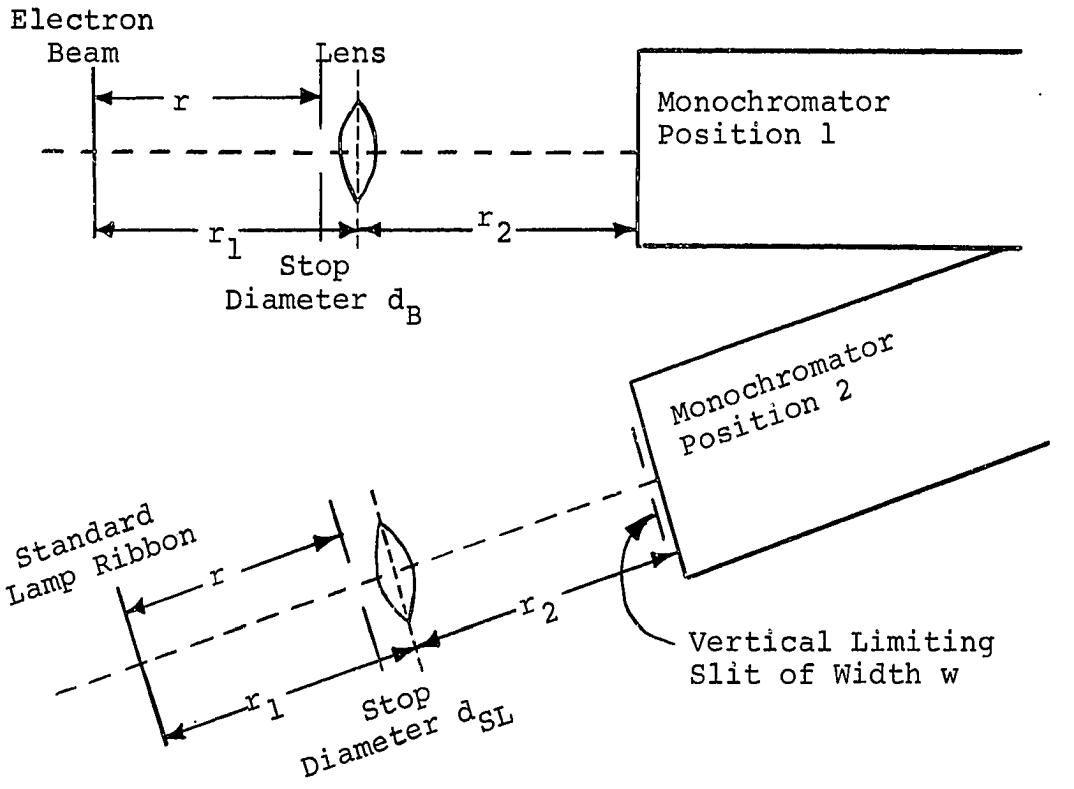

Figure 6. Configuration for Standardization with the Static System.

standard lamp and electron beam measurements. Fig. 6 shows

$$Q_{ij} = \frac{P_{ij}\ \Delta\lambda\ P_{16\,\mathring{A}}}{P_{SL}\ N^{*} I}\left[\frac{d_{SL}^{2}\ 4\pi\ w r_1 e}{d_B^{2}\ r_2\ 16\ \mathring{A}}\right] \quad (35)$$

the meaning of the new quantities in Eq. (35). The bandpass $\Delta\lambda$ can be obtained by the use of Eq. (36) below or it can be measured from a recorded scan of the monochromator past a monochromatic line.

$$\Delta\lambda = \frac{W}{f \frac{d\theta}{d\lambda}} \qquad (36)$$

where W is the width of the monochromatic slits,

f is the focal length of the monochromator, and

$\frac{d\theta}{d\lambda}$ is the angular dispersion of the monochromator.

The same monochromator slit widths were used for the measurement of the radiation from the electron beam and the standard lamp.

Implicit in Eq. (35) is that the response of the optical and detection systems are directly proportional to the aperture diameter squared d^2 and to the width of the vertical limiting slit w for a uniform source. The limits on these relations are when d becomes large enough that the light overfills the monochromator surfaces and when w becomes wider than the detector. These limits can be determined experimentally and empirical correction factors can be introduced when work at these limits is desired. Reducing w to approximately 0.1 mm can introduce the factor of local detector sensivitity. Reducing d to approximately 1 mm can introduce the factor of local transmission variations of the monochromator. Both of these factors can be eliminated by applying averaging techniques.

CHAPTER III

CROSSED ELECTRON-ATOMIC HYDROGEN BEAM SYSTEM

Wood's Discharge Tube

Radio frequency discharge, glow discharge, and thermal techniques are widely accepted for their success in dissociating hydrogen molecules. Langmuir[48] discovered that high degrees of dissociation could be obtained from a tungsten surface at 2500°K. Fite and Brackmann[3] measured the degree of dissociation in a tungsten oven to be 92% at 2530°K. Fite and Brackmann[3] and later Long *et al.*[6] made crossed atomic hydrogen and electron beam measurements of atomic hydrogen excitation cross sections using a tungsten oven source. However, this technique yielded atomic hydrogen densities of only 1×10^{7} to 1×10^{8} cm^{-3} in the electron beam which limited their measurements to optical excitation cross sections of the n = 2 state. Since the technique of thermal dissociation has been essentially exhausted by these workers and other workers mentioned in Chapter I and since

the technique requires considerable design, construction, and expense, it was rejected for this work.

A radio frequency or rf discharge is capable of essentially 100% dissociation of hydrogen molecules. It has been applied by Ramsey[50] in the construction of an atomic hydrogen maser. Schultz[51] used an rf source in the measurement of the atomic hydrogen electronic elastic cross section. Although this technique should supply a greater quantity of hydrogen atoms than the tungsten oven, the anticipated interference of the rf source with other circuits in the experiment and the expense of the rf source led to the rejection of this idea.

By far the simplest and the most easily constructed device for obtaining hydrogen atoms is a glow discharge of the type discovered by R. W. Wood[11]. Wood and later other workers[52,53] reported that essentially 100% dissociation was obtained with such glow discharges or Wood's tubes. However, for reasons which were not apparent at the outset of this work, the Wood's tube technique has been used very little recently compared with the thermal and rf techniques by workers in the field of atomic and molecular physics. In spite of this the Wood's tube technique was adopted in this work. Fite[54] communicated to the author after the completion of this work that he experimented with a Wood's

tube but rejected it in favor of a tungsten oven after he found that his Wood's tube: 1) was unstable in its degree of dissociation; 2) produced excessive electrical noises which interfered with other circuits; and 3) produced great amounts of radiation which interfered with radiation measurements in the electron beam. In the following discussion it will be shown that these problems were adequately solved.

When Wood[11] constructed a glow discharge in order to observe the atomic hydrogen Balmer lines he had the good fortune to use an electrolytic source of molecular hydrogen. By observing the atomic and molecular spectra from the discharge he deduced that the hydrogen, which was moistened with approximately 2% water vapor by volume, became essentially 100% dissociated. By running the discharge with and without water vapor Wood concluded that its effect was to hinder the recombination of hydrogen atoms on the glass discharge tube walls. By switching the discharge off and on he found that the population of hydrogen atoms remained in the tube treated with water for 1/5 sec. The dimensions of Wood's discharge tube were 6.5 mm inner diameter by 2 meters length. The electrodes were hollow aluminum cylinders approximately 2.5 cm in diameter by 8 cm in length. The pressure at which Wood obtained the purest atomic spectrum was 0.5 mm Hg. Up to 200 ma current was produced in the discharge by a 25 KV transformer.

Since Wood reported the successful operation of the Wood's tube others have expended considerable work to explain its operation. Poole[55] measured the rate of dissociation of molecular hydrogen by electron impact in a glow discharge. He continuously flowed hydrogen molecules into a glow discharge and out onto a platinum calorimeter where the number of hydrogen atoms produced was measured by their heat of recombination. The rate of dissociation of hydrogen molecules in a glow discharge is

$$\frac{dN_{H_2}}{dt} = - N_{H_2} n_e \int_0^\infty v_e \, Q_{H_2}(v_e) \, f(v_e) \, dv_e, \qquad (37)$$

where N_{H_2} is the density of hydrogen molecules,

$Q_{H_2}(v_e)$ is the dissociation cross section for molecular hydrogen for an incident electron velocity of v_e,

$f(v_e)$ is the distribution function of electron velocities v_e,

n_e is the density of free electrons, and

N_H is the density of hydrogen atoms.

The Schottky theory, which is presented by Francis[56], for the uniform positive column of a glow discharge applies where the electron and ion mean free paths are much less than

the tube radius R. The basis of the Schottky theory is that a steady state is reached in the positive column where ions are created as rapidly as they are lost at the walls. In a straightforward manner we obtain the result that the electron temperature T_e, longitudinal electric field divided by gas pressure E/P, and the longitudinal drift velocity of the electrons v_d are functions of p·R. Measured values of the drift velocity are reported by Brown[57]. We can obtain the electron density in the positive column from the discharge current I_D, the cross-sectional area A of the discharge, and the drift velocity as

$$n_e = \frac{I_D}{v_d A} . \tag{38}$$

Numerical solutions for the integral in Eq. (37) for several electron temperatures are given in Table 1. The solutions were obtained with an IBM 360 computer using a program written by R. Day and I. Latimer. The cross section for the dissociation of H_2 by electron impact used in the calculation was measured by Corrigan[58] by the pressure increment technique. A Maxwellian velocity distribution was assumed for the electrons.

In order to obtain the rate of dissociation of H_2 in the positive column of a glow discharge we measure the discharge radius, current, and pressure. From these measurements the electron temperature and density are obtained by

TABLE 1

DISSOCIATION RATE OF MOLECULAR HYDROGEN

Electron Energy (in units of eV) $E = \frac{3}{2}kT$	Dissociation Rate (in units of cm^3/sec) $\int_{-\infty}^{\infty} Q_{H_2}(v_e)\, f(v_e)\, v_e dv_e$
1.5	2.45×10^{-12}
3.0	2.93×10^{-10}
4.5	1.40×10^{-9}
6.0	2.99×10^{-9}
7.5	4.63×10^{-9}
9.0	6.10×10^{-9}
10.5	7.32×10^{-9}
12.0	8.30×10^{-9}
13.5	9.07×10^{-9}
15.0	9.65×10^{-9}
16.5	1.01×10^{-8}
18.0	1.04×10^{-8}
19.5	1.06×10^{-8}
21.0	1.07×10^{-8}

use of the Schottky theory. The value of the electron density is then combined with the numerical value of the integral in Eq. (37) for the proper electron temperature.

As a check on the accuracy of the calculation of the rate of dissociation, a comparison with Poole's Fig. 3c[55] was made. Poole measured the fraction of hydrogen molecules dissociated to be 0.37; by use of Eq. (37) 0.29 was obtained. This correlation lends support to the application of the Schottky theory and the Maxwellian electron velocity distribution to the nonuniform, or striated, positive columns of the discharges obtained at the high currents necessary to dissociate hydrogen molecules.

Wood measured the time between turning on his tube and the disappearance of the molecular spectrum to be 0.01 and 0.04 sec for 20 and 2 amperes of primary transformer current. Assuming 50 ma for Wood's discharge current (which was not specified in his paper but represents a nominal current used in his work) we calculate by the above method that e^{-1} of the molecules are dissociated in 4×10^{-3} sec. The discrepancy between this time and Wood's observed time is probably due to the delay in the establishment of the glow discharge.

In 4×10^{-3} sec a hydrogen atom makes approximately 5×10^{2} collisions with the walls in Wood's tube. Therefore, a recombination coefficient much less than $(5 \times 10^{2})^{-1}$ is

required to explain the nearly 100% dissociation observed by him. The recombination coefficients compiled by Wood and Wise[43] for moist Pyrex which averaged 3×10^{-4} satisfy this requirement. The mechanism for surface recombination is the adsorption of atoms and subsequent recombination due to collisions with impinging gas atoms. If a small fraction of the area of a surface is comprised of adsorbed atoms, its recombination coefficient is low.

The review article by Wood and Wise[43] indicates that there are few known surfaces with recombination coefficients of 1×10^{-4} or less. Since a surface is largely determined by the top monolayer, obtaining an arbitrary surface in a vacuum system is quite difficult. For example, an impurity in the vacuum system with a pressure of 1×10^{-6} mm Hg and a sticking coefficient of 0.1 would form a monolayer in less than two minutes. It is therefore apparent that the surface in Wood's tube was not formed in a straightforward manner.

In order to answer questions such as the surface condition in a Wood's tube, a tube was constructed closely following Wood's design. The electrodes of the discharge were constructed of unalloyed aluminum hollow cylinders 2.5 cm in diameter by 7.6 cm in length. These were enclosed in 7740 Pyrex bulbs 3.5 cm in diameter by 12 cm in length. The discharge tube of 6.5 mm inner diameter by 2 meter length was also constructed of 7740 Pyrex. The discharge tube was cleaned

with hot chromic acid and rinsed first with distilled water and then ethyl alcohol.

The water used to moisten the hydrogen was triple distilled. The first distillation was done in a Barnstead distillation apparatus. The next two stages were carried out in the three bulb apparatus shown in Fig. 7. After cleaning the apparatus in a manner similar to that of the Wood's tube, the distilled water was introduced into bulb 1 and the excess gas in the bulb was pumped out. After closing stopcock 1 the remainder of the apparatus was evacuated and outgassed using a high vacuum system. After closing stopcock 3, distillation from bulb 1 to bulb 2 was carried out with bulb 1 at room temperature and bulb 2 at ice temperature. In a similar manner distillation was carried out from bulb 2 to bulb 3 and stopcock 2 was then closed. Stopcock 2 and bulb 3 with the distilled water were removed from the distillation apparatus and joined to the hydrogen supply system as shown in Fig. 8. A cylinder of Matheason prepurified grade hydrogen with a Matheason model 19 all metal regulator was used to supply hydrogen at atmospheric pressure. Approximately two percent by volume of water vapor was added to the hydrogen from the water bulb. The pressure of the hydrogen was then reduced by a Matheason model A 12TP-B stainless steel needle valve with a Kel-F plastic tip. The diffusion pump used to evacuate the Wood's tube was a CVC

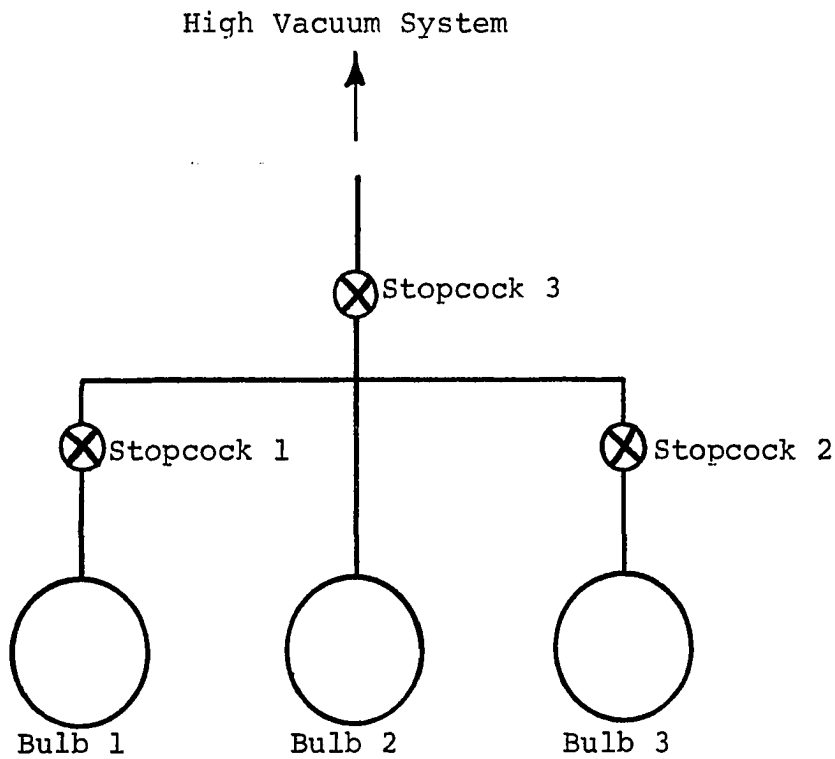

Figure 7. H_2O Distillation Apparatus.

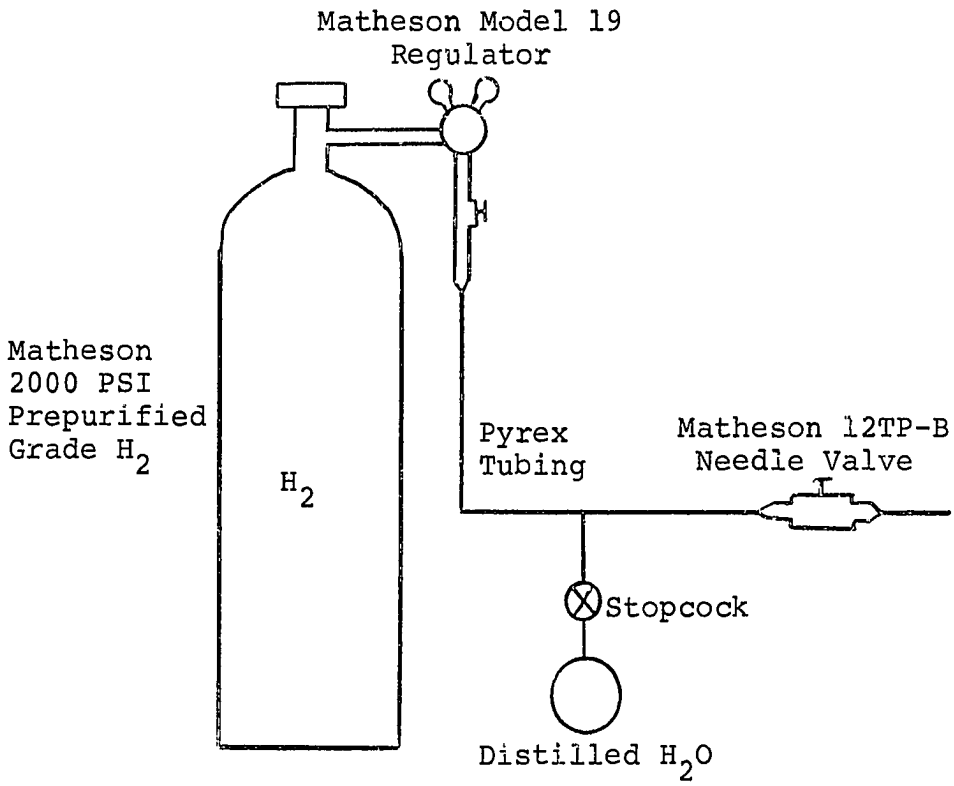

Figure 8. Hydrogen Supply System for the Wood's Tube.

115 PMC with DC 704 fluid. A water baffle was used to reduce oil backstreaming.

The Wood's tube operated with complete success. With 100 μ pressure and 80 ma ac current the tube lighted the entire room with the deep red of the H_α line. Wood describes this as "fiery purple". Moist hydrogen was slowly flowed through the Wood's tube in order to insure its purity. Using

a 1/2-meter Jarrell-Ash monochromator and an EMI 9558 PMT, the molecular spectrum could not be detected in the Wood's tube. Using the noise level of the detection system for the molecular intensity, a Balmer to molecular intensity ratio of 1×10^5 was obtained. Very near the electrodes in the "molecular" discharge this ratio was 45. We therefore obtained an increase in the ratio of at least 2,000. This can be compared to the increase of 40 obtained by Wood. Wood attributed an increase of 40 to essentially 100% dissociation. From the intensity of the atomic hydrogen spectrum it was deduced that the degree of dissociation in the discharge was constant to within 2% over a 20 minute period. With a hand spectroscope it was observed that the molecular hydrogen spectrum was not found further than 2 cm from the electrode bulb.

In order to produce a throughput of 1000 μ.liters/sec of atomic hydrogen a large diameter Wood's tube must be used to avoid excessive pressure differences. The relation of throughput Q in μ·liters/sec to conductance C in liters/sec and pressure difference ΔP in microns is given by Dushman[59] as

$$Q = C\Delta P. \qquad (39)$$

For a tube 2 cm in diameter by 150 cm in length, the tube conductance was calculated by the formula given by Dushman[60]

to be 3.5 liters/sec. The conductance was calculated for molecular flow which holds where gas-wall collisions are more frequent than gas-gas collisions. For a conductance of 3.5 liters/sec and a throughput of 1000 μ.liters/sec of atomic hydrogen, we obtain by Eq. (29) a pressure difference in the tube of 286 μ. For an outlet pressure of 163 μ, which was the approximate pressure obtained in this work, an inlet pressure of 449 μ is obtained for the above conductance and throughput. It should be noted that viscous flow is significant at these pressures and therefore adds to the molecular flow conductance and reduces the above pressure differences. A throughput of 1000 μ·liters/sec of atomic hydrogen is equivalent to a throughput of 500 μ·liters/sec of molecular hydrogen for equal mass flow. At a 500 μ·liters/sec throughput of molecular hydrogen the inlet and outlet pressures of the discharge tube are 316 μ and 115 μ. The average transit time for a hydrogen molecule through the 150 cm discharge tube was calculated to be 0.2 sec. For 100 ma current and 217 μ pressure we calculate that e^{-1} of the hydrogen molecules are dissociated in the tube in 0.01 sec. Although these factors indicate that essentially 100% concentrations of hydrogen atoms could be produced by this tube at a throughput of 1000 μ·liters/sec of atomic hydrogen, Melville and Gowenlock[61] have reported that in a 2 cm diameter by 2 meter long Wood's tube the concentration of hydrogen atoms is very low near the electrodes and increases monotonically to a high

concentration at one meter from the electrodes. The explanation of this effect is that the conductance of a tube under conditions of molecular flow varies as the tube radius cubed. In the 2 cm diameter discharge tube then the flow of hydrogen atoms to the electrodes where they recombine on the metal surfaces greatly reduces the net atomic hydrogen production rate. A proof of this conclusion can be obtained by solving the differential equations for the transport of H and H_2 coupled by the dissociation rate per unit time $k_d N_{H_2}$, where k_d is the probability of dissociation per unit time. The solution of these equations for the density of hydrogen molecules at a distance x from an electrode is given as

$$N_{H_2} = N^{o}_{H_2} e^{-\sqrt{\frac{k_d A}{C'}}\, x}, \qquad (40)$$

where $N^{o}_{H_2}$ is the density of hydrogen molecules at the electrode,

A is the cross-sectional area of the discharge tube, and

C' is the conductance per unit length of the tube for H_2.

Using the value of k_d of 92/sec calculated previously for the 2 cm diameter tube we find that $N_{H_2}/N^{o}_{H_2}$ is 0.135 at 70 cm from the electrode which agrees well with the value reported by Melville and Gowenlock. Using the value of k_d

of 244/sec calculated for the 6.5 mm diameter tube reported by Wood[11] we find that $N_{H_2}/N^{o}_{H_2}$ is 0.135 at 26 cm from the electrode which agrees well with the 30 cm distance reported by Wood. The 2 cm distance from the electrode bulb required in the 6.5 mm diameter Wood's tube constructed in this work for the disappearance of the molecular spectrum is attributed to a much higher electron temperature than obtained by Wood.

In the design of the 2 cm diameter by 2 meter long Wood's tube used in this work the loss of hydrogen atoms at the electrodes was minimized by using a 10 cm length of 6.5 mm inner diameter tubing between the electrodes and the discharge tube as shown in Fig. 9. The electrodes and electrode bulbs from the previous Wood's tube were used with the 2 cm diameter tube. The tube was constructed of 7740 Pyrex and cleaned in the same manner as the previous Wood's tube. The same moist hydrogen supply was also used. The degree of dissociation obtained in the tube agreed closely with the calculated value at a throughput of 1000 μ·liters/sec. With a Balmer to molecular intensity ratio near the nozzle of 1×10^{4}, the degree of dissociation was essentially 100%. A 5 KVA power transformer was used to construct a 0-10KV dc power supply for this Wood's tube. The stability of the intensity of the Balmer lines in the Wood's tube indicated that the combined stability of the flow system and the degree of dissociation was better than 2% over a 20 minute period.

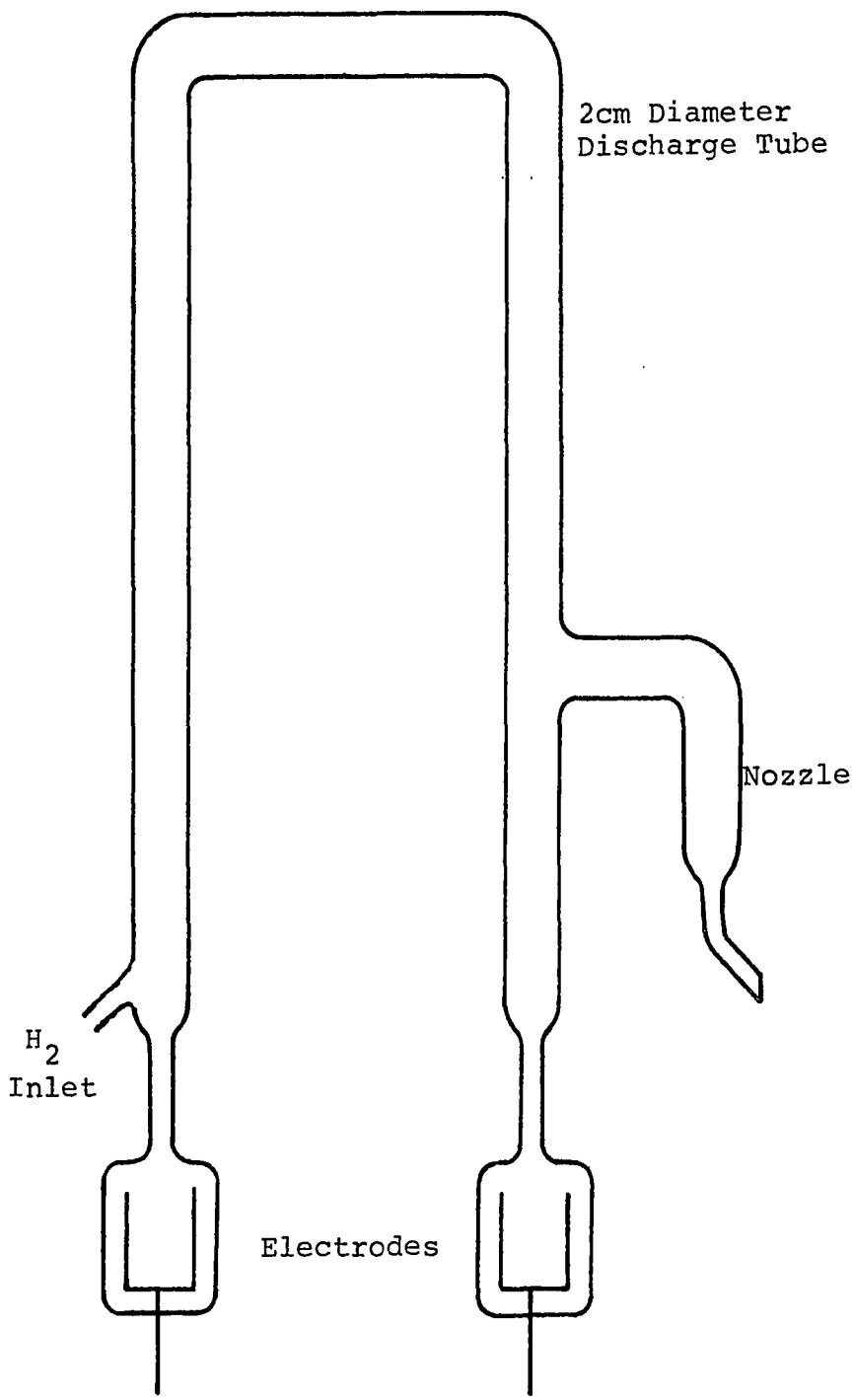

Figure 9. The 2cm Diameter Wood's Tube.

Design and Construction of the Crossed Beam Apparatus

A general problem encountered in crossed electron-atomic beam experiments is background atom density. It causes error and noise in measurements. In order to reduce the background density we can use a high throughput diffusion pump and a high conductance beam chamber. Further, we can design the beam system so that a large fraction of the atoms in the atomic beam pass through the volume of the crossed beams. A technique for accomplishing this is to employ collimating skimmers and differential pumping such as Fite and Brackmann[3] and Long et al.[6] have done. The technique employed here was to inject the atoms into the electron beam with the nozzle shown in Fig. 2. In order to maximize the fraction of atoms passing through the electron beam, the end of the nozzle was placed 0.5 cm from the electron beam. Further, the emission in the forward direction from the nozzle was maximized by the use of Clausing's "beaming effect"[62]. In order to obtain this effect the length of the final straight section of the nozzle was four times its radius. The large segment of the nozzle was 2 cm in diameter by 34 cm in length, while the small segment was 1 cm in diameter by 3.5 cm in length. The conductance of the nozzle was calculated to be 6.7 liters/sec for atomic hydrogen under molecular flow conditions. With a head pres-

sure of 163 μ and a throughput of 1000 μ·liters/sec of hydrogen atoms, the mean drift velocity in the 2 cm diameter portion of the nozzle was calculated to be 2.6×10^3 cm/sec. The average transit time for an atom through this portion of the nozzle was therefore 1.3×10^{-2} sec. With an average velocity of 2.5×10^5 cm/sec for atomic hydrogen at room temperature, at least 300 collisions with the wall occurred during this time.

Corning 6" inner diameter Pyrex conical pipeline was used to facilitate the construction of the atomic beam system. A tee, a 90° ell, and an end cap were assembled in the manner shown in Fig. 1. Teflon gaskets and flanges supplied by Corning were used to connect these parts making high vacuum seals. The electron gun was mounted on a 3" cap in such a way that, with the cap mounted on the tee, the collision area of the electron gun was in the center of the tee. Two holes were ground in the tee with a carborundum compound. Through one the nozzle was inserted, and in the other a Pirani gauge was placed. Both were sealed with Apiezon black wax. No window for the chamber was required since the radiation from the crossed beams could be measured through the Pyrex chamber wall.

Rather than using an optically dense baffle which would decrease the conductance to the diffusion pump, the 90° ell was connected directly to the diffusion pump and used to condense the backstreaming diffusion pump oil. To

facilitate condensation the ell was cooled to 5°C below room temperature by a room airconditioner. According to Power and Crawley[63] a "one bounce" trap of this sort reduces backstreaming by a factor of 3000. Since they also determined that most backstreaming occurs from the top jet of a diffusion pump and that a room temperature "cold cap" above this jet reduced backstreaming by a factor of 30, such a cap was constructed and installed in the CVC 720 PMC 4" diffusion pump used here. With this configuration the Dow Corning 704 silicone diffusion pump oil which was used condensed in the 90° ell and the beam chamber showed no trace of oil. The conductance for H_2 from the electron gun to the pump inlet obtained with this configuration was 2,000 liters/sec. For a throughput of 500 μ·liters/sec, therefore, a pressure difference between these points of only 0.25 μ was obtained.

Since silicone oil can "glaze" the plates of an electron gun with an electrically insulating layer, care must be taken to prevent this. Heddle[64] has stated that a 24 hour baking at 300°K removes such glazing. Since the electron gun operated at elevated temperatures due to its thermionic cathode, it is possible that the glaze would be removed during its operation. After many hours of operation no glazing on the electron gun was detected with an ohmmeter.

A Kinney KC-5 compound mechanical pump with a speed of 4.2 CFM was used to back the diffusion pump. The specifications supplied by CVC for their 720 PMC diffusion pump indicate that a throughput of 500 μ·liters/sec is obtained for an inlet pressure of approximately 1 μ. Since a) at the limiting forepressure of the diffusion pump of 0.35 mm Hg 500 μ·liters/sec was the maximum throughput of the KC-5 forepump and b) above 1 μ diffusion pump inlet pressure backstreaming becomes excessive, a throughput of 500 μ·liters/sec was used in this work. Using this throughput the background density in the region of the electron gun was approximately 1 μ or 3.5×10^{13} cm^{-3}. The atomic beam density was $3 - 6 \times 10^{13}$ cm^{-3}.

Noise in the electron and atomic beams results from fluctuations in the densities of the beams. Shot noise which is proportional to the square root of the beam density is always present in each beam. For narrow atomic beams fluctuations in the beam density occur due to atom-atom collisions. Since Bederson[65] points out that the cross section for small angle scattering is much greater than the momentum transfer cross section which is readily available, care must be taken in estimating this type of beam noise. Due to the approximately 3 cm width of the atomic beam in this work and due to the 0.5 cm distance from the nozzle to the electron beam, beam density fluctuations due to atomic scattering was con-

sidered insignificant. Since the thermionic and Wood's tube sources of the electron and atomic beams were stable, shot noise should therefore comprise most of the beam noise in this work. Consequently, the signal to noise ratio in the combined electron and atomic beams was directly proportional to the square root of the product of the electron and atomic beam densities. Since the atomic beam density in this work was approximately 10^5 greater than that of Long et al.[6] and the electron beam current was approximately 10^2 greater, a significant improvement in signal to noise ratio was made. Bächler[66] has demonstrated that eruptive boiling in diffusion pumps can make them quite noisy. This type of noise is due to background density fluctuations which follow pumping speed fluctuations. If these fluctuations are coherent in the sense that they maintain a constant phase relation with the chopping frequency used in the cross section measurement, they can displace the average level of the signal. Bächler reported that an oil stirrer reduced pumping speed fluctuations. The effects of pumping speed fluctuations can be reduced by increasing the time constant of the beam chamber, defined as the ratio of the chamber volume to the pumping speed, and by increasing the ratio of beam to background density.

A pentode type electron gun was used in this work which produced a 1 cm diameter monoenergetic electron beam

as shown in Fig. 2. The plates of the electron gun were constructed of 303 stainless steel. The cathode was a 1 cm diameter hollow nickel cylinder coated with RCA 33-C-337 barium, calcium, and strontium oxide material. The cathode was indirectly heated by a Semicon alumina coated tungsten heater. The pentode electrode structure gave beam currents which were relatively independent of anode to cathode voltage in the 100-500 volt range used here. A typical beam current with an accelerating voltage of 100 V was 1 ma. By the retarding potential technique Jobe[67] showed this gun to have an energy spread of approximately 0.5 eV at 23 eV beam energy. The operating temperature of the cathode was measured with a Leeds and Northrup optical pyrometer to be 930°C. The crossed beam region could not be enclosed in a solid metal Faraday electric field shield in this work due to the recombination properties of metal for hydrogen atoms. Therefore, this region was enclosed by an 80% transmission nickel screen. Although the electron gun had been operated in a satisfactory manner previously in a static all metal system over the energy range of 20-500 eV, it would not operate below approximately 50 eV in the atomic beam system. The cause of this could not be determined although charging of the glass chamber walls, the glass nozzle, and electrodes which might have become glazed were the most probable explanations.

Operation of Crossed Beam Apparatus

The configuration of the equipment used to make measurements with the atomic beam system is shown in Fig. 10. The types of measurements made with this equipment were discussed in Chapter II. Note that the reference signal from the PAR Model 122 Lock-In Amplifier is amplified to chop the electron beam. By using this technique instead of a light beam chopping wheel, the Balmer radiation from the Wood's tube was not included in the amplified signal from the crossed beams. With this system an excitation function could be recorded by a Tektronix C-12 oscilloscope camera on Polaroid film in five minutes. The measurement of relative atomic and molecular cross sections as described in Chapter II was accomplished by recording excitation functions with the Wood's tube on and off. The equality, within experimental error, of the scale factors of the excitation functions with the Wood's tube on and off was obtained by holding all instrument settings constant during the recording of the two functions. After each set of excitation functions were recorded, $N^*_{H_2T}$ and $N^{*'}_{H_2T}$ were measured by observation of the H_2 lines at 5550 Å. These measurements, made at 200 eV electron beam energy, were recorded on a Bausch and Lomb V.O.M. time base chart recorder. $N^{*'}_{H_2}$ was measured with the Wood's tube on while $N^*_{H_2}$ was measured with the Wood's tube off. Again all instrument settings were held

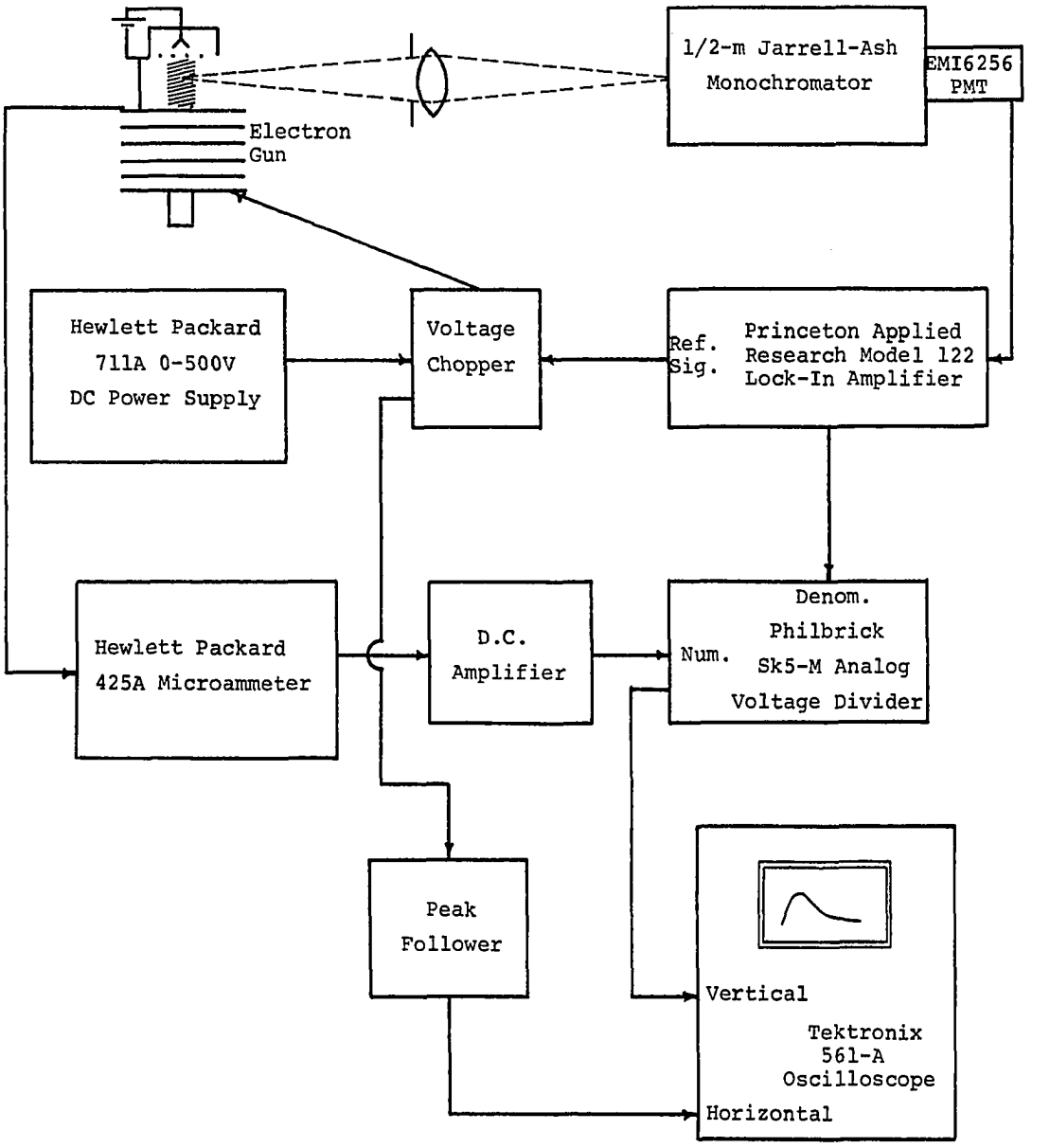

Figure 10. Configuration of Equipment for Measurements with the Crossed Beam System.

constant during the measurements of $N^*_{H_2}$ and $N^{*'}_{H_2}$ in order to obtain equal scale factors.

CHAPTER IV

PRESENTATION AND DISCUSSION OF THE MEASUREMENTS

Balmer Optical Excitation Functions

In the measurement of an optical excitation cross section of a state, any radiative decay channel from the state can be observed. The choice of channels is usually determined by the facility with which radiation in the various regions of the spectrum can be resolved and detected. For visible radiation, resolving instruments are available which operate near the diffraction limit. Photomultiplier tubes for this region yield signal to noise ratios which are near the thermodynamic shot noise limit. Although resolving instruments in the infrared operate near the diffraction limit, the linear relation between the diffraction limit and wavelength leads to a resolution problem. Photomultiplier tubes which operate to 1.2 μ have considerable dark noise. Lead sulfide photoconductive detectors which operate to 4.5 μ are detector noise limited. The resolution and detection of ultraviolet radiation is hampered by low reflectivities,

transmission factors, and photoelectric quantum efficiencies. Therefore visible radiation channels are chosen whenever possible.

The Balmer series in atomic hydrogen, which arises from transitions terminating in the n = 2 state, provides visible radiation channels for the study of the excitation of states greater than n = 2. The energy level diagram of atomic hydrogen is shown in Fig. 11. By observation of the Balmer lines from the crossed electron-atomic beams, optical excitation functions for the n = 3 through the n = 13 states were measured with the Wood's tube on and off in the manner described in Chapter III. These functions with the measured value of $N^{*'}_{H_2T}/N^{*}_{H_2T}$ for each pair of functions are shown in Fig. 12. The shapes of the atomic hydrogen Balmer optical excitation functions can be readily obtained from the data in Fig. 12 by use of the relation given in Eq. (29).

Absolute Balmer Optical Excitation Cross Sections

Due to the near degeneracy of the angular momentum states for a given n state in atomic hydrogen, it was not possible to spectroscopically resolve these states. Therefore a measured Balmer optical excitation cross section for a given n state is the sum of the optical excitation cross sections for the individual angular momentum states of the n state. The dipole radiation selection rule of $\Delta l = \pm 1$,

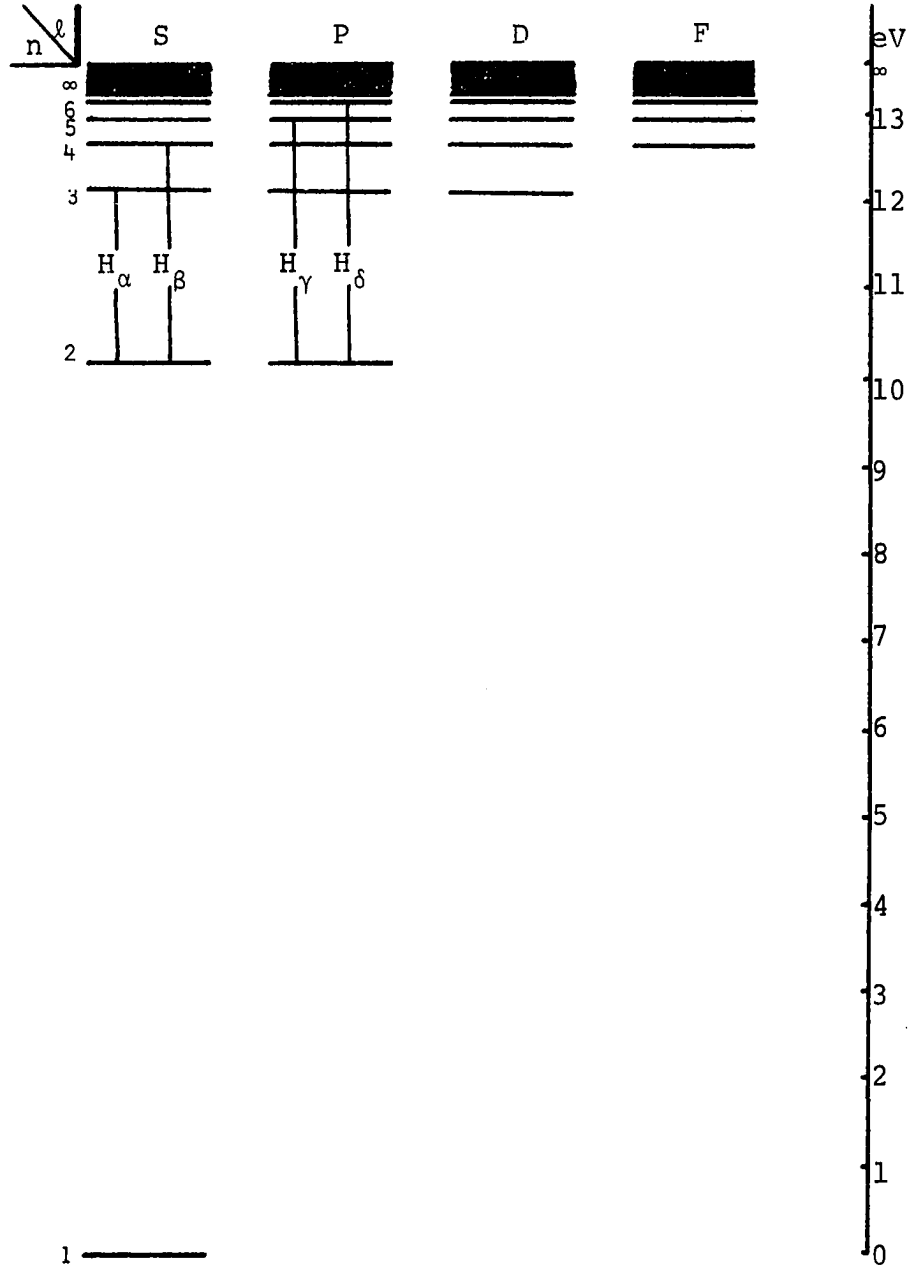

Figure 11. Atomic Hydrogen Energy Level Diagram.

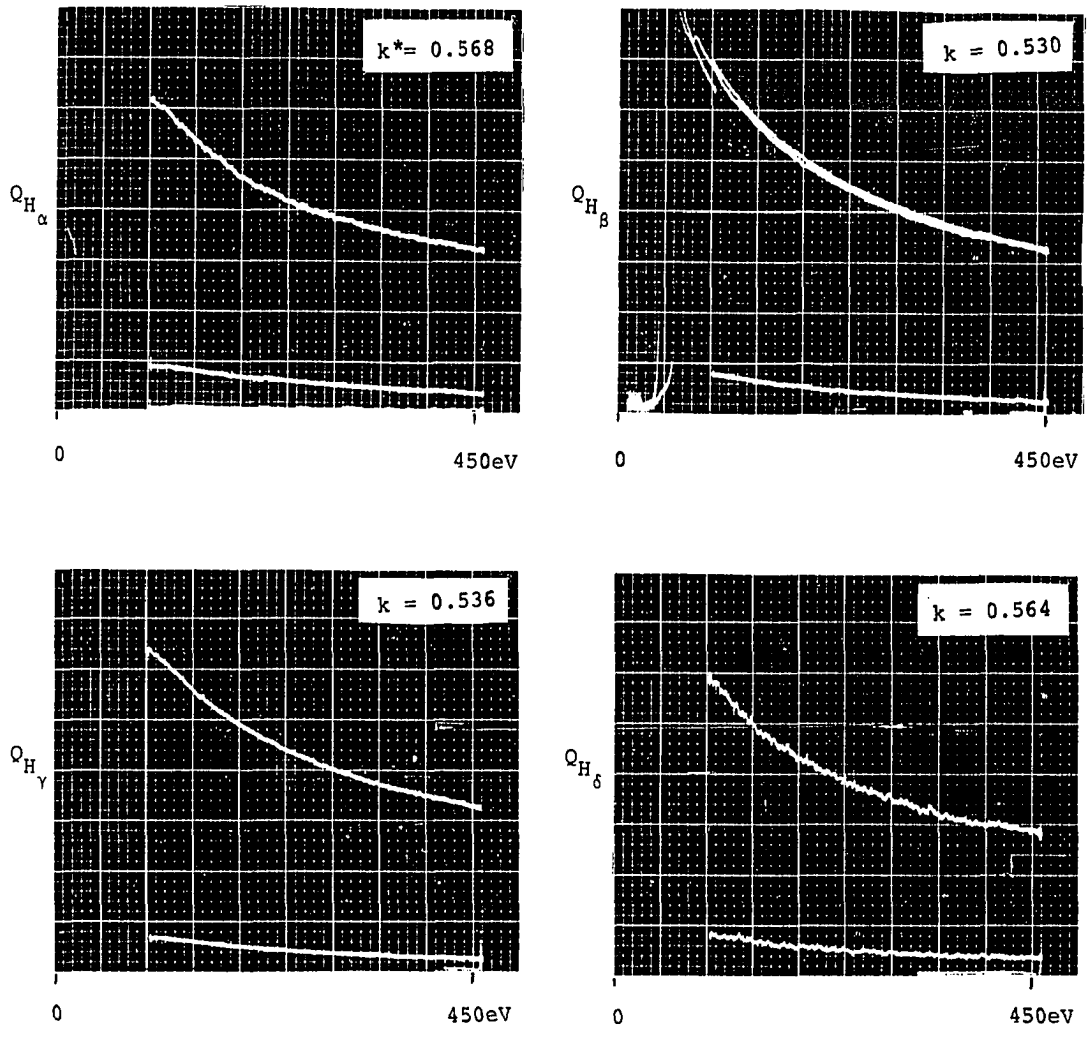

Figure 12. Balmer Optical Excitation Functions from the Crossed Beam System

* $k = N^{*'}_{H_2T} / N^{*}_{H_2T}$

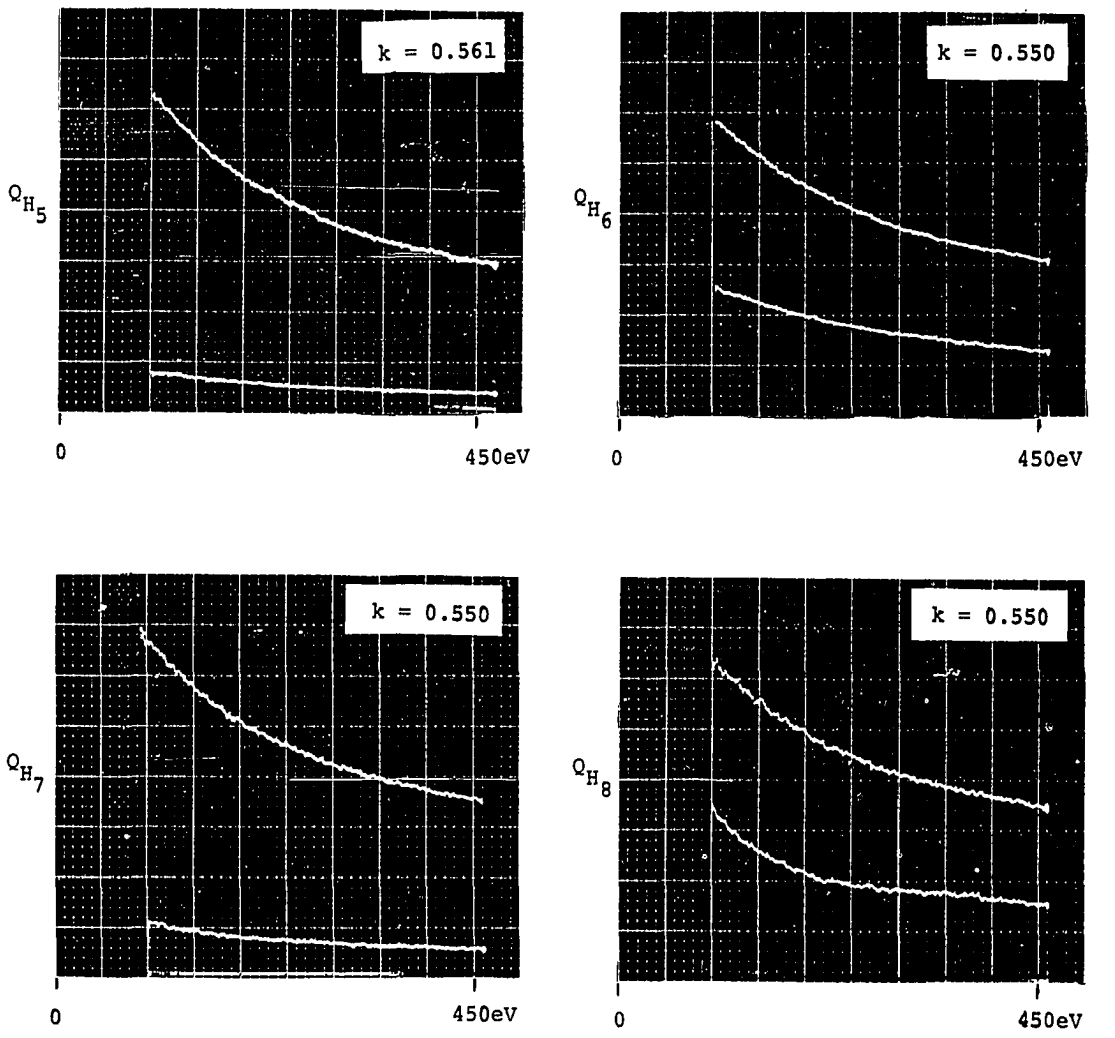

Figure 12. (Continued)

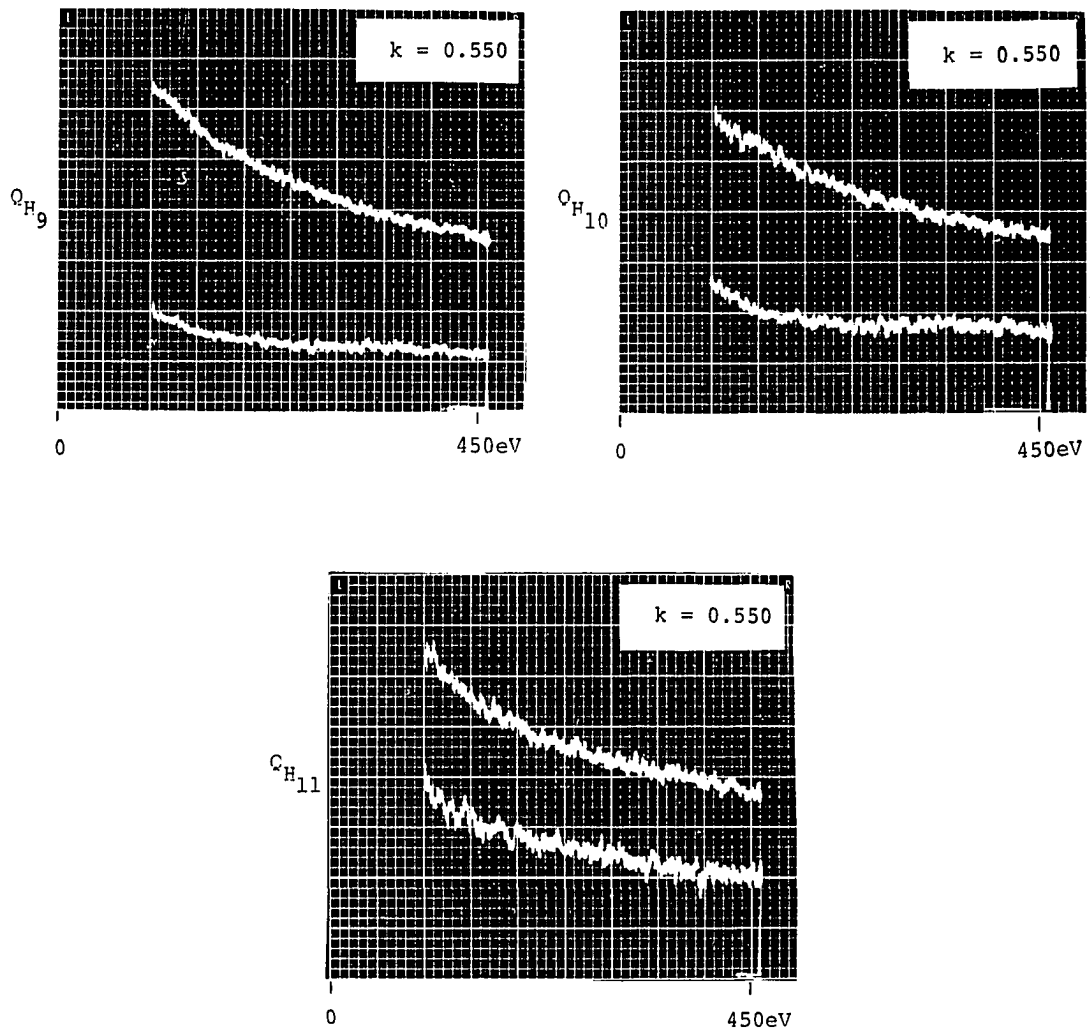

Figure 12. (Continued)

where l is the orbital angular momentum quantum number of the electron, determines that only upper S, P, and D states can radiate to the S and P states of the n = 2 state. The measured Balmer optical excitation cross sections, $Q_{Hn,2}$, are therefore given by

$$Q_{Hn,2} = Q'_{HnS}/B_{nS,2} + Q'_{HnP}/B_{nP,2} + Q'_{HnD}/B_{nD,2}. \quad (41)$$

The absolute optical excitation cross sections of molecular hydrogen were measured at the Balmer wavelengths with the static system as described in Chapter III. The results of these measurements for an electron energy of 200 eV are given in Table 2. The accuracy of these measurements of $Q_{H_2n,2}$ was 15%. Since the effective optical excitation cross section of a many line spectrum molecule such as H_2 is dependent on the monochromator bandpass, the same bandpasses were used in the absolute measurements with the static system and the corresponding measurements with the crossed beam system.

For the measurement of the absolute Balmer optical excitation cross sections of atomic hydrogen, (P_{H_2ij}/I_{off}) and $(P_{Hij} + P'_{H_2ij})/I_{on}$ from the crossed beam system at 200 eV were recorded on a Bausch and Lomb V.O.M. time base chart recorder in order to make use of an expanded scale

TABLE 2

BALMER OPTICAL EXCITATION CROSS SECTIONS
AT 200 eV (UNITS ARE 10^{-20} cm^2)

n	$Q_{H_2 n,2}$	$Q_{Hn,2}$
3	61.5	697.4
4	11.9	165.9
5	3.9	62.9
6	1.7	21.9
7	0.98	14.0
8	1.74	4.6
9	0.60	5.2
10	1.16	3.2
11	0.40	1.9
12	0.33	1.1
13	0.35	0.55

and signal averaging. Combining these measurements with the measurements of $N^{*'}_{H_2T}/N^{*}_{H_2T}$ and $Q_{H_2n,2}$ by Eq. (30), we obtain the absolute values of $Q_{Hn,2}$ shown in Table 2. The accuracy of the measurements of $Q_{Hn,2}$ is estimated to be 30%.

Comparison Between Theory and Experiment

Only level excitation cross sections are calculated by theoreticians for atomic or molecular systems. In order to convert a measured optical excitation cross section to a level cross section, it is transformed to an apparent cross section by the use of its branching ratio. The cascade component is then subtracted by the use of upper apparent cross sections and their branching ratios. For each measured Balmer optical excitation cross section, however, we have the sum of the optical excitation cross sections of the S, P, and D states. Therefore, we cannot obtain the apparent cross sections for these states without making an assumption about their relative magnitude. Such an assumption cannot be based on the relative magnitude of their theoretically calculated level cross sections since the apparent cross sections include cascade. In a straightforward manner, however, the theoretical level cross sections can be converted to Balmer optical excitation cross sections.

Since the compilation of transition probabilities by Wiese, Smith, and Glennon[68] gives only the transition probabilities for atomic hydrogen through n = 6, the dipole matrix element calculations of Green, Rush, and Chandler[69] which include all angular momentum states for n through 20 were used here. The dipole matrix element can be readily converted to a transition probability by Eq. (7) given by Green et al.[69] These conversions were carried out for S, P, and D transitions through n = 20 with a General Electric 430 time sharing computer. The resulting transition probabilities are given in Table 3. The reciprical of the branching ratios, which are defined by Eq. (4), were computed from the transition probabilities in Table 3 and are given in Table 4. The lifetime τ of state i is defined as

$$\tau = 1/\sum_k A_{ik}, \qquad (42)$$

where k is summed over all lower states to which state i radiatively decays. The lifetimes of atomic hydrogen were computed from the transition probabilities in Table 3 and are given in Table 5.

Vainshtein[70] has calculated the level excitation cross sections for atomic hydrogen for the S, P, and D states for n = 2 through 9 for electron energies of 1.16

ATØMIC HYDRØGEN TRANSITIØN PRØBABILITIES

N, NP	S TØ P	P TØ S	P TØ D	D TØ P
2, 1	0.00000E+00	0.62616E+09	0.00000E+00	0.00000E+00
3, 1	0.00000E+00	0.16717E+09	0.00000E+00	0.00000E+00
3, 2	0.63138E+07	0.22449E+08	0.00000E+00	0.64653E+08
4, 1	0.00000E+00	0.68151E+08	0.00000E+00	0.00000E+00
4, 2	0.25782E+07	0.96684E+07	0.00000E+00	0.20626E+08
4, 3	0.18355E+07	0.30652E+07	0.34754E+06	0.70377E+07
5, 1	0.00000E+00	0.34357E+08	0.00000E+00	0.00000E+00
5, 2	0.12837E+07	0.49485E+07	0.00000E+00	0.94257E+07
5, 3	0.90470E+06	0.16377E+07	0.14954E+06	0.33915E+07
5, 4	0.64506E+06	0.73718E+06	0.18846E+06	0.14858E+07
6, 1	0.00000E+00	0.19718E+08	0.00000E+00	0.00000E+00
6, 2	0.73503E+06	0.28584E+07	0.00000E+00	0.51452E+07
6, 3	0.50717E+06	0.95510E+06	0.78242E+05	0.18778E+07
6, 4	0.35823E+06	0.44561E+06	0.94166E+05	0.86216E+06
6, 5	0.26818E+06	0.24296E+06	0.95934E+05	0.44949E+06
7, 1	0.00000E+00	0.12355E+08	0.00000E+00	0.00000E+00
7, 2	0.45867E+06	0.17972E+07	0.00000E+00	0.31312E+07
7, 3	0.31232E+06	0.60254E+06	0.46362E+05	0.11495E+07
7, 4	0.21738E+06	0.28281E+06	0.53909E+05	0.53380E+06
7, 5	0.16173E+06	0.15909E+06	0.53074E+05	0.29024E+06
7, 6	0.12652E+06	0.97904E+05	0.51048E+05	0.17043E+06
8, 1	0.00000E+00	0.82505E+07	0.00000E+00	0.00000E+00
8, 2	0.30542E+06	0.12025E+07	0.00000E+00	0.20524E+07
8, 3	0.20668E+06	0.40379E+06	0.29861E+05	0.75585E+06
8, 4	0.14195E+06	0.18975E+06	0.33959E+05	0.35245E+06
8, 5	0.10399E+06	0.10711E+06	0.32455E+05	0.19334E+06
8, 6	0.81042E+05	0.67790E+05	0.30403E+05	0.11794E+06
8, 7	0.65698E+05	0.45344E+05	0.28729E+05	0.75412E+05
9, 1	0.00000E+00	0.57818E+07	0.00000E+00	0.00000E+00
9, 2	0.21361E+06	0.84387E+06	0.00000E+00	0.14203E+07
9, 3	0.14377E+06	0.28357E+06	0.20417E+05	0.52403E+06
9, 4	0.97944E+05	0.13327E+06	0.22877E+05	0.24434E+06
9, 5	0.70933E+05	0.75205E+05	0.21431E+05	0.13463E+06
9, 6	0.54475E+05	0.47681E+05	0.19555E+05	0.82728E+05
9, 7	0.44072E+05	0.32725E+05	0.18098E+05	0.54792E+05
9, 8	0.36771E+05	0.23268E+05	0.17033E+05	0.37346E+05
10, 1	0.00000E+00	0.42083E+07	0.00000E+00	0.00000E+00
10, 2	0.15525E+06	0.61477E+06	0.00000E+00	0.10246E+07
10, 3	0.10408E+06	0.20663E+06	0.14602E+05	0.37348E+06
10, 4	0.70498E+05	0.97110E+05	0.16192E+05	0.17703E+06
10, 5	0.50637E+05	0.54750E+05	0.14962E+05	0.97479E+05
10, 6	0.38454E+05	0.34664E+05	0.13404E+05	0.59974E+05
10, 7	0.30682E+05	0.23804E+05	0.12114E+05	0.39936E+05
10, 8	0.25582E+05	0.17335E+05	0.11215E+05	0.28127E+05
10, 9	0.21848E+05	0.12914E+05	0.10575E+05	0.20144E+05

ATØMIC HYDRØGEN TRANSITIØN PRØBABILITIES

N,NP	S TØ P	P TØ S	P TØ D	D TØ P
11, 1	0.00000E+00	0.31581E+07	0.00000E+00	0.00000E+00
11, 2	0.11637E+06	0.46165E+06	0.00000E+00	0.76390E+06
11, 3	0.77797E+05	0.15524E+06	0.10817E+05	0.28240E+06
11, 4	0.52468E+05	0.72924E+05	0.11905E+05	0.13218E+06
11, 5	0.37464E+05	0.41077E+05	0.10893E+05	0.72815E+05
11, 6	0.28219E+05	0.25963E+05	0.96347E+04	0.44312E+05
11, 7	0.22268E+05	0.17789E+05	0.85598E+04	0.29353E+05
11, 8	0.18320E+05	0.12948E+05	0.77530E+04	0.21114E+05
11, 9	0.15656E+05	0.98664E+04	0.72132E+04	0.15596E+05
11,10	0.13629E+05	0.76243E+04	0.68270E+04	0.11618E+05
12, 1	0.00000E+00	0.24304E+07	0.00000E+00	0.00000E+00
12, 2	0.89484E+05	0.35545E+06	0.00000E+00	0.58497E+06
12, 3	0.59689E+05	0.11955E+06	0.82431E+04	0.21638E+06
12, 4	0.40126E+05	0.56143E+05	0.90213E+04	0.10131E+06
12, 5	0.28523E+05	0.31599E+05	0.81951E+04	0.55825E+05
12, 6	0.21354E+05	0.19942E+05	0.71806E+04	0.34351E+05
12, 7	0.16716E+05	0.13633E+05	0.63028E+04	0.22881E+05
12, 8	0.13605E+05	0.98947E+04	0.56175E+04	0.16177E+05
12, 9	0.11476E+05	0.75301E+04	0.51207E+04	0.11985E+05
12,10	0.10007E+05	0.59455E+04	0.47943E+04	0.91934E+04
12,11	0.88538E+04	0.47333E+04	0.45589E+04	0.70737E+04
13, 1	0.00000E+00	0.19102E+07	0.00000E+00	0.00000E+00
13, 2	0.70287E+05	0.27948E+06	0.00000E+00	0.45801E+06
13, 3	0.46803E+05	0.94013E+05	0.64298E+04	0.16949E+06
13, 4	0.31385E+05	0.44140E+05	0.70063E+04	0.79387E+05
13, 5	0.22234E+05	0.24826E+05	0.63296E+04	0.43743E+05
13, 6	0.16570E+05	0.15649E+05	0.55075E+04	0.26910E+05
13, 7	0.12892E+05	0.10677E+05	0.47912E+04	0.17914E+05
13, 8	0.10409E+05	0.77291E+04	0.42214E+04	0.12656E+05
13, 9	0.86888E+04	0.58619E+04	0.37897E+04	0.93683E+04
13,10	0.74819E+04	0.46195E+04	0.34806E+04	0.72012E+04
13,11	0.66346E+04	0.37538E+04	0.32804E+04	0.56963E+04
13,12	0.59502E+04	0.30624E+04	0.31341E+04	0.45014E+04
14, 1	0.00000E+00	0.15286E+07	0.00000E+00	0.00000E+00
14, 2	0.56215E+05	0.22371E+06	0.00000E+00	0.36540E+06
14, 3	0.37382E+05	0.75260E+05	0.51142E+04	0.13527E+06
14, 4	0.25018E+05	0.35328E+05	0.55538E+04	0.63369E+05
14, 5	0.17676E+05	0.19859E+05	0.49960E+04	0.34918E+05
14, 6	0.13126E+05	0.12505E+05	0.43238E+04	0.21475E+05
14, 7	0.10166E+05	0.85192E+04	0.37362E+04	0.14288E+05
14, 8	0.81591E+04	0.61528E+04	0.32637E+04	0.10083E+05
14, 9	0.67559E+04	0.46517E+04	0.28973E+04	0.74539E+04
14,10	0.57578E+04	0.36522E+04	0.26227E+04	0.57224E+04
14,11	0.50442E+04	0.29606E+04	0.24273E+04	0.45328E+04
14,12	0.45376E+04	0.24636E+04	0.23027E+04	0.36754E+04

ATØMIC HYDRØGEN TRANSITION PRØBABILITIES

N,NP	S TØ P	P TØ S	P TØ D	D TØ P
14,13	0.41194E+04	0.20526E+04	0.22113E+04	0.29745E+04
15, 1	0.00000E+00	0.12422E+07	0.00000E+00	0.00000E+00
15, 2	0.45666E+05	0.18185E+06	0.00000E+00	0.29623E+06
15, 3	0.30333E+05	0.61180E+05	0.41360E+04	0.10963E+06
15, 4	0.20269E+05	0.28714E+05	0.44792E+04	0.51393E+05
15, 5	0.14290E+05	0.16134E+05	0.40157E+04	0.28318E+05
15, 6	0.10532E+05	0.10150E+05	0.34608E+04	0.17412E+05
15, 7	0.81662E+04	0.69066E+04	0.29748E+04	0.11573E+05
15, 8	0.65235E+04	0.49790E+04	0.25817E+04	0.81646E+04
15, 9	0.53699E+04	0.37552E+04	0.22732E+04	0.60232E+04
15,10	0.45403E+04	0.29381E+04	0.20356E+04	0.46195E+04
15,11	0.39370E+04	0.23718E+04	0.18576E+04	0.36524E+04
15,12	0.34999E+04	0.19680E+04	0.17319E+04	0.29661E+04
15,13	0.31868E+04	0.16703E+04	0.16529E+04	0.24590E+04
15,14	0.29224E+04	0.14162E+04	0.15943E+04	0.20271E+04
16, 1	0.00000E+00	0.10232E+07	0.00000E+00	0.00000E+00
16, 2	0.37601E+05	0.14981E+06	0.00000E+00	0.24351E+06
16, 3	0.24954E+05	0.50405E+05	0.33932E+04	0.90186E+05
16, 4	0.16652E+05	0.23653E+05	0.36666E+04	0.42260E+05
16, 5	0.11719E+05	0.13285E+05	0.32781E+04	0.23285E+05
16, 6	0.86598E+04	0.83530E+04	0.28156E+04	0.14315E+05
16, 7	0.66634E+04	0.56773E+04	0.24102E+04	0.95143E+04
16, 8	0.53038E+04	0.40868E+04	0.20811E+04	0.67041E+04
16, 9	0.43451E+04	0.30756E+04	0.18206E+04	0.49436E+04
16,10	0.36524E+04	0.24001E+04	0.16174E+04	0.37829E+04
16,11	0.31426E+04	0.19305E+04	0.14608E+04	0.29849E+04
16,12	0.27658E+04	0.15948E+04	0.13437E+04	0.24167E+04
16,13	0.24897E+04	0.13494E+04	0.12614E+04	0.20058E+04
16,14	0.22915E+04	0.11650E+04	0.12108E+04	0.16939E+04
16,15	0.21186E+04	0.10020E+04	0.11719E+04	0.14189E+04
17, 1	0.00000E+00	0.85283E+06	0.00000E+00	0.00000E+00
17, 2	0.31329E+05	0.12488E+06	0.00000E+00	0.20262E+06
17, 3	0.20776E+05	0.42019E+05	0.28138E+04	0.75055E+05
17, 4	0.13850E+05	0.19716E+05	0.30404E+04	0.35173E+05
17, 5	0.97332E+04	0.11069E+05	0.27119E+04	0.19379E+05
17, 6	0.71788E+04	0.69560E+04	0.23230E+04	0.11911E+05
17, 7	0.55112E+04	0.47239E+04	0.19819E+04	0.79139E+04
17, 8	0.43739E+04	0.33964E+04	0.17043E+04	0.55728E+04
17, 9	0.35707E+04	0.25522E+04	0.14838E+04	0.41062E+04
17,10	0.29870E+04	0.19863E+04	0.13098E+04	0.31373E+04
17,11	0.25550E+04	0.15935E+04	0.11738E+04	0.24711E+04
17,12	0.22314E+04	0.13114E+04	0.10688E+04	0.19977E+04
17,13	0.19858E+04	0.11044E+04	0.99031E+03	0.16524E+04
17,14	0.18099E+04	0.95016E+03	0.93552E+03	0.13951E+04
17,15	0.16816E+04	0.83253E+03	0.90290E+03	0.11972E+04

ATØMIC HYDRØGEN TRANSITION PRØBABILITIES

N,NP	S TØ P	P TØ S	P TØ D	D TØ P
17,16	0.15668E+04	0.72547E+03	0.37726E+03	0.10174E+04
18, 1	0.00000E+00	0.71826E+06	0.00000E+00	0.00000E+00
18, 2	0.26380E+05	0.10519E+06	0.00000E+00	0.17041E+06
18, 3	0.17483E+05	0.35394E+05	0.23675E+04	0.63134E+05
18, 4	0.11644E+05	0.16606E+05	0.25496E+04	0.29589E+05
18, 5	0.81737E+04	0.93209E+04	0.22701E+04	0.16302E+05
18, 6	0.60193E+04	0.58545E+04	0.19400E+04	0.10018E+05
18, 7	0.46121E+04	0.39729E+04	0.16506E+04	0.66538E+04
18, 8	0.36517E+04	0.28536E+04	0.14148E+04	0.46330E+04
18, 9	0.29721E+04	0.21413E+04	0.12266E+04	0.34475E+04
18,10	0.24775E+04	0.16642E+04	0.10777E+04	0.26315E+04
18,11	0.21094E+04	0.13315E+04	0.96000E+03	0.20695E+04
18,12	0.18313E+04	0.10923E+04	0.86750E+03	0.16696E+04
18,13	0.16199E+04	0.91636E+03	0.79591E+03	0.13775E+04
18,14	0.14598E+04	0.78455E+03	0.74237E+03	0.11597E+04
18,15	0.13412E+04	0.68473E+03	0.70540E+03	0.99438E+03
18,16	0.12560E+04	0.60739E+03	0.68331E+03	0.86492E+03
18,17	0.11798E+04	0.53609E+03	0.66764E+03	0.74548E+03
19, 1	0.00000E+00	0.61059E+06	0.00000E+00	0.00000E+00
19, 2	0.22420E+05	0.89433E+05	0.00000E+00	0.14470E+06
19, 3	0.14851E+05	0.30093E+05	0.20079E+04	0.53613E+05
19, 4	0.98837E+04	0.14117E+05	0.21596E+04	0.25128E+05
19, 5	0.69311E+04	0.79222E+04	0.19198E+04	0.13844E+05
19, 6	0.50978E+04	0.49739E+04	0.16375E+04	0.85064E+04
19, 7	0.38997E+04	0.33733E+04	0.13901E+04	0.56480E+04
19, 8	0.30816E+04	0.24209E+04	0.11881E+04	0.39732E+04
19, 9	0.25021E+04	0.18145E+04	0.10269E+04	0.29231E+04
19,10	0.20793E+04	0.14080E+04	0.89855E+03	0.22283E+04
19,11	0.17640E+04	0.11244E+04	0.79562E+03	0.17508E+04
19,12	0.15245E+04	0.92026E+03	0.71563E+03	0.14102E+04
19,13	0.13406E+04	0.76946E+03	0.65163E+03	0.11609E+04
19,14	0.11990E+04	0.65606E+03	0.60206E+03	0.97461E+03
19,15	0.10909E+04	0.56970E+03	0.56500E+03	0.83304E+03
19,16	0.10107E+04	0.50344E+03	0.53969E+03	0.72394E+03
19,17	0.95351E+03	0.45162E+03	0.52554E+03	0.63747E+03
19,18	0.90051E+03	0.40237E+03	0.51439E+03	0.55527E+03
20, 1	0.00000E+00	0.52341E+06	0.00000E+00	0.00000E+00
20, 2	0.19216E+05	0.76671E+05	0.00000E+00	0.12391E+06
20, 3	0.12723E+05	0.25799E+05	0.17178E+04	0.45917E+05
20, 4	0.84619E+04	0.12101E+05	0.18456E+04	0.21522E+05
20, 5	0.59288E+04	0.67897E+04	0.16384E+04	0.11856E+05
20, 6	0.43558E+04	0.42614E+04	0.13952E+04	0.72843E+04
20, 7	0.33279E+04	0.28887E+04	0.11321E+04	0.48356E+04
20, 8	0.26254E+04	0.20717E+04	0.10032E+04	0.34004E+04
20, 9	0.21275E+04	0.15514E+04	0.86901E+03	0.25002E+04

ATOMIC HYDROGEN TRANSITION PROBABILITIES

N,NP	S TO P	P TO S	P TO D	D TO P
20,10	0.17639E+04	0.12024E+04	0.75806E+03	0.19052E+04
20,11	0.14919E+04	0.95879E+03	0.66943E+03	0.14949E+04
20,12	0.12845E+04	0.78300E+03	0.59850E+03	0.12022E+04
20,13	0.11244E+04	0.65303E+03	0.54188E+03	0.98802E+03
20,14	0.99985E+03	0.55492E+03	0.49695E+03	0.82750E+03
20,15	0.90302E+03	0.47984E+03	0.46203E+03	0.70523E+03
20,16	0.82856E+03	0.42179E+03	0.43597E+03	0.61075E+03
20,17	0.77360E+03	0.37694E+03	0.41859E+03	0.53725E+03
20,18	0.73495E+03	0.34169E+03	0.40949E+03	0.47848E+03
20,19	0.69809E+03	0.30726E+03	0.40212E+03	0.42111E+03

Reciprocal Atomic Hydrogen Branching Ratios

N,NP	S TO P	P TO S	P TO D	D TO P
2, 1	0.00000E+00	0.10000E+01	0.00000E+00	0.00000E+00
3, 1	0.00000E+00	0.83161E+00	0.00000E+00	0.00000E+00
3, 2	0.10000E+01	0.11839E+00	0.00000E+00	0.10000E+01
4, 1	0.00000E+00	0.83897E+00	0.00000E+00	0.00000E+00
4, 2	0.58414E+00	0.11902E+00	0.00000E+00	0.74560E+00
4, 3	0.41586E+00	0.37734E-01	0.42784E-02	0.25440E+00
5, 1	0.00000E+00	0.81767E+00	0.00000E+00	0.00000E+00
5, 2	0.45401E+00	0.11777E+00	0.00000E+00	0.65900E+00
5, 3	0.31873E+00	0.38976E-01	0.35589E-02	0.23712E+00
5, 4	0.22726E+00	0.17544E-01	0.44852E-02	0.10388E+00
6, 1	0.00000E+00	0.80520E+00	0.00000E+00	0.00000E+00
6, 2	0.39336E+00	0.11672E+00	0.00000E+00	0.61733E+00
6, 3	0.27142E+00	0.39002E-01	0.31951E-02	0.22530E+00
6, 4	0.19171E+00	0.18197E-01	0.38453E-02	0.10344E+00
6, 5	0.14352E+00	0.99214E-02	0.39175E-02	0.53930E-01
7, 1	0.00000E+00	0.79715E+00	0.00000E+00	0.00000E+00
7, 2	0.35914E+00	0.11595E+00	0.00000E+00	0.59357E+00
7, 3	0.24494E+00	0.38876E-01	0.29913E-02	0.21791E+00
7, 4	0.17021E+00	0.18247E-01	0.34782E-02	0.10119E+00
7, 5	0.12664E+00	0.10264E-01	0.34244E-02	0.55020E-01
7, 6	0.99067E-01	0.63168E-02	0.32936E-02	0.32303E-01
8, 1	0.00000E+00	0.79163E+00	0.00000E+00	0.00000E+00
8, 2	0.33756E+00	0.11537E+00	0.00000E+00	0.57457E+00
8, 3	0.22843E+00	0.38743E-01	0.23651E-02	0.21307E+00
8, 4	0.15639E+00	0.18206E-01	0.32583E-02	0.99355E-01
8, 5	0.11493E+00	0.10277E-01	0.31140E-02	0.54502E-01
8, 6	0.89571E-01	0.65044E-02	0.29171E-02	0.33247E-01
8, 7	0.72612E-01	0.43507E-02	0.27565E-02	0.21253E-01
9, 1	0.00000E+00	0.78762E+00	0.00000E+00	0.00000E+00
9, 2	0.32288E+00	0.11495E+00	0.00000E+00	0.56841E+00
9, 3	0.21731E+00	0.38629E-01	0.27813E-02	0.20972E+00
9, 4	0.14805E+00	0.18155E-01	0.31164E-02	0.97936E-01
9, 5	0.10721E+00	0.10244E-01	0.29194E-02	0.53900E-01
9, 6	0.82341E-01	0.64953E-02	0.26639E-02	0.33108E-01
9, 7	0.66617E-01	0.44580E-02	0.24654E-02	0.21928E-01
9, 8	0.55561E-01	0.31697E-02	0.23210E-02	0.14946E-01
10, 1	0.00000E+00	0.78463E+00	0.00000E+00	0.00000E+00
10, 2	0.31235E+00	0.11462E+00	0.00000E+00	0.56119E+00
10, 3	0.20940E+00	0.38535E-01	0.27225E-02	0.20730E+00
10, 4	0.14134E+00	0.18106E-01	0.30190E-02	0.96962E-01
10, 5	0.10187E+00	0.10206E-01	0.27897E-02	0.53391E-01
10, 6	0.77367E-01	0.64631E-02	0.24992E-02	0.32849E-01
10, 7	0.61731E-01	0.44332E-02	0.22586E-02	0.21774E-01
10, 8	0.51470E-01	0.32321E-02	0.20910E-02	0.15496E-01
10, 9	0.43957E-01	0.24073E-02	0.19717E-02	0.11033E-01

Reciprocal Atomic Hydrogen Branching Ratios

N,NP	S TO P	P TO S	P TO D	D TO P
11, 1	0.00000E+00	0.78233E+00	0.00000E+00	0.00000E+00
11, 2	0.30448E+00	0.11436E+00	0.00000E+00	0.55565E+00
11, 3	0.20356E+00	0.38456E-01	0.26796E-02	0.20549E+00
11, 4	0.13728E+00	0.18065E-01	0.29491E-02	0.96130E-01
11, 5	0.93024E-01	0.10175E-01	0.26984E-02	0.52734E-01
11, 6	0.73835E-01	0.64316E-02	0.23367E-02	0.33607E-01
11, 7	0.58264E-01	0.44067E-02	0.21205E-02	0.21726E-01
11, 8	0.47934E-01	0.32075E-02	0.19206E-02	0.15364E-01
11, 9	0.40964E-01	0.24441E-02	0.17869E-02	0.11345E-01
11,10	0.35660E-01	0.18887E-02	0.16912E-02	0.84538E-02
12, 1	0.00000E+00	0.78051E+00	0.00000E+00	0.00000E+00
12, 2	0.29845E+00	0.11415E+00	0.00000E+00	0.55174E+00
12, 3	0.19907E+00	0.38393E-01	0.26472E-02	0.20410E+00
12, 4	0.13333E+00	0.18030E-01	0.28971E-02	0.95562E-01
12, 5	0.95129E-01	0.10147E-01	0.26318E-02	0.52658E-01
12, 6	0.71219E-01	0.64043E-02	0.23060E-02	0.32402E-01
12, 7	0.55751E-01	0.43782E-02	0.20241E-02	0.21583E-01
12, 8	0.45375E-01	0.31776E-02	0.18040E-02	0.15259E-01
12, 9	0.38275E-01	0.24183E-02	0.16445E-02	0.11305E-01
12,10	0.33375E-01	0.19094E-02	0.15397E-02	0.86716E-02
12,11	0.29529E-01	0.15201E-02	0.14641E-02	0.66724E-02
13, 1	0.00000E+00	0.77904E+00	0.00000E+00	0.00000E+00
13, 2	0.29363E+00	0.11398E+00	0.00000E+00	0.54660E+00
13, 3	0.19555E+00	0.38342E-01	0.26223E-02	0.20301E+00
13, 4	0.13113E+00	0.18002E-01	0.28574E-02	0.95063E-01
13, 5	0.92399E-01	0.10124E-01	0.25814E-02	0.52345E-01
13, 6	0.69233E-01	0.63822E-02	0.22461E-02	0.32232E-01
13, 7	0.53866E-01	0.43544E-02	0.19540E-02	0.21457E-01
13, 8	0.43491E-01	0.31522E-02	0.17216E-02	0.15159E-01
13, 9	0.36304E-01	0.23907E-02	0.15456E-02	0.11221E-01
13,10	0.31261E-01	0.18840E-02	0.14195E-02	0.86255E-02
13,11	0.27721E-01	0.15309E-02	0.13379E-02	0.66229E-02
13,12	0.24361E-01	0.12489E-02	0.12782E-02	0.53917E-02
14, 1	0.00000E+00	0.77765E+00	0.00000E+00	0.00000E+00
14, 2	0.28963E+00	0.11383E+00	0.00000E+00	0.54605E+00
14, 3	0.19273E+00	0.38297E-01	0.26024E-02	0.20215E+00
14, 4	0.12899E+00	0.17977E-01	0.28261E-02	0.94679E-01
14, 5	0.91134E-01	0.10105E-01	0.25423E-02	0.52181E-01
14, 6	0.67675E-01	0.63633E-02	0.22002E-02	0.32092E-01
14, 7	0.52414E-01	0.43351E-02	0.19012E-02	0.21352E-01
14, 8	0.42067E-01	0.31309E-02	0.16603E-02	0.15063E-01
14, 9	0.34832E-01	0.23671E-02	0.14743E-02	0.11139E-01
14,10	0.29636E-01	0.18555E-02	0.13346E-02	0.85516E-02
14,11	0.26007E-01	0.15065E-02	0.12351E-02	0.67733E-02
14,12	0.23395E-01	0.12536E-02	0.11717E-02	0.54970E-02

Reciprocal Atomic Hydrogen Branching Ratios

N,NP	S TO P	P TO S	P TO D	D TO P
14,13	0.21239E-01	0.10444E-02	0.11252E-02	0.44451E-04
15, 1	0.00000E+00	0.77635E+00	0.00000E+00	0.00000E+00
15, 2	0.28669E+00	0.11372E+00	0.00000E+00	0.54401E+00
15, 3	0.19043E+00	0.38261E-01	0.25866E-02	0.20142E+00
15, 4	0.12725E+00	0.17957E-01	0.23012E-02	0.94381E-01
15, 5	0.89713E-01	0.10039E-01	0.25113E-02	0.52005E-01
15, 6	0.66434E-01	0.63476E-02	0.21643E-02	0.31976E-01
15, 7	0.51263E-01	0.43193E-02	0.18604E-02	0.21262E-01
15, 8	0.40955E-01	0.31138E-02	0.16145E-02	0.14994E-01
15, 9	0.33712E-01	0.23484E-02	0.14216E-02	0.11070E-01
15,10	0.28504E-01	0.18374E-02	0.12730E-02	0.84835E-02
15,11	0.24717E-01	0.14833E-02	0.11617E-02	0.67075E-02
15,12	0.21972E-01	0.12307E-02	0.10831E-02	0.54471E-02
15,13	0.20007E-01	0.10445E-02	0.10336E-02	0.45158E-02
15,14	0.18347E-01	0.88566E-03	0.99704E-03	0.37227E-02
16, 1	0.00000E+00	0.77602E+00	0.00000E+00	0.00000E+00
16, 2	0.28408E+00	0.11362E+00	0.00000E+00	0.54231E+00
16, 3	0.18853E+00	0.38229E-01	0.25735E-02	0.20085E+00
16, 4	0.12531E+00	0.17939E-01	0.27308E-02	0.94115E-01
16, 5	0.88540E-01	0.10075E-01	0.24862E-02	0.51657E-01
16, 6	0.65427E-01	0.63351E-02	0.21354E-02	0.31300E-01
16, 7	0.50343E-01	0.43058E-02	0.18280E-02	0.21139E-01
16, 8	0.40071E-01	0.30995E-02	0.15784E-02	0.14930E-01
16, 9	0.32828E-01	0.23326E-02	0.13808E-02	0.11009E-01
16,10	0.27595E-01	0.18203E-02	0.12266E-02	0.84247E-02
16,11	0.23743E-01	0.14641E-02	0.11079E-02	0.66475E-02
16,12	0.20896E-01	0.12095E-02	0.10191E-02	0.53866E-02
16,13	0.18810E-01	0.10234E-02	0.95668E-03	0.44670E-02
16,14	0.17313E-01	0.88357E-03	0.91830E-03	0.37724E-02
16,15	0.16007E-01	0.75994E-03	0.88880E-03	0.31600E-02
17, 1	0.00000E+00	0.77532E+00	0.00000E+00	0.00000E+00
17, 2	0.28188E+00	0.11353E+00	0.00000E+00	0.54090E+00
17, 3	0.18693E+00	0.38200E-01	0.25626E-02	0.20036E+00
17, 4	0.12461E+00	0.17924E-01	0.27641E-02	0.93895E-01
17, 5	0.87573E-01	0.10063E-01	0.24654E-02	0.51733E-01
17, 6	0.64590E-01	0.63238E-02	0.21119E-02	0.31797E-01
17, 7	0.49586E-01	0.42946E-02	0.18018E-02	0.21126E-01
17, 8	0.39354E-01	0.30877E-02	0.15494E-02	0.14877E-01
17, 9	0.32127E-01	0.23202E-02	0.13489E-02	0.10961E-01
17,10	0.26875E-01	0.18062E-02	0.11907E-02	0.83751E-02
17,11	0.22938E-01	0.14487E-02	0.10671E-02	0.65967E-02
17,12	0.20077E-01	0.11922E-02	0.97166E-03	0.53329E-02
17,13	0.17894E-01	0.10040E-02	0.90031E-03	0.44111E-02
17,14	0.16284E-01	0.86381E-03	0.85050E-03	0.37242E-02
17,15	0.15130E-01	0.75687E-03	0.82084E-03	0.31960E-02

Reciprocal Atomic Hydrogen Branching Ratios

N,N'	S TO P	P TO S	P TO D	D TO P
17,16	0.14097E-01	0.65954E-03	0.79753E-03	0.27160E-02
18, 1	0.00000E+00	0.77471E+00	0.00000E+00	0.00000E+00
18, 2	0.23001E+00	0.11345E+00	0.00000E+00	0.53970E+00
18, 3	0.18557E+00	0.38176E-01	0.25536E-02	0.19995E+00
18, 4	0.12359E+00	0.17911E-01	0.27500E-02	0.93710E-01
18, 5	0.86760E-01	0.10053E-01	0.24485E-02	0.51629E-01
18, 6	0.63892E-01	0.63146E-02	0.20925E-02	0.31725E-01
18, 7	0.48955E-01	0.42352E-02	0.17303E-02	0.21073E-01
18, 8	0.38761E-01	0.30779E-02	0.15260E-02	0.14331E-01
18, 9	0.31547E-01	0.23096E-02	0.13230E-02	0.10913E-01
18,10	0.26297E-01	0.17950E-02	0.11624E-02	0.83341E-02
18,11	0.22390E-01	0.14362E-02	0.10354E-02	0.65542E-02
18,12	0.19438E-01	0.11781E-02	0.93568E-03	0.52577E-02
18,13	0.17194E-01	0.98838E-03	0.85847E-03	0.43626E-02
18,14	0.15495E-01	0.84621E-03	0.80072E-03	0.36723E-02
18,15	0.14236E-01	0.73855E-03	0.76084E-03	0.31493E-02
18,16	0.13332E-01	0.65513E-03	0.73756E-03	0.27393E-02
18,17	0.12523E-01	0.57823E-03	0.72011E-03	0.23610E-02
19, 1	0.00000E+00	0.77419E+00	0.00000E+00	0.00000E+00
19, 2	0.27841E+00	0.11339E+00	0.00000E+00	0.53370E+00
19, 3	0.18442E+00	0.38156E-01	0.25459E-02	0.19959E+00
19, 4	0.12273E+00	0.17899E-01	0.27382E-02	0.93548E-01
19, 5	0.86069E-01	0.10044E-01	0.24342E-02	0.51539E-01
19, 6	0.63303E-01	0.63066E-02	0.20762E-02	0.31663E-01
19, 7	0.48425E-01	0.42771E-02	0.17626E-02	0.21027E-01
19, 8	0.38266E-01	0.30696E-02	0.15064E-02	0.14722E-01
19, 9	0.31070E-01	0.23007E-02	0.13020E-02	0.10832E-01
19,10	0.25920E-01	0.17853E-02	0.11393E-02	0.82975E-02
19,11	0.21905E-01	0.14257E-02	0.10100E-02	0.65130E-02
19,12	0.18931E-01	0.11663E-02	0.90737E-03	0.52500E-02
19,13	0.16647E-01	0.97563E-03	0.82629E-03	0.43219E-02
19,14	0.14839E-01	0.83184E-03	0.76337E-03	0.36233E-02
19,15	0.13547E-01	0.72234E-03	0.71638E-03	0.31013E-02
19,16	0.12551E-01	0.63833E-03	0.68429E-03	0.26951E-02
19,17	0.11840E-01	0.57263E-03	0.66635E-03	0.23732E-02
19,18	0.11132E-01	0.51013E-03	0.65221E-03	0.20672E-02
20, 1	0.00000E+00	0.77373E+00	0.00000E+00	0.00000E+00
20, 2	0.27701E+00	0.11333E+00	0.00000E+00	0.53781E+00
20, 3	0.18341E+00	0.38138E-01	0.25393E-02	0.19930E+00
20, 4	0.12193E+00	0.17883E-01	0.27283E-02	0.93413E-01
20, 5	0.85467E-01	0.10036E-01	0.24220E-02	0.51459E-01
20, 6	0.62792E-01	0.62994E-02	0.20625E-02	0.31616E-01
20, 7	0.47974E-01	0.42702E-02	0.17474E-02	0.20993E-01
20, 8	0.37847E-01	0.30625E-02	0.14904E-02	0.14759E-01
20, 9	0.30669E-01	0.22934E-02	0.12846E-02	0.10851E-01

Reciprocal Atomic Hydrogen Branching Ratios

N,NP	S TO P	P TO S	P TO D	D TO P
20,10	0.25428E-01	0.17775E-02	0.11206E-02	0.82692E-03
20,11	0.21507E-01	0.14173E-02	0.98959E-03	0.64864E-03
20,12	0.18517E-01	0.11574E-02	0.83474E-03	0.52180E-03
20,13	0.16209E-01	0.96535E-03	0.80104E-03	0.42884E-03
20,14	0.14413E-01	0.82031E-03	0.73462E-03	0.35916E-03
20,15	0.13018E-01	0.70933E-03	0.68300E-03	0.30609E-03
20,16	0.11944E-01	0.62351E-03	0.64448E-03	0.26509E-03
20,17	0.11151E-01	0.55721E-03	0.61378E-03	0.23319E-03
20,18	0.10594E-01	0.50511E-03	0.60533E-03	0.20766E-03
20,19	0.10063E-01	0.45421E-03	0.59444E-03	0.18278E-03

ATOMIC HYDROGEN LIFETIMES

N	S	P	D
2	0.00000E+00	0.15970E-08	0.00000E+00
3	0.15838E-06	0.52737E-08	0.15467E-07
4	0.22657E-06	0.12310E-07	0.36148E-07
5	0.35230E-06	0.23799E-07	0.69915E-07
6	0.53516E-06	0.40836E-07	0.11998E-06
7	0.78301E-06	0.64521E-07	0.18957E-06
8	0.11052E-05	0.95949E-07	0.28190E-06
9	0.15115E-05	0.13622E-06	0.40021E-06
10	0.20119E-05	0.18645E-06	0.54771E-06
11	0.26165E-05	0.24772E-06	0.72765E-06
12	0.33352E-05	0.32115E-06	0.94327E-06
13	0.41782E-05	0.40763E-06	0.11977E-05
14	0.51558E-05	0.50886E-06	0.14944E-05
15	0.62780E-05	0.62533E-06	0.18365E-05
16	0.75552E-05	0.75843E-06	0.22271E-05
17	0.89974E-05	0.90912E-06	0.26695E-05
18	0.10614E-04	0.10786E-05	0.31671E-05
19	0.12417E-04	0.12679E-05	0.37229E-05
20	0.14416E-04	0.14783E-05	0.43404E-05

through 24.04 threshold units. Since the thresholds are different for each state, Vainshtein's digital data was graphically interpolated to yield level cross sections at equal electron energies. For several energies the cross sections of the S, P, and D states were log-log plotted against n. The linear nature of these plots allowed extrapolation of the cross sections through n = 20. Vainshtein's cross sections and the branching ratios in Table 4 were used to compute the apparent cross sections of the S, P, and D states for n through 20 given in Table 6. The Balmer optical excitation cross sections as well as the sum of the apparent and the sum of the level cross sections for n through 20 are also given in Table 6.

The measured optical excitation cross sections and those computed from Vainshtein's calculations are shown in a log-log plot against n in Fig. 13. By measuring the slopes of the curves we find that for n = 3-9 the computed cross sections vary as $n^{-3.64}$ and the measured cross sections vary as $n^{-4.5}$. The computed cross sections are less than the measured cross sections for n = 3, but they cross over at n = 11.

The effect of the adsorption of resonance radiation from a state by ground state atoms is to increase the value of the optical excitation cross section of the state when it is measured by a nonresonant radiative decay channel. The

Apparent Excitation Cross Sections (20eV)

n\L	S	P	D
1	0.151E-15	0.000E+00	0.000E+00
2	0.235E-16	0.120E-15	0.000E+00
3	0.420E-17	0.203E-16	0.124E-17
4	0.147E-17	0.664E-17	0.912E-18
5	0.699E-18	0.313E-17	0.444E-18
6	0.375E-18	0.171E-17	0.256E-18
7	0.231E-18	0.105E-17	0.164E-18
8	0.150E-18	0.654E-18	0.104E-18
9	0.103E-18	0.455E-18	0.770E-19
10	0.749E-19	0.326E-18	0.542E-19
11	0.557E-19	0.234E-18	0.397E-19
12	0.421E-19	0.180E-18	0.306E-19
13	0.330E-19	0.139E-18	0.242E-19
14	0.258E-19	0.107E-18	0.192E-19
15	0.213E-19	0.890E-19	0.156E-19
16	0.173E-19	0.711E-19	0.129E-19
17	0.142E-19	0.585E-19	0.106E-19
18	0.114E-19	0.486E-19	0.885E-20
19	0.970E-20	0.406E-19	0.759E-20
20	0.836E-20	0.352E-19	0.651E-20

n	Balmer Optical	Total Apparent	Total Direct (20eV)
3	0.354E-17	0.264E-16	0.242E-16
4	0.233E-17	0.902E-17	0.836E-17
5	0.954E-18	0.432E-17	0.406E-17
6	0.505E-18	0.234E-17	0.223E-17
7	0.303E-18	0.145E-17	0.139E-17
8	0.190E-18	0.939E-18	0.906E-18
9	0.125E-18	0.632E-18	0.612E-18
10	0.912E-19	0.455E-18	0.443E-18
11	0.653E-19	0.330E-18	0.322E-18
12	0.499E-19	0.252E-18	0.247E-18
13	0.383E-19	0.196E-18	0.193E-18
14	0.302E-19	0.152E-18	0.150E-18
15	0.247E-19	0.126E-18	0.124E-18
16	0.200E-19	0.101E-18	0.100E-18
17	0.164E-19	0.833E-19	0.827E-19
18	0.135E-19	0.690E-19	0.686E-19
19	0.113E-19	0.579E-19	0.577E-19
20	0.981E-20	0.501E-19	0.501E-19

Table 6. Optical, Apparent, and Level Cross Sections of Atomic Hydrogen from Vainshtein's Calculations in Units of 10^{-20} cm^2

Apparent Excitation Cross Sections (40eV)

n\L	S	P	D
1	0.140E-15	0.000E+00	0.000E+00
2	0.156E-16	0.111E-15	0.000E+00
3	0.291E-17	0.189E-16	0.153E-17
4	0.995E-18	0.659E-17	0.727E-18
5	0.465E-18	0.310E-17	0.387E-18
6	0.253E-18	0.171E-17	0.225E-18
7	0.155E-18	0.104E-17	0.142E-18
8	0.100E-18	0.681E-18	0.960E-19
9	0.702E-19	0.476E-18	0.661E-19
10	0.468E-19	0.331E-18	0.472E-19
11	0.346E-19	0.246E-18	0.362E-19
12	0.258E-19	0.187E-18	0.271E-19
13	0.198E-19	0.142E-18	0.216E-19
14	0.153E-19	0.115E-18	0.175E-19
15	0.125E-19	0.837E-19	0.143E-19
16	0.980E-20	0.735E-19	0.115E-19
17	0.843E-20	0.610E-19	0.977E-20
18	0.708E-20	0.512E-19	0.797E-20
19	0.574E-20	0.432E-19	0.689E-20
20	0.484E-20	0.361E-19	0.581E-20

n	Balmer Optical Total Apparent	Total Direct (40eV)
3	0.667E-17	0.233E-16	0.215E-16
4	0.191E-17	0.832E-17	0.779E-17
5	0.831E-18	0.395E-17	0.375E-17
6	0.437E-18	0.218E-17	0.209E-17
7	0.261E-18	0.134E-17	0.130E-17
8	0.168E-18	0.877E-18	0.851E-18
9	0.114E-18	0.612E-18	0.597E-18
10	0.791E-19	0.425E-18	0.416E-18
11	0.583E-19	0.316E-18	0.311E-18
12	0.440E-19	0.240E-18	0.236E-18
13	0.339E-19	0.184E-18	0.181E-18
14	0.271E-19	0.148E-18	0.147E-18
15	0.214E-19	0.115E-18	0.114E-18
16	0.174E-19	0.948E-19	0.942E-19
17	0.146E-19	0.792E-19	0.788E-19
18	0.120E-19	0.662E-19	0.660E-19
19	0.102E-19	0.558E-19	0.557E-19
20	0.855E-20	0.467E-19	0.467E-19

Table 6. (Continued)

Apparent Excitation Cross Sections (60eV)

n\L	S	P	D
1	0.116E-15	0.000E+00	0.000E+00
2	0.114E-16	0.920E-16	0.000E+00
3	0.209E-17	0.157E-16	0.114E-17
4	0.721E-18	0.558E-17	0.546E-18
5	0.336E-18	0.260E-17	0.233E-18
6	0.181E-18	0.148E-17	0.170E-18
7	0.110E-18	0.830E-18	0.106E-18
8	0.710E-19	0.575E-18	0.742E-19
9	0.499E-19	0.399E-18	0.504E-19
10	0.343E-19	0.236E-18	0.365E-19
11	0.248E-19	0.214E-18	0.273E-19
12	0.191E-19	0.160E-18	0.208E-19
13	0.145E-19	0.124E-18	0.162E-19
14	0.112E-19	0.975E-19	0.135E-19
15	0.897E-20	0.797E-19	0.107E-19
16	0.750E-20	0.654E-19	0.892E-20
17	0.623E-20	0.500E-19	0.739E-20
18	0.514E-20	0.450E-19	0.620E-20
19	0.424E-20	0.379E-19	0.533E-20
20	0.361E-20	0.326E-19	0.440E-20

n	Balmer Optical	Total Apparent	Total Direct (60eV)
3	0.510E-17	0.120E-16	0.176E-16
4	0.149E-17	0.490E-17	0.639E-17
5	0.648E-18	0.322E-17	0.306E-17
6	0.344E-18	0.179E-17	0.171E-17
7	0.205E-18	0.102E-17	0.106E-17
8	0.132E-18	0.719E-18	0.696E-18
9	0.906E-19	0.499E-18	0.487E-18
10	0.639E-19	0.357E-18	0.349E-18
11	0.472E-19	0.265E-18	0.261E-18
12	0.355E-19	0.200E-18	0.197E-18
13	0.273E-19	0.155E-18	0.153E-18
14	0.217E-19	0.122E-18	0.121E-18
15	0.175E-19	0.994E-19	0.986E-19
16	0.144E-19	0.819E-19	0.813E-19
17	0.117E-19	0.665E-19	0.662E-19
18	0.939E-20	0.563E-19	0.561E-19
19	0.833E-20	0.474E-19	0.473E-19
20	0.706E-20	0.406E-19	0.406E-19

Table 6. (Continued)

Apparent Excitation Cross Sections (80eV)

n\L	S	P	D
1	0.922E-16	0.[illegible]E+00	0.000E+00
2	0.913E-17	0.777E-16	0.000E+00
3	0.165E-17	0.134E-16	0.992E-17
4	0.566E-18	0.469E-17	0.432E-17
5	0.263E-18	0.222E-17	0.228E-17
6	0.140E-18	0.122E-17	0.134E-18
7	0.855E-19	0.755E-18	0.843E-19
8	0.562E-19	0.496E-18	0.567E-19
9	0.330E-19	0.342E-18	0.395E-19
10	0.269E-19	0.238E-18	0.275E-19
11	0.229E-19	0.179E-18	0.205E-19
12	0.195E-19	0.134E-18	0.154E-19
13	0.171E-19	0.102E-18	0.122E-19
14	0.147E-19	0.820E-19	0.973E-20
15	0.129E-19	0.667E-19	0.790E-20
16	0.115E-19	0.533E-19	0.635E-20
17	0.101E-19	0.443E-19	0.534E-20
18	0.873E-20	0.363E-19	0.444E-20
19	0.802E-20	0.309E-19	0.371E-20
20	0.722E-20	0.264E-19	0.317E-20

n	Balmer Optical	Total Apparent	Total Direct (80eV)
3	0.414E-17	0.159E-16	0.148E-16
4	0.121E-17	0.569E-17	0.538E-17
5	0.531E-18	0.271E-17	0.256E-17
6	0.281E-18	0.150E-17	0.144E-17
7	0.168E-18	0.924E-18	0.892E-18
8	0.108E-18	0.603E-18	0.590E-18
9	0.740E-19	0.419E-18	0.403E-18
10	0.511E-19	0.292E-18	0.285E-18
11	0.389E-19	0.223E-18	0.218E-18
12	0.297E-19	0.169E-18	0.166E-18
13	0.234E-19	0.133E-18	0.130E-18
14	0.189E-19	0.106E-18	0.105E-18
15	0.156E-19	0.875E-19	0.865E-19
16	0.123E-19	0.712E-19	0.705E-19
17	0.107E-19	0.593E-19	0.594E-19
18	0.893E-20	0.495E-19	0.493E-19
19	0.773E-20	0.426E-19	0.425E-19
20	0.669E-20	0.363E-19	0.363E-19

Table 6. (Continued)

Apparent Excitation Cross Sections (100eV)

n\L	S	P	D
1	0.372E-16	0.[illegible]E+00	0.000E+00
2	0.759E-17	0.522E-16	0.000E+00
3	0.137E-17	0.116E-16	0.733E-17
4	0.469E-18	0.413E-17	0.354E-17
5	0.216E-18	0.193E-17	0.182E-17
6	0.116E-18	0.106E-17	0.112E-17
7	0.706E-19	0.663E-18	0.716E-19
8	0.461E-19	0.436E-18	0.472E-19
9	0.312E-19	0.296E-18	0.322E-19
10	0.224E-19	0.215E-18	0.230E-19
11	0.167E-19	0.161E-18	0.174E-19
12	0.163E-19	0.125E-18	0.129E-19
13	0.140E-19	0.937E-19	0.999E-20
14	0.122E-19	0.757E-19	0.795E-20
15	0.108E-19	0.622E-19	0.639E-20
16	0.950E-20	0.497E-19	0.520E-20
17	0.841E-20	0.407E-19	0.423E-20
18	0.751E-20	0.345E-19	0.355E-20
19	0.679E-20	0.291E-19	0.301E-20
20	0.619E-20	0.246E-19	0.255E-20

n	Balmer Optical	Total Apparent	Total Direct (100eV)
3	0.348E-17	0.134E-16	0.125E-16
4	0.103E-17	0.425E-17	0.467E-17
5	0.452E-18	0.234E-17	0.223E-17
6	0.240E-18	0.133E-17	0.134E-17
7	0.145E-18	0.856E-18	0.778E-18
8	0.938E-19	0.580E-18	0.514E-18
9	0.640E-19	0.409E-18	0.360E-18
10	0.446E-19	0.296E-18	0.254E-18
11	0.338E-19	0.197E-18	0.193E-18
12	0.263E-19	0.154E-18	0.152E-18
13	0.208E-19	0.117E-18	0.115E-18
14	0.165E-19	0.959E-19	0.946E-19
15	0.137E-19	0.795E-19	0.786E-19
16	0.111E-19	0.644E-19	0.638E-19
17	0.931E-20	0.534E-19	0.531E-19
18	0.793E-20	0.455E-19	0.453E-19
19	0.681E-20	0.389E-19	0.388E-19
20	0.587E-20	0.334E-19	0.334E-19

Table 6. (Continued)

Apparent Excitation Cross Sections (140eV)

n\L	S	P	D
1	0.697E-14	0.000E+00	0.000E+00
2	0.562E-17	0.552E-16	0.000E+00
3	0.102E-17	0.243E-17	0.556E-18
4	0.349E-18	0.329E-17	0.267E-18
5	0.155E-18	0.156E-17	0.141E-18
6	0.857E-19	0.859E-18	0.825E-19
7	0.515E-19	0.531E-18	0.523E-19
8	0.329E-19	0.350E-18	0.343E-19
9	0.228E-19	0.242E-18	0.245E-19
10	0.164E-19	0.170E-18	0.175E-19
11	0.138E-19	0.125E-18	0.128E-19
12	0.113E-19	0.952E-19	0.967E-20
13	0.103E-19	0.740E-19	0.754E-20
14	0.896E-20	0.587E-19	0.606E-20
15	0.785E-20	0.471E-19	0.486E-20
16	0.693E-20	0.381E-19	0.394E-20
17	0.620E-20	0.310E-19	0.326E-20
18	0.548E-20	0.265E-19	0.271E-20
19	0.494E-20	0.220E-19	0.230E-20
20	0.440E-20	0.185E-19	0.194E-20

n	Balmer Optical Total Apparent	Total Direct (140eV)	
3	0.270E-17	0.110E-16	0.103E-16
4	0.795E-18	0.391E-17	0.369E-17
5	0.347E-18	0.186E-17	0.177E-17
6	0.185E-18	0.102E-17	0.937E-18
7	0.111E-18	0.635E-18	0.614E-18
8	0.717E-19	0.413E-18	0.406E-18
9	0.491E-19	0.289E-18	0.282E-18
10	0.344E-19	0.204E-18	0.199E-18
11	0.257E-19	0.152E-18	0.149E-18
12	0.201E-19	0.119E-18	0.117E-18
13	0.156E-19	0.919E-19	0.905E-19
14	0.125E-19	0.738E-19	0.723E-19
15	0.102E-19	0.597E-19	0.591E-19
16	0.844E-20	0.490E-19	0.486E-19
17	0.703E-20	0.404E-19	0.402E-19
18	0.600E-20	0.347E-19	0.345E-19
19	0.511E-20	0.293E-19	0.292E-19
20	0.435E-20	0.248E-19	0.248E-19

Table 6. (Continued)

Apparent Excitation Cross Sections (180eV)

n\L	S	P	D
1	0.590E-16	0.000E+00	0.000E+00
2	0.442E-17	0.468E-16	0.000E+00
3	0.817E-18	0.790E-17	0.437E-17
4	0.276E-18	0.273E-17	0.218E-17
5	0.124E-18	0.131E-17	0.113E-17
6	0.673E-19	0.731E-18	0.659E-18
7	0.412E-19	0.449E-18	0.422E-18
8	0.264E-19	0.296E-18	0.293E-18
9	0.182E-19	0.206E-18	0.199E-18
10	0.128E-19	0.147E-18	0.139E-18
11	0.106E-19	0.109E-18	0.925E-19
12	0.914E-20	0.837E-19	0.699E-19
13	0.779E-20	0.649E-19	0.581E-19
14	0.674E-20	0.515E-19	0.482E-19
15	0.590E-20	0.426E-19	0.413E-19
16	0.516E-20	0.337E-19	0.344E-19
17	0.457E-20	0.283E-19	0.292E-19
18	0.409E-20	0.238E-19	0.161E-19
19	0.362E-20	0.196E-19	0.129E-19
20	0.326E-20	0.172E-19	0.105E-19

n	Balmer Optical Total Apparent	Total Direct (180eV)
3	0.219E-17	0.916E-17	0.855E-17
4	0.650E-18	0.327E-17	0.309E-17
5	0.286E-18	0.155E-17	0.143E-17
6	0.153E-18	0.865E-18	0.802E-18
7	0.922E-19	0.533E-18	0.517E-18
8	0.600E-19	0.351E-18	0.342E-18
9	0.409E-19	0.244E-18	0.238E-18
10	0.287E-19	0.174E-18	0.170E-18
11	0.209E-19	0.130E-18	0.127E-18
12	0.161E-19	0.999E-19	0.982E-19
13	0.126E-19	0.780E-19	0.769E-19
14	0.100E-19	0.623E-19	0.615E-19
15	0.826E-20	0.516E-19	0.511E-19
16	0.661E-20	0.413E-19	0.409E-19
17	0.557E-20	0.348E-19	0.346E-19
18	0.470E-20	0.295E-19	0.293E-19
19	0.395E-20	0.247E-19	0.247E-19
20	0.341E-20	0.215E-19	0.213E-19

Table 6. (Continued)

Apparent Excitation Cross Sections (220eV)

n\L	S	P	D
1	0.509E-16	0.000E+00	0.000E+00
2	0.371E-17	0.403E-16	0.000E+00
3	0.633E-18	0.633E-17	0.367E-18
4	0.230E-18	0.246E-17	0.179E-18
5	0.109E-18	0.114E-17	0.926E-19
6	0.559E-19	0.581E-18	0.547E-19
7	0.340E-19	0.346E-18	0.338E-19
8	0.215E-19	0.251E-18	0.246E-19
9	0.143E-19	0.174E-18	0.158E-19
10	0.112E-19	0.120E-18	0.106E-19
11	0.871E-20	0.899E-19	0.740E-20
12	0.749E-20	0.677E-19	0.544E-20
13	0.634E-20	0.534E-19	0.404E-20
14	0.557E-20	0.416E-19	0.311E-20
15	0.491E-20	0.337E-19	0.237E-20
16	0.436E-20	0.275E-19	0.181E-20
17	0.391E-20	0.221E-19	0.143E-20
18	0.336E-20	0.185E-19	0.120E-20
19	0.309E-20	0.159E-19	0.976E-21
20	0.278E-20	0.132E-19	0.793E-21

n	Balmer Optical Total Apparent	Total Direct (220eV)	
3	0.157E-17	0.723E-17	0.742E-17
4	0.560E-18	0.286E-17	0.272E-17
5	0.242E-18	0.134E-17	0.128E-17
6	0.129E-18	0.741E-18	0.715E-18
7	0.779E-19	0.454E-18	0.440E-18
8	0.504E-19	0.297E-18	0.289E-18
9	0.338E-19	0.205E-18	0.200E-18
10	0.233E-19	0.143E-18	0.139E-18
11	0.170E-19	0.105E-18	0.103E-18
12	0.130E-19	0.806E-19	0.793E-19
13	0.101E-19	0.637E-19	0.628E-19
14	0.806E-20	0.504E-19	0.493E-19
15	0.653E-20	0.410E-19	0.406E-19
16	0.534E-20	0.336E-19	0.334E-19
17	0.439E-20	0.274E-19	0.272E-19
18	0.370E-20	0.231E-19	0.230E-19
19	0.313E-20	0.199E-19	0.199E-19
20	0.264E-20	0.167E-19	0.167E-19

Table 6. (Continued)

Apparent Excitation Cross Sections (240eV)

n\L	S	P	D
1	0.433E-16	0.000E+00	0.000E+00
2	0.348E-17	0.384E-16	0.000E+00
3	0.625E-18	0.641E-17	0.344E-17
4	0.210E-18	0.227E-17	0.162E-17
5	0.931E-19	0.107E-17	0.852E-18
6	0.509E-19	0.594E-18	0.509E-19
7	0.302E-19	0.359E-18	0.310E-19
8	0.196E-19	0.233E-18	0.223E-19
9	0.134E-19	0.161E-18	0.144E-19
10	0.945E-20	0.116E-18	0.974E-20
11	0.796E-20	0.829E-19	0.666E-20
12	0.676E-20	0.624E-19	0.439E-20
13	0.585E-20	0.480E-19	0.367E-20
14	0.512E-20	0.373E-19	0.274E-20
15	0.446E-20	0.302E-19	0.209E-20
16	0.396E-20	0.244E-19	0.163E-20
17	0.350E-20	0.199E-19	0.126E-20
18	0.309E-20	0.168E-19	0.104E-20
19	0.283E-20	0.141E-19	0.825E-21
20	0.255E-20	0.118E-19	0.673E-21

n	Balmer Optical	Total Apparent	Total Direct (240eV)
3	0.173E-17	0.736E-17	0.691E-17
4	0.514E-18	0.265E-17	0.251E-17
5	0.225E-18	0.125E-17	0.120E-17
6	0.120E-18	0.696E-18	0.671E-18
7	0.709E-19	0.420E-18	0.407E-18
8	0.464E-19	0.275E-18	0.268E-18
9	0.310E-19	0.189E-18	0.184E-18
10	0.217E-19	0.135E-18	0.132E-18
11	0.156E-19	0.976E-19	0.957E-19
12	0.113E-19	0.740E-19	0.728E-19
13	0.922E-20	0.575E-19	0.566E-19
14	0.723E-20	0.452E-19	0.446E-19
15	0.535E-20	0.367E-19	0.363E-19
16	0.478E-20	0.300E-19	0.297E-19
17	0.393E-20	0.247E-19	0.245E-19
18	0.333E-20	0.209E-19	0.206E-19
19	0.283E-20	0.178E-19	0.177E-19
20	0.242E-20	0.151E-19	0.151E-19

Table 6. (Continued)

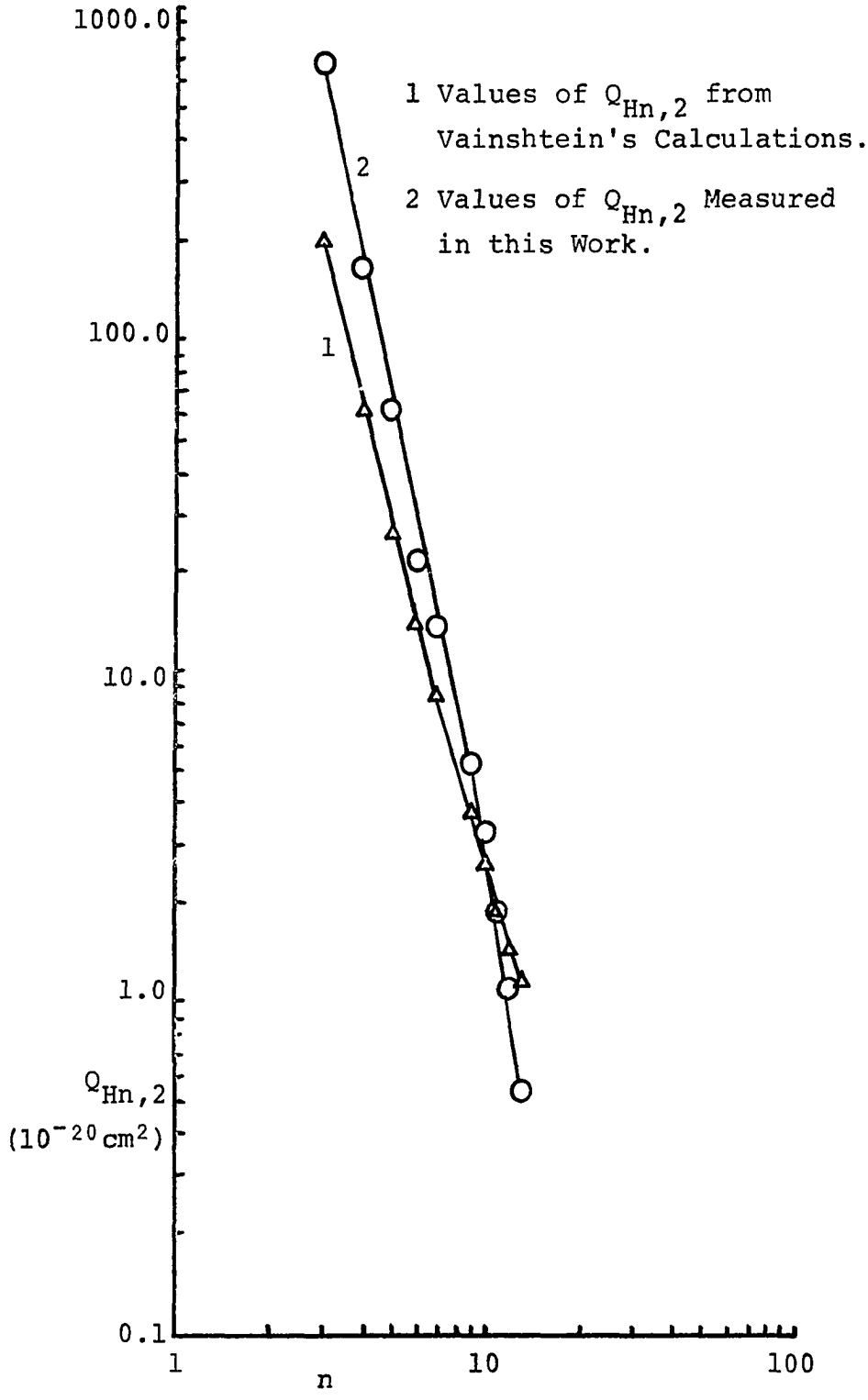

Figure 13. Theoretical and Experimental Values of $Q_{Hn,2}$ at 200 eV.

methods for calculating adsorption coefficients are given by Mitchell[71]. We find that the peak of the adsorption curve for 3 P resonance radiation in helium is approximately twice the corresponding peak for hydrogen. Heddle and Lucas[72] determined that the 5016 Å line optical excitation cross section of the 3 P helium state at one micron pressure was 2.5 times the same cross section at 1×10^{-5} mm Hg due to resonance adsorption. Since the geometry in the collision region and the shape of the adsorption curve affects the amount of resonance adsorption, the results of Heddle and Lucas cannot be applied directly to hydrogen. However, it is estimated that between 25% and 50% of the H_α optical excitation cross section measured in this work with an atomic hydrogen pressure of approximately two microns was due to resonance adsorption. The procedure for eliminating this effect by lowering the pressure could not be carried out since the thermionic cathode of the electron gun failed to operate at pressures lower than approximately two microns in the electron beam. Since the adsorption coefficient for the resonance radiation of a state is inversely proportional to the lifetime of that state, Table 5 indicates that above the n = 3 state resonance adsorption in this work was negligible. Therefore, resonance adsorption cannot explain the differences between the measured and computed optical excitation cross sections shown in Fig. 13.

The estimated 20% error in the measurement of $N^*_{HT}/N^*_{H_2T}$ cannot fully explain the differences in the cross sections in Fig. 13. It should be noted that a portion of the 20% error in the measurement of $N^*_{HT}/N^*_{H_2T}$ is expected to be systematic or constant. The effect of such an error is to translate but not alter the slope of the log-log plot of the measured cross sections against n. This is of interest since the occurrence of errors in the measurement of $N^*_{HT}/N^*_{H_2T}$ in addition to the anticipated 20% error should be systematic.

Since the dependence of the Balmer optical excitation cross sections on n is very nearly independent of electron energy, the effect of retarded or mixed electron energies in the electron beam would have the same effect as a systematic error on the plot of the measured cross sections in Fig. 13.

Errors in the absolute measurement of $Q_{H_2n,2}$ could both translate and change the slope of the measured $Q_{Hn,2}$ in Fig. 13. However, the limit on the error in the measurement of $Q_{H_2n,2}$ was 15%. Therefore, with the averaging process of curve fitting in Fig. 13, these errors could not account for the differences in the measured and the calculated cross sections.

The lifetimes for atomic hydrogen given in Table 5 indicate that at the average velocity of 2.5×10^5 cm/sec

for hydrogen atoms at room temperature a negligible fraction of the excited states through n = 13 escaped from the electron beam before radiatively decaying.

A consideration which must be made is the effect of the electric fields in the electron beam on the near degenerate states in atomic hydrogen. In the Dirac theory which includes spin there are $2n^2$ independent states for each value of n for atomic hydrogen. The $2n^2$ states are split into n energy levels, one for each value of j, the total angular momentum quantum number of the electron. The energies of the j states for a given value of n are called the fine structure. The Lamb shift splits the energies of the two l states for a given value of j. This energy splitting is much less than that of the fine structure.

If the energy shift in an electric field, or the Stark effect, is small compared to the energy differences between two states, they remain independent. If the Stark effect is comparable to or greater than this energy difference, the states become mixed. In order to have meaningful l quantum numbers for atomic hydrogen therefore, the Stark effect must be smaller than the Lamb shift. Bethe and Salpeter[73] give the electric field strengths at which the Lamb shifted S and P states with j = 1/2 become mixed to be 475, 58, 12, and 1.7 Volts/cm for n = 2, 3, 4, and 6, respectively. The necessary electric field strength for

mixing these states varies inversely as $n^4\sqrt{n^2 - 1}$. Bethe and Salpeter[73] state that the Lamb shift is negligible for $j \geq 3/2$.

If two or more states are mixed by an electric field, the wavefunction for each resulting state is a linear sum of the wavefunctions of the original or pure states. The relative number of atoms excited to a given pure state component of a mixed state depends on the mode of excitation and the strength of the perturbing electric field. A hydrogen atom excited to a given component of a mixed state radiatively decays according to the selection rules for the wavefunction of that component. The lifetime of each component of a mixed state is a function of the lifetimes of the constituent pure states of the mixed state and the perturbing electric field.

The level cross sections for the excitation of mixed states of atomic hydrogen have not been calculated. However, the calculated level cross section for a mixed state should be significantly different than the calculated level cross section of any of its constituent pure states.

The electric field due to the space charge of the electrons in the electron beam in this work was calculated to be less than 2 mV/cm. This value should have been considerably reduced by positive ion neutralization. Stray electric fields were shielded from the electron beam by the

Faraday screen described in Chapter III. It should be noted, however, that charging of parts of the electron gun which may have become glazed could have introduced stray electric fields. In spite of the Faraday screen, charging of the glass nozzle and chamber walls may have introduced small stray electric fields. The lack of operation of the electron beam below 50 eV gives some weight to these possibilities. However, when the electron beam formed above 50 eV, the conductive path formed to the anode by the weak plasma would tend to prevent electrons from straying to nonconducting parts which would cause charging and stray electric fields. Therefore, above 100 eV it is assumed that space charge contributes the only significant electric field in the electron beam.

We therefore conclude that through n = 13 the j = 1/2 states were not mixed. Since Bethe and Salpeter say only that for $j \geq 3/2$ the Lamb shift is negligible, we cannot determine at which n state these j states become mixed. The constant slope of the measured cross sections in Fig. 13 for n = 3-10 suggests that effects due to mixing of states do not occur in this range. It is estimated that the Balmer optical excitation cross sections computed in this work on the basis of pure states would deviate less than 20% at 100 eV above n = 6 from the same computation based on the partially mixed states occurring in this work. For $n \leq 6$ smaller deviations are estimated. Therefore, a) since the

cross sections for mixed states have not been calculated, b) since the exact electric field in the electron beam is not known, and c) since treating the states as pure is expected to contribute only small error in the computed Balmer optical excitation cross sections, the cross sections computed on the basis of pure states are convenient and valid expressions for comparison with experimental measurements.

Fig. 14 shows the log-log plots of the H_α optical excitation function computed from Vainshtein's calculations and the one measured here. The slope of the computed function is -0.812 while the slope of the measured function is -0.425. An effective retarding potential of approximately 100 V on the electron beam would be required to bring these slopes into agreement. However, the existance of such a retarding potential was very unlikely as discussed previously.

The best check on the operation of the electron gun is to measure a known excitation function. This was done for the H_α optical excitation function of molecular hydrogen shown in Fig. 15. The slopes of the functions measured with the static and crossed beam systems are -0.65 and -0.69. The very close agreement of these functions strongly indicates that no significant distortion of the electron beam energy occurred.

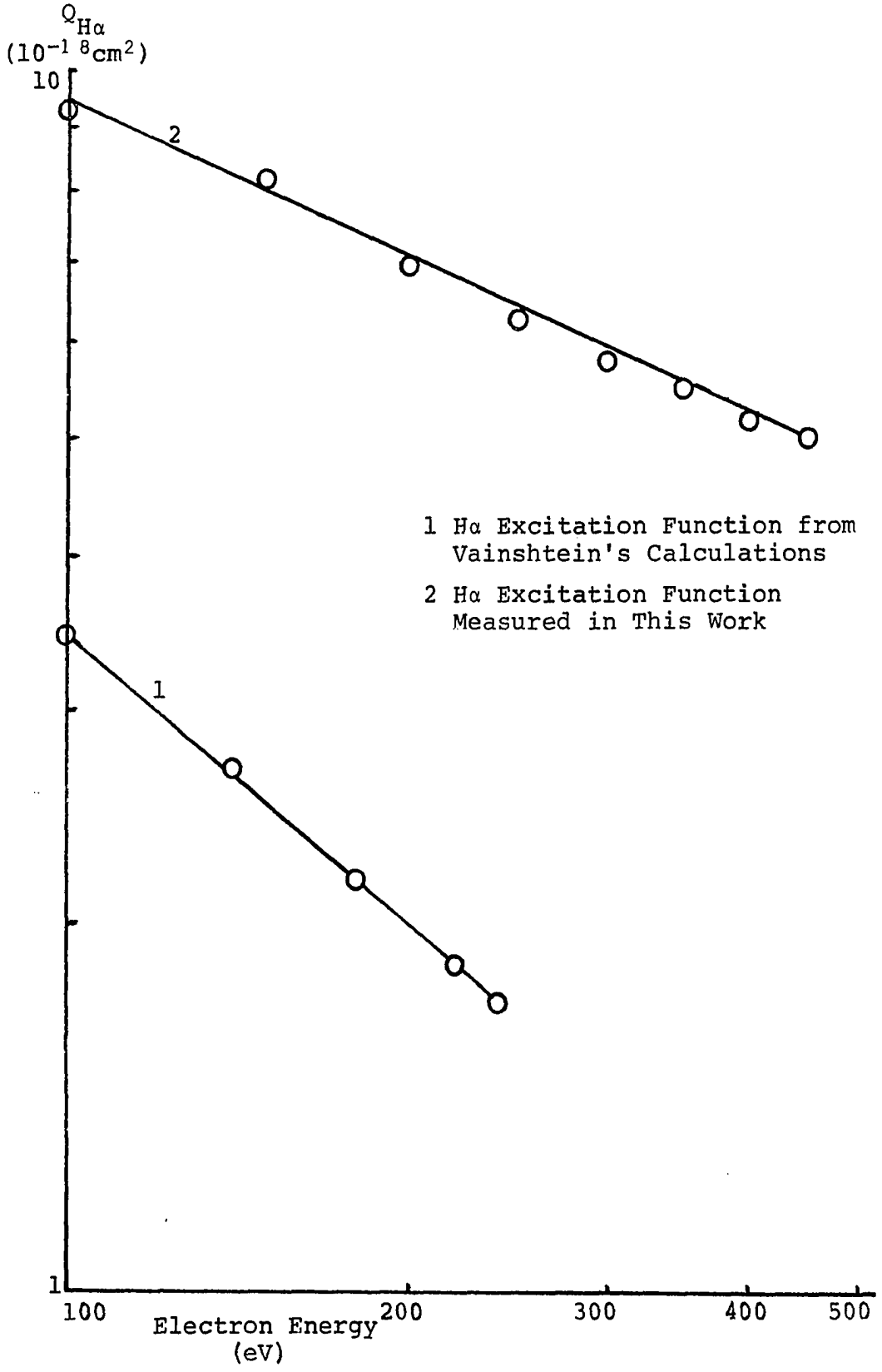

Figure 14. Theoretical and Measured Hα Optical Excitation Functions.

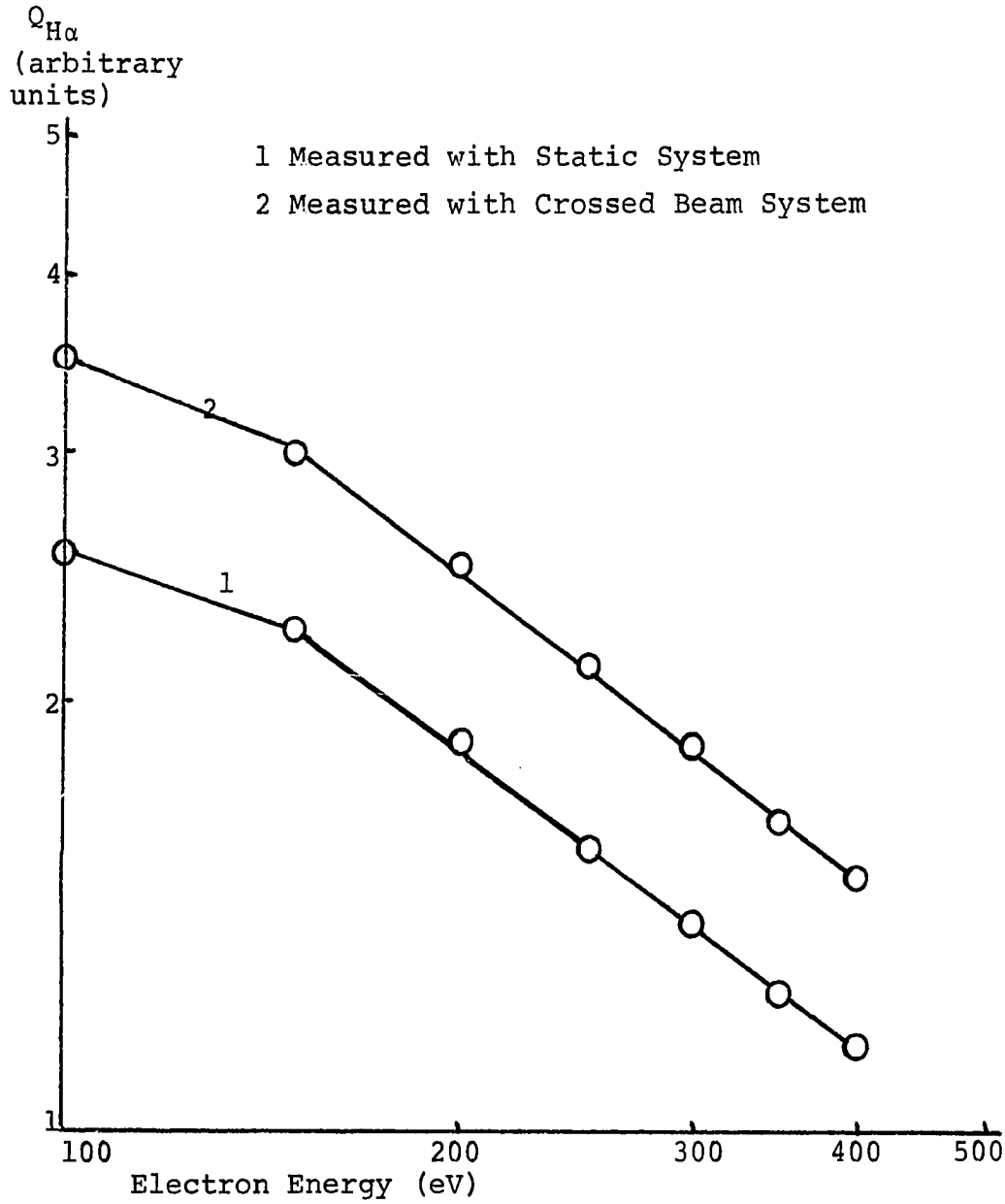

Figure 15. The Hα Optical Excitation Functions of H_2 Measured with the Static and Atomic Beam Systems.

CHAPTER V

CONCLUSION

The significant accomplishments of this work were: the development of a Wood's discharge tube source of hydrogen atoms which produced essentially 100% dissociation at a throughput of 1000 μ·liters/sec; the development of a simplified crossed electron-atomic beam apparatus which yielded an atomic hydrogen density in the electron beam of 3-6 x 10^{13} cm^{-3}; and the measurements of the absolute Balmer optical excitation cross sections of atomic hydrogen for n = 3-13. The error in the measurements was estimated to be 30%.

The excitation cross sections calculated for the pure states of atomic hydrogen by Vainshtein were converted to Balmer optical excitation cross sections by using the Einstein transition probabilities for the pure states. The theoretical Balmer optical excitation cross sections for hydrogen atoms with partially mixed states due to an electric field of the magnitude found in the electron beam in this work were expected to deviate only a relatively small amount from the

corresponding cross sections calculated on the basis of pure states, although the calculations for mixed states have not been carried out.

The differences in the calculated and measured Balmer optical excitation cross sections were in most cases greater than the sum of the errors expected for both. We must conclude, therefore, that systematic errors which are difficult to identify and assess remain in the calculations and/or measurements. The sources of these possible systematic errors in the measurements would be expected to be stray electric fields in the electron beam large enough to significantly distort the electron energy, and the different gas-gas scattering properties of hydrogen atoms and molecules which could affect the measurement of $N^*_{HT}/N^*_{H_2T}$. By altering the design of the crossed beam apparatus it may be possible to greatly reduce the magnitude of these systematic errors. These alterations include in-line liquid nitrogen trapping above the diffusion pump to reduce the possibility of glazing the electron gun and the shielding of all glass parts exposed to the electron beam by grounded conductors. The in-line trap should allow the operation of the thermionic cathode at lower hydrogen densities which would reduce the gas-gas scattering. A further effect of these changes in design may be the proper operation of the electron beam down to the onset of excitation of atomic hydrogen. However, due

to limitations in time and equipment these design changes were not carried out. They remain as a potential check and extension of this work.

LIST OF REFERENCES

1. L. S. Ornstein and H. Lindeman, Z. Physik 80, 525 (1933).

2. W. E. Lamb, Jr. and R. C. Retherford, Phys. Rev. 79, 549 (1950).

3. W. L. Fite and R. T. Brackmann, Phys. Rev. 112, 1151 (1958).

4. W. L. Fite, R. F. Stebbings, and R. T. Brackmann, Phys. Rev. 116, 356 (1959).

5. G. E. Chamberlain, S. J. Smith, and D. W. O. Heddle, Phys. Rev. Letters 12, 647 (1964).

6. R. L. Long, Jr., D. M. Cox, and S. J. Smith, J. of Res. 72 A, 521 (1968).

7. J. F. Williams, E. K. Curley, and J. W. McGowan, Bull. Am. Phys. Soc. 13, 214 (1968).

8. W. Lichten and S. Schultz, Phys. Rev. 116, 1132 (1959).

9. R. F. Stebbings, W. L. Fite, D. G. Hummer, and R. T. Brackmann, Phys. Rev. 119, 1939 (1960).

10. H. Kleinpoppen and E. Kraiss, Phys. Rev. Letters 20, 361 (1967).

11. R. W. Wood, Proc. Roy. Soc. 97 A, 455 (1920).

12. B. J. Wood and H. Wise, Rarefied Gas Dynamics Supp. 1, 51 (New York: Academic Press, 1961).

13. J. D. Cobine, Gaseous Conductors, 26 (New York: Dover Publications, Inc. 1941).

14. Ibid., 18.

15. Ibid., 23.

16. J. T. Vanderslice, S. Weissman, E. A. Mason, and R. J. Fallon, Phys. of Fluids 5, 155 (1962).

17. J. E. Scott, Jr., H. S. Morton, Jr., J. A. Phipps, and J. F. Moonan, Rarefied Gas Dynamics Vol. 11, Supp. 3, 331 (New York: Academic Press, 1966).

18. P. M. Marcus and J. H. McFee, Recent Research in Molecular Beams, 43 (New York: Academic Press, 1959).

19. J. P. Hartnett, Rarefied Gas Dynamics Supp. 1, 1 (New York: Academic Press, 1961).

20. W. H. Keesom and G. Schmidt, Physica 4, 828 (1937).

21. S. Dushman, Scientific Foundations of Vacuum Technique, 9 (New York: John Wiley and Sons, Inc., 1949).

22. Knudsen, Ann. Physik 25, 983 (1908).

23. S. Dushman, op. cit., 94.

24. W. Jawtusch, Rarefied Gas Dynamics Vol. 1, Supp. 2, 414 (New York: Academic Press, 1963).

25. S. Datz, G. E. Moore, and E. H. Taylor, Rarefied Gas Dynamics Vol. 1, Supp. 2, 347 (New York: Academic Press, 1963).

26. J. N. Smith, Jr. and W. L. Fite, Rarefied Gas Dynamics Vol. 1, Supp. 2, 430 (New York: Academic Press, 1963).

27. J. N. Smith, Jr. and W. L. Fite, J. Chem. Phys. 37, 898 (1962).

28. D. R. O'Keefe, J. N. Smith, Jr., P. L. Palmer, and H. Saltzburg, Surface Science 20, 27 (1970).

29. F. C. Hurlbut, RAND Report 339, 21-1 (June 1959).

30. J. J. Hinchen and E. F. Shepherd, Rarefied Gas Dynamics, 239 (New York: Academic Press, 1967).

31. R. E. Stickney, Advances in Atomic and Molecular Physics Vol. 3, 143 (New York: Academic Press, 1967).

32. E. C. Beder, Advances in Atomic and Molecular Physics Vol. 3, 205 (New York: Academic Press, 1967).

33. M. Navez and C. Sella, C. R. Acad. Sci. (Paris) Vol. 250, No. 26, 4325 (1960).

34. J. R. Stalder, G. Goodwin, and M. O. Creager, National Advisory Comm. Aeronaut. Report No. 1032 (1951).

35. D. H. Davis, L. L. Levenson, and N. Milleron, Rarefied Gas Dynamics Supp. 1, 99 (New York: Academic Press, 1961).

36. L. L. Levenson, N. Milleron, and D. H. Davis, UCRL-6014, Lawrence Radiation Laboratory, Livermore, Calif.

37. R. W. Zwanzig, J. Chem. Phys. 32, 1173 (1960).

38. W. Bayh and H. Pflug, Z. Angew. Phys. 25, 358 (1968).

39. F. C. Hurlbut, J. Applied Phys. 28, 844 (1957).

40. F. C. Hurlbut, Recent Research in Molecular Beams, 145 (New York: Academic Press, 1959).

41. S. Dushman, op. cit., 10.

42. W. V. Smith, J. Chem. Phys. 11, 110 (1943).

43. H. Wise and B. J. Wood, Advances in Atomic and Molecular Physics Vol. 3, 291 (New York: Academic Press, 1967).

44. F. A. Sharpton, Excitation of Neon Atoms by Electron Impact (a Ph.D. dissertation), 6 (University of Oklahoma, 1968).

45. H. J. Kostkowski and R. D. Lee, Theory and Methods of Optical Pyrometry (NBS Monograph 41), (Washington, D.C.: U.S. Government Printing Office, 1962).

46. J. D. Jobe, Excitation Processes in Helium (a Ph.D. dissertation), 14 (University of Oklahoma, 1968).

47. J. C. DeVos, Physica 20, 690 (1954).

48. I. Langmuir, J. Am. Chem. Soc. 34 No. 17, 1310 (1912).

49. W. L. Fite and R. T. Brackmann, Phys. Rev. 112, 1141 (1958).

50. N. F. Ramsey, Am. Scientist 56 No. 4, 420 (1968).

51. G. J. Schultz, Phys. Rev. Letters 13 No. 20, 583 (1964).

52. J. M. B. Kellogg, J. I. Rabi, and J. R. Zacharias, Phys. Rev. 50, 472 (1936).

53. E. W. R. Steacie, Atomic and Free Radical Reactions, 33 (New York: Rinehold, 1954).

54. Private Communication from W. L. Fite (1970).

55. H. G. Poole, Proc. Roy. Soc. London 163 A, 415 (1937).

56. G. Francis, Encyclopedia of Physics Vol. 12, Gas Discharges 2, 53 (Berlin: Springer-Verlag, 1956).

57. S. C. Brown, Basic Data of Plasma Physics, (Cambridge: Cambridge Technology Press of the Massachusetts Institute of Technology, 1959).

58. S. J. B. Corrigan, J. Chem. Phys. 43, 4381 (1965).

59. S. Dushman, op. cit., 91.

60. Ibid., 94.

61. H. Melville and B. G. Gowenlock, Experimental Methods in Gas Reactions, 182 (New York: St. Martin's Press, 1964).

62. P. Clausing, Z. Physik 66, 471 (1930).

63. B. D. Power and D. J. Crawley, Vacuum 4, 415 (1954).

64. Private Communication from D. W. O. Heddle (1970).

65. B. Bederson, Methods of Experimental Physics Vol. 7, Part A, 73 (New York: Academic Press, 1968).

66. W. Bächler, Am. Vacuum Soc. Trans., (1962).

67. J. D. Jobe, op. cit., 22.

68. W. L. Wiese, M. W. Smith, and B. M. Glennon, Atomic Transition Probabilities Volume 1 Hydrogen Through Neon, 1 (Washington, D.C.: U.S. Government Printing Office, 1966).

69. L. C. Green, P. P. Rush, and C. D. Chandler, Astrophys. J. Supp. Ser. 3, 37 (1957).

70. L. A. Vainshtein, Opt. Spectry. USSR 18, 538 (1965).

71. A. C. G. Mitchell and M. W. Zemansky, Resonance Radiation and Excited Atoms, 96 (New York: Macmillan Co., 1934).

72. D. W. O. Heddle and C. B. Lucas, Proc. Roy. Soc. London 271A, 129 (1963).

73. H. A. Bethe and E. E. Salpeter, Quantum Mechanics of One and Two Electron Atoms, 288 (Berlin: Springer-Verlag, 1957).